POLITECNICO DI TORINO

Department of Mechanical and Aerospace Engineering

Master's Degree in
Biomedical Engineering

Master's Thesis

Raman spectroscopy for dentistry: effects of irrigations treatments on dentin

Supervisors

Prof. Sabrina Grassini
Prof. Leonardo Iannucci
Prof. Nicola Scotti

Candidate

Matilde Iafelice

AY 2025/2026

To my brother,
who lit the way
whenever I felt lost.

Abstract

In recent years, restorative dentistry has increasingly focused on understanding the interactions between restorative materials and dental tissues, since the long-term stability and clinical success of dental restorations depend largely on the integrity of the adhesive interface. In this context, dentin represents a complex biological substrate whose chemical composition and structural organization can be significantly altered by endodontic irrigation protocols. Specifically, commonly employed solutions such as sodium hypochlorite (NaOCl) and ethylenediaminetetraacetic acid (EDTA), while essential for the cleaning and disinfection of the dental root canal, can induce alterations in both the organic (collagen) and inorganic (apatite) components of dentin. These alterations negatively affect the formation and stability of the hybrid layer and, consequently, the overall durability of the dental restorations.

In light of these clinical challenges, this Master thesis, developed in collaboration with the Dental School of the University of Turin, aims to investigate the chemical alterations in dentin induced by irrigation protocols based on NaOCl and EDTA, evaluating the effect of exposure time and the protective role of an adhesive layer applied prior to irrigation. Two experimental conditions were compared: dentin subjected to direct irrigation and dentin protected by the preventive application of a universal adhesive system. This comparison was designed to assess the effect of the irrigants and the efficacy of the adhesive in preserving the chemical integrity of the dentinal substrate.

Raman spectroscopy was employed for the analysis, as it is a non-destructive technique that allows for the in situ chemical characterization of dentin, providing in-depth information on mineral and organic components. This approach enabled the evaluation of dentin variations induced by the treatments, specifically monitoring parameters related to mineral content, collagen integrity, and the stability of the dentin matrix. The results highlight that irrigation protocols lead to significant chemical alterations, which are influenced by both exposure time and the presence of a protective adhesive layer. These

findings provide an objective basis for optimizing clinical protocols aimed at preserving the integrity of the dentinal substrate and enhancing the longevity of dental restorations.

Abstract

Negli ultimi anni, l'odontoiatria restaurativa ha rivolto crescente attenzione alla comprensione delle interazioni tra materiali restaurativi e tessuti dentali, poiché la stabilità a lungo termine e il successo clinico dei restauri dentali dipendono in larga misura dall'integrità dell'interfaccia adesiva. In questo contesto, la dentina rappresenta un substrato biologico complesso, la cui composizione chimica e organizzazione strutturale possono essere significativamente alterate dai protocolli di irrigazione endodontica. In particolare, soluzioni comunemente impiegate come l'ipoclorito di sodio (NaOCl) e l'acido etilendiamminotetraacetico (EDTA), pur essendo essenziali per la detersione e disinfezione del sistema canalare, possono indurre alterazioni nella componente organica (collagene) e in quella inorganica (apatite) della dentina, influenzando negativamente la formazione e la stabilità dello strato ibrido e, di conseguenza, la durabilità dei restauri.

Alla luce di queste problematiche cliniche, la presente tesi, sviluppata in collaborazione con la Dental School dell'Università degli Studi di Torino, ha lo scopo di investigare le alterazioni chimiche della dentina indotte da protocolli irriganti a base di NaOCl ed EDTA, valutando l'effetto del tempo di esposizione e il ruolo protettivo di uno strato adesivo applicato prima dell'irrigazione. Sono state confrontate due condizioni sperimentali: dentina sottoposta a irrigazione diretta e dentina protetta mediante applicazione preventiva di un sistema adesivo universale al fine di valutare l'effetto degli irriganti e l'efficacia dell'adesivo nel preservare l'integrità chimica del substrato dentinale.

Per l'analisi è stata impiegata la spettroscopia Raman, tecnica non distruttiva che consente la caratterizzazione chimica in situ della dentina, fornendo informazioni quantitative sulle componenti minerale e organica. Questo approccio ha permesso di valutare le variazioni della dentina indotte dai diversi trattamenti, valutando parametri correlati al contenuto minerale, all'integrità del collagene e alla stabilità della matrice dentinale. I risultati evidenziano che i protocolli irriganti determinano alterazioni chimiche significative, influenzate

dal tempo di esposizione e dalla presenza di uno strato adesivo protettivo. Tali evidenze forniscono basi oggettive per l'ottimizzazione dei protocolli clinici volti a preservare l'integrità del substrato dentinale e migliorare la longevità dei restauri dentali.

Contents

Chapter 1

Introduction

1.1 Clinical Relevance of Dentin-Adhesive Interfaces

The integrity of dentin adhesive interfaces is one of the most critical and determinant aspect when concerning the long term clinical longevity and predictability of restorative dental procedures, notably following endodontic treatments. Therefore, endodontically treated teeth are routinely restored using adhesive techniques, wherein bonding to dentin plays a central role.

Irrigating agents employed during root canal therapy are known to induce chemical and structural modifications in dentin [1], potentially leading to a compromise of the substrate and its intrinsic properties, with negative implications for subsequent adhesive restorations [2]. Although indispensable for ensuring effective disinfection and procedural success, these agents lack substrate specificity [3] and may therefore induce unintended alterations within the dentinal structure.

Among those most used for such applications, of particular relevance, sodium hypochlorite (NaOCl) exhibits strong oxidative and proteolytic activity, resulting in degradation of the collagen matrix [4]. In contrast, ethylenediaminetetraacetic acid (EDTA) primarily exerts its effect through calcium chelation, targeting the inorganic hydroxyapatite phase and inducing partial demineralization of the dentin surface [3].

For this reason it is important to underline that while essential for accomplishing their endodontic function, these chemical agents are not devoid of potential drawbacks and may exert negative effects on the dentinal substrate, including a reduction in mechanical stability [5] and an impairment of its ability to form a stable and durable hybrid layer when resin based adhesive systems are employed [5] [6]. The hybrid layer must therefore be understood as a unit consisting of the smear layer created following the preparation of the dentin substrate and the adhesive monomer chosen to be applied. [7]. To fully appreciate the implications of these chemically induced effects, it is essential to consider the structural and compositional characteristics of dentin as a biological substrate, as it will be discussed in Section 1.2.

Traditional analytical techniques such as scanning electron microscopy (SEM), transmission electron microscopy (TEM), and energy dispersive spectroscopy (EDS) [8] are widely used to investigate morphological and elemental changes in dentin [9]. However, despite their usefulness, these methods are limited in providing in situ molecular level information, particularly with regard to collagen degradation [10] and alterations in the mineral phase [11].

In this context, Raman spectroscopy has emerged as a robust [12], non destructive analytical technique with high molecular specificity [13]. Its growing adoperation in dental research stems from its ability to precisely map compositional shifts in dentin [14], from assessing collagen scaffold integrity to quantifying mineral phase variations post treatments [15].

Starting from these premises, therefore, by enabling the simultaneous characterization of both organic and inorganic components while preserving specimen integrity [14] [16], Raman spectroscopy allows the identification of specific spectral markers associated with hydroxyapatite and collagen [17], as well as the assessment of their relative modifications following chemical exposure, as discussed in Section 3.2.

1.2 Dentin as a complex biological substrate

Dentin is a hierarchically organized biological tissue composed primarily of type I collagen fibrils embedded within a mineralized matrix of hydroxyapatite crystals [18]. The organization and relative proportion of its organic and inorganic components are critical for maintaining mechanical integrity and ensuring effective interaction with adhesive systems [19] [20].

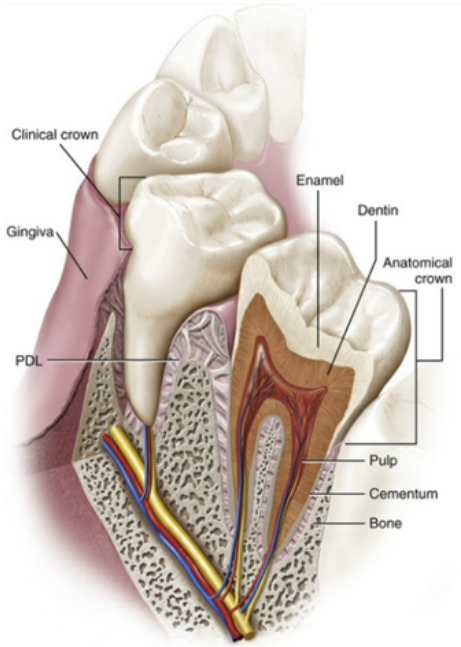

Figure 1.1: Schematic representation of tooth anatomy highlighting enamel, dentin, pulp, cementum, and surrounding periodontal tissues [18].

Any disruption of this chemical and mechanical balance, whether through deproteinization or demineralization [21], may impair monomer diffusion and compromise hybrid layer formation [22], ultimately affecting the quality and durability of adhesive restorations.

The specific mechanical behavior of dentin, together with its intrinsic permeability and structural complexity [12], makes it a central substrate in both operative dentistry and adhesive restorative procedures. From an ultrastructural perspective, dentin exhibits a tubular microarchitecture, characterized by approximately 15,000 to 45,000 dentinal tubules per mm^2 extending radially from the pulp chamber [23] toward the dentino-enamel junction (DEJ) [24].

These tubules are embedded within an intertubular matrix composed of mineralized collagen fibrils [25], while the peritubular dentin surrounding each tubule is more highly mineralized and characterized by a reduced collagen content [26] [27].

Both the density and diameter of dentinal tubules increase with proximity to the pulp, rendering deep dentin more permeable, less mineralized, and more reactive to chemical stimuli than superficial dentin [27] [5] . This regional variability results in differences in chemical reactivity, adhesive behavior, and susceptibility to degradation. In particular, deeper dentin facilitates greater penetration of irrigating solutions and presents additional challenges for stable hybrid layer formation due to its higher water content and increased tubule density [28] [6].

Dentin's composite structure, arising from the intimate association between collagen fibrils, nanocrystalline hydroxyapatite, and water, renders the tissue especially vulnerable to chemical challenges. Irrigating agents commonly employed during endodontic procedures may selectively affect the organic or inorganic components of dentin [19], inducing collagen degradation through oxidative mechanisms, as observed with NaOCl, or promoting calcium chelation from hydroxyapatite in the case of chelating agents such as EDTA [27]. These processes may lead to significant alterations in dentin structure and properties [5], with potential consequences for both mechanical integrity and adhesive performance.

Understanding how dentin architecture and composition influence its response to chemical treatments is therefore essential for interpreting the effects of endodontic irrigation and for refining adhesive strategies.

1.2.1 Chemical composition and structural organization

Dentin is a tripartite composite material (as clarified in Table 1.1). The inorganic phase primarily consists of nanocrystalline hydroxyapatite ($Ca_{10}(PO_4)_6(OH)_2$), tightly associated with a fibrous collagen type I matrix [2](organized in fibrils that provide tensile strength and contribute to

the overall toughness of the tissue [2]).

From a compositional and functional perspective, the organic matrix of dentin is dominated by a three dimensional collagen network that provides tensile strength, fracture resistance [29]. This matrix also contains non-collagenous proteins (NCPs) that play a regulatory role in mineralization processes, water retention, and molecular signaling within dentin [2] as summarized in Table 1.2.

Table 1.1: Compositional and structural features of dentin

Component	**Fraction (%)**	**Main constituents**	**Structural localization**	**Functional role**
Inorganic phase	~ 70	Nanocrystalline hydroxyapatite	Intra and extrafibrillar spaces	Stiffness, hardness, load-bearing capacity
Organic matrix	~ 20	Type I collagen fibrils	Intertubular dentin	Tensile strength, toughness, crack resistance
Water	~ 10	Free and bound water	Dentinal tubules and interfibrillar spaces	Permeability, diffusion, chemical reactivity

Hydroxyapatite crystals are not uniformly distributed throughout the entire tissue but are predominantly located in intrafibrillar and extrafibrillar regions, contributing to both stiffness and hardness of the tissue [28].

Dentin's microstructural organization is further defined by the presence of dentinal tubules extending radially from the pulp toward the dentino-enamel junction (DEJ). The progressive increase in tubule density and diameter toward the pulp results in deep dentin exhibiting greater permeability and enhanced reactivity to chemical agents compared to more superficial regions [6] [26].

This architecture results in biomechanical properties intermediate between enamel and pulp [28].

At the same time, its composite nature makes it particularly susceptible to chemical alterations, especially when exposed to oxidizing or chelating agents used in endodontic treatments [28].

Such agents may selectively affect either the organic or the mineral components, leading to significant modifications of dentin structure and properties [5] [6].

Table 1.2: Microstructural features and biological components of dentin

Component	**Main characteristics**	**Structural localization and functional relevance**
Non-collagenous proteins (NCPs)	DPP and DMP1 promote mineral nucleation and crystal growth; osteocalcin and osteonectin mediate collagen mineral coupling; proteoglycans regulate hydration and ionic balance.	Primarily associated with the organic matrix and the mineralized collagen network; contribute to controlled mineralization, matrix organization, and mechanical performance.
Water phases	Free water (FW) supports fluid transport and diffusion; bound water (BW) is confined at the collagen/hydroxyapatite interface and stabilizes fibril conformation.	FW: mainly within dentinal tubules and interfibrillar spaces; BW: concentrated at the collagen–HA interface, influencing permeability, chemical reactivity, and mechanical damping.
Dentin regions	Intertubular dentin (ID): collagen rich and the main bonding substrate; peritubular dentin (PD): hypermineralized and more susceptible to erosion and chemical challenges.	ID: constitutes the bulk between tubules and governs adhesive infiltration; PD: surrounds tubules and can be preferentially affected by demineralizing/chelating agents, altering local permeability and bonding behavior.

This hydrated framework, while mechanically advantageous, is inherently sensitive to chemical perturbations. Oxidizing agents such as sodium hypochlorite may induce collagen degradation [10], whereas chelating agents such as EDTA preferentially dissolve the mineral phase, leading to alterations in mechanical properties [20], surface energy, wettability, and monomer infiltration capacity [21].

These chemically induced modifications play a decisive role in determining the effectiveness and durability of adhesive restorations [2].

1.2.2 Susceptibility to Chemical Degradation

The susceptibility of dentin to chemical degradation arises from its composite organization (as reported in Table 1.1), which integrates nanocrystalline hydroxyapatite, type I collagen, and water into a finely balanced structural system [28].While it is important to emphasize that this arrangement offers functional versatility, it also makes dentin particularly sensitive to chemical challenges [1], especially during endodontic irrigation procedures.

Irrigating agents commonly employed for root canal disinfection interact with dentin in a non selective manner [5], affecting both its organic and inorganic components [6]. In particular, the organic matrix, is highly susceptible to sodium hypochlorite, which acts as a strong oxidizing agent [27] and it is precisely this type of induced oxidative degradation that can lead to partial or complete breakdown of the collagen fibrillar architecture [28], resulting in reduced tensile strength, increased brittleness, and compromised adhesive performance.

Moreover, exposed and denatured collagen becomes more susceptible to enzymatic degradation by matrix metalloproteinases (MMPs) and cysteine cathepsins [7], enzymes naturally present in dentin and activated under conditions of demineralization or oxidative stress [13] [26] .

By contrast, EDTA acts primarily on the inorganic phase by chelating divalent calcium ions (Ca^2+) from the hydroxyapatite mineral lattice [27]. This mechanism results in dentin demineralization, particularly affecting peritubular dentin (characterized by a higher degree of mineralization and more susceptible to EDTA induced erosion [25]).

The depletion of calcium ions compromises dentin stiffness and hardness and may increase tissue permeability by enlarging the lumens of dentinal tubules [5] [28] .

In clinical protocols, NaOCl and EDTA are often used in combination and may produce synergistic or additive degradation effects [6], depending on parameters such as irrigant concentration, exposure time, and dentin depth.

While superficial dentin may undergo partial structural alteration, deeper dentin, characterized by higher tubule density and water content, is more chemically reactive and therefore more extensively affected [6] [26]

Thus, a detailed understanding of the depth dependent and component specific effects of endodontic irrigants is essential for optimizing clinical protocols and preserving dentin's structural and chemical integrity [13].

1.3 Endodontic Irrigants and Their Chemical Effects

Chemical irrigation is an essential phase of endodontic treatment, aimed at enhancing canal cleanliness through antimicrobial action and dissolution of organic and inorganic debris.

The primary goal of endodontic irrigation is to efficiently disinfect the root canal system [30] and eliminate residual debris [1], including the smear layer formed during the use of mechanical instrumentation for cavity preparation. Among the various agents employed, NaOCl and EDTA represent the most commonly used solutions, owing to their well documented tissue dissolving and chelating properties, respectively [4] [6].

Beyond its antimicrobial activity, NaOCl is uniquely capable of dissolving necrotic and vital pulp tissue, thus facilitating canal cleaning.

NaOCl predominantly exerts its antimicrobial and tissue, dissolving effects through a strong oxidative mechanism, leading to protein degradation through chlorination and oxidation reactions [27].

However, these non specific effects also extend to the organic matrix of dentin,

especially type I collagen. Indeed, prolonged exposure to NaOCl has been shown to decrease collagen integrity, reduce dentin flexural strength, and increase the brittleness of the substrate, potentially compromising bonding performance [5] [26].

EDTA, on the other hand, is a chelating agent with a strong affinity for divalent cations, particularly calcium (Ca^2+)and when applied to dentin, it demineralizes the inorganic phase, primarily targeting hydroxyapatite crystals.
This process promotes smear layer removal [3], enlargement of dentinal tubules, and increased surface permeability [4] [5]. However, overexposure may lead to pronounced mineral content loss, erosion of peritubular dentin, and exposure of unsupported collagen fibrils [3] [6].

The combined use of NaOCl and EDTA is common in clinical protocols, and this sequence enhances smear layer removal and canal cleanliness [3], but it may also lead to synergistic structural damage as NaOCl can denature exposed collagen, while EDTA weakens the mineral support. Such alterations are more pronounced in deep dentin, where increased tubule density and water content enhance the diffusion and action of irrigants [18]. For this reason, optimization of irrigation protocols—through appropriate control of irrigant concentration, exposure time, and the potential use of protective strategies represents a crucial aspect in minimizing structural damage while ensuring adequate canal decontamination [2] [18].

1.3.1 NaOCl and EDTA: Mechanisms of Action

Assessing the efficacy of an endodontic treatment requires consideration of several parameters related to the chemical properties of the substances used during the procedural phases.

A clear example is the pronounced proteolytic and antimicrobial activity exhibited by NaOCl, a potent oxidizing and chlorinating agent capable of degrading proteins through amino acid chlorination and oxidation [19], leading to fragmentation of peptide chains [28]. This may contribute to type I collagen denaturation and to a reduction in mechanical and adhesive properties.

However, its mechanism of action and reactivity are neither specific nor substrate selective, and it can therefore affect both peritubular and intertubular dentin [31].

These alterations are reflected in macroscopic changes in dentin properties, including reduced tensile strength and flexural modulus, loss of elasticity, and increased brittleness [18] [27].
In addition to its direct oxidative action, NaOCl may also promote the activation of endogenous proteolytic enzymes notably MMPs and cathepsins [3]. The activation of these enzymes can further exacerbate collagen degradation [31].

EDTA is a polyaminocarboxylic chelating agent with a strong affinity for divalent metal ions such as Ca^{2+}, Mg^{2+}, and Zn^{2+}. When applied to mineralized tissues, it removes calcium ions from the hydroxyapatite ($Ca_10(PO_4)_6(OH)_2$) matrix, inducing a superficial demineralization of dentin [28].

Figure 1.2: Schematic representation of elements involved in irrigation protocols ***(A)*** *Extracted tooth selected for treatment;* ***(B)*** *Sodium hypochlorite (NaOCl) solution for the dissolution of the organic component;* ***(C)*** *Ethylenediaminetetraacetic acid (EDTA) solution for smear layer removal [3] and superficial demineralization.*

Its primary clinical function is the removal of the smear layer and the opening of dentinal tubules [30], thereby enhancing both canal disinfection and sealer penetration. However, excessive EDTA exposure may result in erosion of peritubular dentin [3], exposure and collapse of collagen fibrils, and increased surface roughness and porosity [6], potentially interfering with uniform adhesive infiltration [26].

When NaOCl and EDTA are present simultaneously, their interaction cannot be considered purely additive. In a combined chemical environment, residual

collagen may remain insufficiently protected and undergo oxidative degradation. At the same time, EDTA can enhance mineral loss by chelating calcium ions from the hydroxyapatite phase, thereby weakening the mineral support of the collagen matrix [13].

The concentration and exposure time of the combined irrigant solution are critical parameters to control to minimize iatrogenic damage and maintain dentin integrity [26] [28] .

1.3.2 Combined Effects and Potential Structural Damage

The combined use of NaOCl and EDTA on dentin can affect both its chemistry and microstructure, leading to cumulative and potentially deleterious alterations (as anticipated in Section 1.3.1).

Individually, NaOCl degrades the organic matrix through collagen oxidation, while EDTA demineralizes the inorganic phase by chelating calcium ions from hydroxyapatite; when used in combination, these agents may affect both major dentin components in a synergistic and depth dependent manner [5] [20]. However, this strategy can result in:

- Collagen matrix destabilization [4] [6],
- Mineral scaffold depletion [4] [6] ,
- Loss of tubular integrity [4] [6].

Experimental findings indicate that this combination increases surface roughness, reduces microhardness, and alters elastic modulus values in a time dependent manner [5] [32]. In deep dentin, where tubule density and water content are higher, the penetration of both chemical agents is facilitated, thereby intensifying the extent of tissue degradation [12] [20].

1.4 Dentin Adhesion: Formation and Stability of the Adhesive Interface

The long-term success of adhesive restorations after endodontic treatment depends on the stability of the dentin adhesive interface. Compared with enamel, dentin presents greater challenges due to its intrinsic moisture and structural heterogeneity [14].

Dentin consists of a hydrated collagen matrix reinforced by hydroxyapatite crystals and crossed by dentinal tubules. This composition requires adhesion strategies that ensure effective resin infiltration [33] into the demineralized collagen network and stable micromechanical interlocking [5] [28] .

The interfacial region formed during bonding is inherently vulnerable. Its durability is influenced by water sorption and nanoleakage [7], incomplete resin penetration, and enzymatic degradation of exposed collagen fibrils [5]. Residual moisture or inadequate solvent evaporation may further impair polymerization [34], leading to structural defects within the adhesive interface [26].

Over time, these factors contribute to interfacial degradation, reducing bond strength and increasing the risk of adhesive failure and secondary caries [13]. This instability is further amplified when dentin has been chemically modified by endodontic irrigants, as discussed in Section 1.3. Loss of mineral content and disruption of collagen integrity following exposure to irrigants further compromise the formation and durability of the bonded interface. For this reason, understanding the interaction between dentin composition, pre treatment procedures, and adhesive strategy is essential to improve clinical outcomes and enhance the longevity of post endodontic restorations [8].

1.4.1 Chemical vulnerability of exposed collagen

Type I collagen represents the main organic component of dentin and plays a key role in maintaining its structural integrity, which is essential for the formation of a stable resin dentin adhesive interface [8].

Following exposure to endodontic irrigants, collagen fibrils may become partially or completely exposed due to demineralization [33], increasing their susceptibility to degradation processes and potentially compromising the long term durability of adhesive bonding.

The enzymes (MMPs, cathepsins) are naturally present in dentin in latent forms and can be activated by acidic environments or oxidative stress [3]. Once activated, they are able to cleave collagen fibrils at multiple sites [16].

The use of sodium hypochlorite (NaOCl) and ethylenediaminetetraacetic acid (EDTA) represents an additional chemical factor contributing to collagen matrix destabilization during endodontic procedures [2]. NaOCl acts as a strong oxidizing and deproteinizing agent, directly targeting the collagen triple helix through peptide bond cleavage and the release of amino acid residues, thereby compromising collagen structural integrity. Raman spectroscopy studies have reported a reduction in amide I and III band intensities, indicative of collagen fragmentation and increased molecular disorder [5] [19].

In contrast, EDTA primarily affects the inorganic component of dentin through calcium chelation. Nevertheless, prolonged exposure to EDTA also induces secondary modifications in collagen organization and hydration, leading to increased fibrillar porosity and swelling [18] [35] . These changes facilitate the penetration of degrading agents and reduce the mechanical resilience of the collagen matrix [5] [6].

These changes can be effectively detected by Raman spectroscopy, which enables selective monitoring of vibrational modes associated with collagen and the mineral phase [36]. In the present study, specific Raman bands were selected to discriminate between alterations affecting the organic matrix and those involving the mineral scaffold of dentin.

These spectroscopic indicators formed the basis of the analytical approach adopted in this study and were evaluated across all experimental groups (A and B) to quantify the chemical effects of endodontic irrigation protocols, in

the presence or absence of an adhesive protective layer.

1.5 Limitations of conventional analytical techniques

Accurate characterization of chemical and structural modifications in dentin induced by endodontic irrigation remains methodologically challenging. Although several analytical techniques are routinely employed in dental research, many of them are limited when non-destructive, localized, and molecular-level information is required to assess chemically induced changes in dentin [9] [11]

Microscopy-based techniques, including SEM, TEM, and CLSM, [25] have been extensively used to investigate dentin surfaces and adhesive interfaces, providing valuable morphological information on surface topography, hybrid layer formation, and resin tag penetration [16] [37].

However, these techniques lack intrinsic chemical specificity and do not allow direct molecularlevel assessment of phenomena such as collagen denaturation, mineral dissolution, or chemical bond disruption induced by irrigation protocols or aging processes [37].

Similarly, analytical methods commonly coupled with electron microscopy, such as energy dispersive X-ray spectroscopy (EDS) [31], provide elemental information (Ca/P ratios) [15] [20] but are unable to resolve organic–inorganic interactions within the dentin matrix or detect molecular alterations affecting collagen integrity [3] [37]. In addition, the extensive sample preparation required for SEM and TEM including dehydration, embedding, sectioning, and metallization may introduce preparation induced artifacts, altering tissue hydration and collagen organization in this highly hydrated composite material [9] [16] .

Bulk analytical techniques, such as Fourier transform infrared spectroscopy

(FTIR) and X-ray diffraction (XRD) [38], have also been applied to investigate dentin composition and mineral crystallinity following endodontic treatments [11] [39]. While these approaches provide useful chemical and structural information, they are inherently limited by low spatial resolution and are unable to discriminate depth dependent modifications within dentin [3]. This limitation is particularly relevant in studies analyzing dentin at different cavity depths, where bulk measurements cannot distinguish superficial alterations from changes occurring in deeper regions [40].

Given that dentin integrity depends on the close interplay between its collagen matrix and hydroxyapatite nanocrystals, analytical methods selectively targeting only one phase fail to capture the coupled degradation processes induced by irrigants such as sodium hypochlorite and EDTA [6]. Furthermore, the destructive nature and limited repeatability of many conventional techniques restrict their applicability in longitudinal investigations [13] and in the evaluation of preventive strategies, such as adhesive application prior to chemical challenge [24] [37]

For these reasons, Raman microspectroscopy was selected in the present study as a non destructive and chemically specific technique, enabling localized, label free molecular characterization of both the organic and inorganic components of dentin while preserving tissue integrity [15] [41]. Its micrometric spatial resolution makes it particularly suitable for investigating depth dependent chemical modifications and for evaluating the protective role of adhesive pre treatment against irrigation induced damage.

1.6 Raman spectroscopy for Dental Applications

Raman spectroscopy is a vibrational spectroscopic technique [36] based on inelastic light scattering [20], allowing localized chemical analysis with micrometric spatial resolution.
Due to its ability to probe the vibrational modes associated with both organic and inorganic bonds without compromising the integrity of the sample, Raman spectroscopy has found increasing application in biomedical research and

in the characterization of dental tissues and materials [15].

In restorative dentistry and endodontics, it is particularly valuable for the investigation of dentin structure (collagenic component and hydroxyapatite), resin dentin interface integrity [8], and chemical modifications induced by irrigation and adhesive protocols allowing evaluation of substrate alterations and chemically induced modifications over time [42].

1.6.1 Principles and Spectroscopic Targets

When incident photons interact with molecular vibrational modes, an energy shift occurs as a consequence of changes in bond polarizability.

The resulting spectrum consists of distinct peaks whose position and intensity are characteristic of specific chemical bonds and molecular structures, effectively providing a molecular fingerprint of the material under investigation.

In dental research, the interest of this technique relies on the possibility to examine both the mineral (phosphate groups ($\nu_1\,PO_4^{3-}$)) and collagen-rich organic matrix (band CH_2) components of dentin at the same time. This dual sensitivity makes it possible to monitor variations in mineral content, changes in crystallinity, alterations in collagen integrity [10], and modifications in mineral matrix interactions that may occur following demineralization, chemical exposure, or adhesive infiltration [25].

Shifts in peak intensity, changes in band ratios, and modifications of spectral profiles provide valuable information about processes such as demineralization, deproteinization, and collagen degradation [10]. Beyond qualitative interpretation, Raman analysis allows quantitative assessment through parameters related to mineral–matrix balance, crystallinity, and collagen structural organization.

Another important advantage of Raman spectroscopy is the possibility of directly comparing different experimental conditions [34]. Quantitative evaluation of exposed dentin versus adhesive covered dentin makes it possible to

estimate the protective effect of adhesive layers against chemically induced degradation [43].

In this way, spectroscopic findings complement morphological observations, enabling an integrated interpretation of microstructural observations and molecular level chemical information at the dentin adhesive interface.

1.7 Aim of the Study

The aim of the present study is to investigate, using Raman spectroscopy technology, the chemical alterations induced by endodontic irrigation protocols on human dentin, with particular focus on their impact on the dentin adhesive interface.
Specifically, the experimental study seeks to distinguish and quantify the alterations produced by two commonly used irrigants (NaOCl and EDTA), on both the mineral and organic components of dentin, including processes related to demineralization, collagen degradation, and changes in Raman spectral features.

A further objective is to evaluate the potential protective role of a universal adhesive system applied to dentin prior to chemical challenge. By comparing dentin specimens with and without adhesive coverage, the study assesses whether the presence of an adhesive layer reduces the extent of chemically induced degradation.

Finally, depth dependent effects are investigated by comparing cavities prepared at 2 mm and 4 mm, in order to examine how dentinal microstructure and proximity to the pulp influence chemical reactivity and substrate vulnerability.
Overall, it can be concluded that this in vitrohis in vitro approach integrates Raman spectroscopic analysis with controlled experimental conditions to support the interpretation of substrate alterations relevant to subsequent adhesive bonding procedures.

Chapter 2

Materials and Methods

2.1 Study Design and Experimental Workflow

This experimental study was designed to evaluate the chemical effects of defined endodontic irrigation protocols on human dentin specimens, with or without prior adhesive application.

Extracted human teeth free of caries, cracks, restorations, or structural defects were selected for this study. All the samples were visually inspected and clinically evaluated by an experienced dentist to confirm their suitability. After extraction, residual soft tissues were carefully removed, and the teeth were thoroughly cleaned. Samples were stored in distilled water at room temperature until testing in order to prevent dehydration and preserve dentin properties.

A cavity was performed on the mesial surface of the tooth using a conical bur to a depth of 2 mm from the coronal margin. The 2 mm depth was measured from the lowest and most mesial point achievable, using the occlusal plane as the reference.

Specimens were divided into two main experimental groups:

- Group A (Unsealed Dentin): no adhesive application prior to irrigation,
- Group B (Adhesive Protected Dentin): adhesive applied before irrigation.

Each condition was further assigned to one of four irrigation protocols: semr

- G1: NaOCl for 30 minutes,

- G2: NaOCl + EDTA for 30 minutes,
- G3: NaOCl for 60 minutes,
- G4: NaOCl + EDTA for 60 minutes.

Raman measurements were conducted on all samples at two defined analytical timepoints:

- T0 (pre-treatment): spectra acquired before irrigation, immediately afeter cavity preparation (Group A) or after adhesive curing (Group B),
- T1 (post-treatment): spectra aqcuired after the irrigation procedure assigned to each specific subgroup

Spectroscopic analysis by Raman, focusing on peaks related to:

- Inorganic phase,
- Organic phase.

(a) 4 mm deep dental cavity preparation

(b) 2 mm deep dental cavity preparation

(c) Occlusal view of both cavity preparations performed on a tooth specimen without the application of dental adhesive pretreatment

Figure 2.1: Cavity preparation at two depths and occlusal view of the specimen.

The experimental setup enabled comparison between irrigated and non-irrigated specimens, evaluation of adhesive-protected versus unsealed dentin, and assessment of depth-related differences.

2.2 Sample Selection and Preparation

Twenty extracted human molars were included, selected trying to exclude those with caries, restorations, fractures, or visible structural defects.

Standardized cavity preparations were performed on both mesial and distal surfaces of each tooth using cylindrical and truncated conical diamond burs (830L) under water cooling (Table 2.1) and with high speed.

All preparations were carried out following the same protocol to ensure consistency across specimens.

Material / Instrument	**Specification / Brand**
Teeth	Human upper and lower molars (6^{th}, 7^{th}, and 8^{th})
Bur for access cavity	Cylindrical diamond bur 880
Burs for cavity preparation	Truncated conical diamond bur 830L
Adhesive	Universal adhesive (3M Scotchbond)
Irrigants	5% sodium hypochlorite, 10% EDTA
Storage solutions	Distilled water
Etchant	37% phosphoric acid

Table 2.1: Materials and instruments used in the experimental protocol.

Specifically, the mesial cavity was prepared to a depth of 2 mm from the occlusal reference plane, while the distal cavity was prepared to a depth of 4 mm.

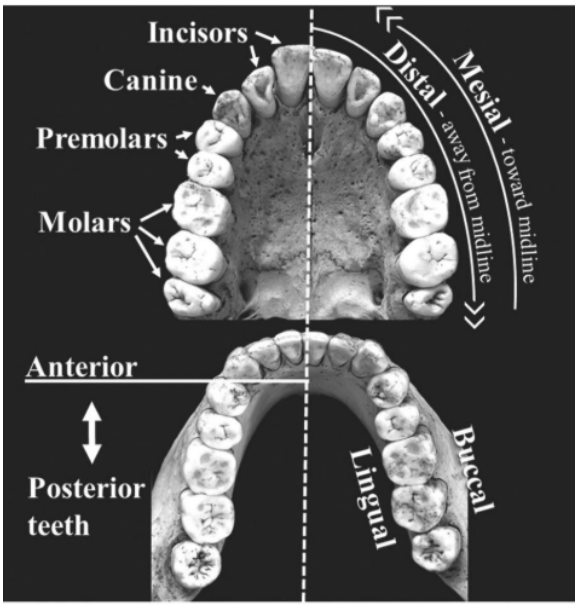

Figure 2.2: General terminology used to identify upper and lower teeth [22]

The adhesive system, for group B samples, was applied using a disposable microbrush applicator (Microbrush Plus, regular 2.0 mm, Young Innovations, Algonquin, USA) (Figure 2.3).

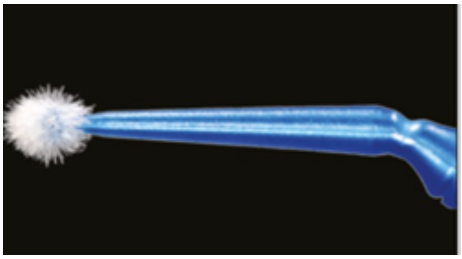

Figure 2.3: Photograph of the disposable microbrush applicator (Microbrush Plus, regular 2.0 mm, blue, Young Innovations, Algonquin, USA), which was used for the application of the adhesive system [23].

The adhesive procedure began with selective etching using a 37% phosphoric acid gel, applied for 30 seconds on enamel and 15 seconds on dentin. The surfaces were then thoroughly rinsed with water for 20–30 seconds and gently air dried, maintaining controlled moisture to prevent collapse of the collagen network.

A universal adhesive system (3M™ Scotchbond™ Universal Plus [32], showed in Fig. 2.4) was subsequently applied to the prepared substrate. The material was actively distributed using a disposable microbrush applicator, followed by a calibrated air stream to promote solvent evaporation and obtain a uniform adhesive layer [34].

Figure 2.4: Adhesive bottle (pre photopolymerization) applied to half of the dental samples in order to perform a comparative analysis between type A and type B samples.

Component	Function
HEMA [38], DEGDMA, 10-MDP [22]	Functional monomers; bonding to dentin and hydroxyapatite
γ-MPTES, APTES	Silane agents; promote bonding to ceramic and filler surfaces
Camphorquinone	Photoinitiator for polymerization
Ethanol, water	Solvent system; aids monomer penetration
Amorphous silica (fumed, crystalline-free)	Nanofillers; mechanical reinforcement
Acetic acid copper(2+) salt, monohydrate	Potential antimicrobial and stabilizing role
N,N-dimethylbenzocaine	Stabilizer; trace component

Table 2.2: Chemical composition and functional role of the universal adhesive system.

Photopolymerization was carried out for 15 seconds using a multi LED curing unit (Valo LED Cordless, Ultradent) with a constant light output of 1200 mW/cm^2. This protocol ensured the formation of a standardized adhesive interface prior to exposure to the endodontic irrigation procedures.

Figure 2.5: Valo LED Cordless, Ultradent used for photo-polimerization

For Group B specimens, Scotchbond Universal Plus Adhesive (3M ESPE, USA) was used (2.2).

The bonding protocol followed these standardized steps:

1. Rinse with air–water syringe,
2. Etching with 37% phosphoric acid: 15 s on dentin and 30 s on enamel,
3. Thorough water rinsing (20–30 s),
4. Gentle air-drying,
5. Application of adhesive using a microbrush,

6. Air-thinning to evaporate solvent,
7. Light curing for 20 s using an LED curing unit.

The adhesive was selected for its chemical affinity to dentin and its ability to form a stable hybrid layer. Its formulation includes functional monomers (such as 10-MDP [44]), nanofillers, solvents, and photoinitiators designed to promote durable adhesion and mechanical integration [44].

This system allows effective chemical interaction with both the mineral and organic phases of dentin and enamel, contributing to stabilization of the interface even under chemically challenging conditions, such as exposure to irrigating solutions.

2.3 Irrigation Protocols

Specimens were subjected to standardized irrigation procedures using NaOCl and EDTA and by static immersion at room temperature.
Two different exposure times were tested: 30 minutes and 60 minutes.
The following experimental conditions were applied to both Group A (exposed dentin), composed of forty specimens and Group B (adhesive protected dentin), composed of the same number of samples:

- NaOCl for 30 minutes,
- NaOCl + EDTA for 30 minutes,
- NaOCl for 60 minutes,
- NaOCl + EDTA for 60 minutes.

For the combined protocol, NaOCl and EDTA were used simultaneously in the same solution.
For Raman analysis, five measurement points were recorded per cavity. Sample identification codes were structured as follows: S indicated the measurement point (1–5), G identified the irrigation protocol, and PA or PB indicated the absence or presence of adhesive, respectively.

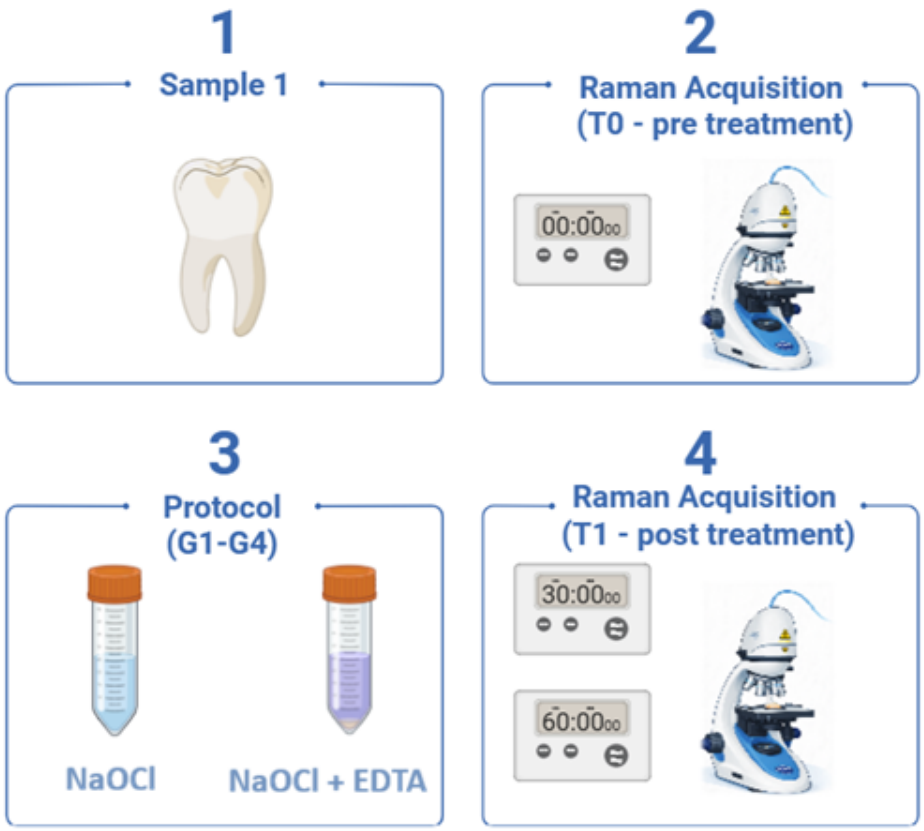

Figure 2.6: Schematic workflow of the experimental protocol. (1) Sample preparation. (2) Baseline Raman acquisition (T0, pre-treatment). (3) Chemical irrigation protocols (G1–G4: NaOCl and NaOCl+EDTA). (4) Post-treatment Raman acquisition (T1) at 30 and 60 minutes.

2.3.1 Sodium Hypochlorite (NaOCl) Treatment

Sodium hypochlorite was used in this study for its antimicrobial activity and ability to dissolve organic tissue [4]. In this specific study, the irrigant was applied at a concentration of 5%, consistent with commonly adopted clinical protocols,in order to evaluate chemically induced alterations in dentin, with and without adhesive protection.

The NaOCl solution was used at room temperature (around 22-25 °C) and freshly prepared for each subsequent treatment to maintain chemical stability and integrity over experimental procedure. Each specimen was fully immersed in the solution for two different time intervals, selected with the intent to simulate, as far as possible, standard clinical irrigation and extended exposure

scenarios:

- 30 minutes: simulating a typical endodontic irrigation duration (Group G1);
- 60 minutes: simulating prolonged or cumulative chemical stress conditions (Group G3).

Following the specific protocol samples were thoroughly rinsed with distilled water for approximately 60 seconds under gentle manual agitation. This step was essential to remove any residual irrigant and continued chemical activity. Furthermore, samples were subsequently stored in distilled water until Raman spectroscopic analysis, in order to preserve their structural and chemical integrity.

2.3.2 NaOCl and EDTA Treatment

NaOCl and EDTA act on the organic and inorganic components of dentin through oxidative and chelating mechanisms, respectively [4] [5] .
When used in combination within the same solution, their chemical action can be complementary and significantly alter dentin composition and structure.

The irrigants used in combination, depending on the specific protocol selected, were applied to the samples for a total exposure time of either 30 or 60 minutes. As with the previous single irrigant treatment, once the irrigation was complete, the samples were thoroughly rinsed with distilled water for 60 seconds under gentle manual agitation to remove any chemical residues and prevent further undesired reactions.
The combined chemical exposure provides a dual action on dentin, affecting both the organic and inorganic phases:

- NaOCl degrades the organic matrix, particularly collagen fibrils, through oxidative mechanisms [3],
- EDTA chelates calcium ions, inducing dissolution of the mineral phase and exposure of the organic matrix [3].

Particular attention was given to the adhesive protected groups (Group B), to assess whether the hybrid layer formed prior to irrigation could mitigate

the depth and severity of chemical degradation. This hypothesis was explored through Raman spectroscopic analysis targeting both mineral and organic vibrational bands, as well as comparative evaluation of pre and post irrigation spectroscopic profiles.

This experimental design allowed evaluation of the protective effect of adhesive pre treatment against combined chemical exposure.

2.4 Raman Spectroscopy Measurements

Raman spectroscopic analyses were performed to investigate compositional and structural modifications of dentin following the different irrigation protocols.

The technique was employed to assess changes in the mineral phase, collagen matrix organization, and mineral organic balance at the dentin surface and adhesive interface.

All measurements were conducted under standardized acquisition conditions to ensure reproducibility across experimental groups.

2.4.1 Instrumentation and acquisition parameters

Raman spectra were acquired using a portable modular spectrometer (BWTEK, Newark, DE, USA) equipped with a 1064 nm monochromatic laser source and a BTC284N spectrometer.

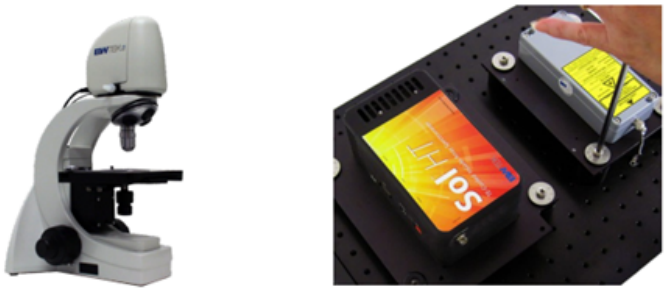

Figure 2.7: Portable modular Raman spectrometer (BWTEK) equipped with a BTC284N detector and a 1064 nm laser source, coupled with the BAC151 compact microscope used for sample observation and laser focusing.

The system operates within a spectral range of 100–2500 cm^{-1}, with a spectral resolution of 10 cm^{-1}.

The spectrometer was coupled to a compact optical microscope (BAC151, BWTEK), allowing direct visualization of the analyzed region and precise focusing of the laser beam on the dentin surface.
Spectra were collected in microscopic configuration with the laser beam oriented perpendicular to the specimen surface.

Before each analytical session, instrument calibration was performed according to the manufacturer's recommendations. Sample positioning was standardized to minimize variability related to surface topography and focusing conditions.

2.4.2 Raman spectral parameters analysed

Spectral analysis was focused on Raman bands associated with hydroxyapatite and collagen components of dentin.
From the acquired spectra, peak intensities, band areas, and full width at half maximum (FWHM) values were extracted to derive compositional and structural indices.

Table 2.3: Characteristic Raman bands selected for the assessment of mineral and organic components of dentin and their corresponding structural significance.

Raman band (cm^{-1})	**Vibrational assignment**	**Dentin component**	**Structural / chemical significance**
∼960	ν_1 PO_4^{3-} symmetric stretching	Mineral phase (hydroxyapatite)	Marker of mineral content and crystallinity; variations indicate demineralization [21] and lattice disorder
∼1070	CO_3^{2-} stretching vibration	Mineral phase (carbonate-substituted apatite)	Indicator of carbonate substitution and mineral lattice stability
∼1250	Amide III (C–N stretching, N–H bending)	Organic matrix (collagen)	Sensitive to collagen secondary structure; intensity reduction suggests chain disruption or unfolding
∼1450	CH_2 deformation	Organic matrix (collagen)	Reflects organization and density of the collagen backbone
∼1650	Amide I (C=O stretching of peptide bonds)	Organic matrix (collagen)	Highly sensitive to collagen triple-helix integrity; shifts or intensity loss indicate structural disorganization or denaturation

The spectral parameters considered, along with the corresponding derived indices and their interpretation, are summarized in Table 2.4.
The Raman intensity and area ratios used for the evaluation of mineral and collagen related properties, as supported by the literature, are reported in Table 2.4.

Table 2.4: Raman spectral parameters and derived indices used for the assessment of mineral and organic components of dentin.

Spectral parameter	**Index**	**Interpretation**
Mineral / Matrix	A_{960}/A_{1660}	Relative amount of the mineral component with respect to the organic matrix
Crystallinity	$1/\mathrm{FWHM}_{960}$	Degree of structural order within hydroxyapatite mineral crystals
Carbonate / Phosphate	I_{1070}/I_{960}	Extent of carbonate incorporation in the hydroxyapatite lattice
Phosphates	I_{960}	Mineral component associated with hydroxyapatite
CH_2 groups	I_{1450}	Structural organization and relative amount of collagen
Amide I	I_{1655}	
Amide III	I_{1246}	
Amide I / Amide III	I_{1655}/I_{1246}	Collagen molecular organization
Amide III / CH_2	I_{1246}/I_{1450}	Differences in collagen structure and quality
Amide I / CH_2	I_{1655}/I_{1450}	

Quantitative outcomes derived from these indices are presented in the Section 3.

2.5 Data Processing and Statistical Analysis

Raman spectra were initially pre processed using BWSpec software (BWTEK, USA) prior to export.
During acquisition, dark current subtraction was applied in order to reduce the noise mainly caused by the instrumental setup itself.
The spectra were then exported in .txtr format and further processed using a custom analysis workflow developed in the Python programming language.

In the first processing step, the exported spectra were restricted to the range 800–1800 cm^{-1} spectral range, corresponding to the main Raman bands of interest for dentin characterization.
Baseline correction was performed in Python using the Asymmetric Least Squares (ALS) algorithm, according to the method described by Eilers and Boelens, with fixed parameters applied to all spectra.

This procedure was adopted to correct background contributions while preserving the shape and relative intensity of the Raman bands.

The baseline-corrected spectra were subsequently smoothed using a Savitzky–Golay filter in order to reduce high-frequency noise without altering peak morphology. The resulting baseline-removed spectra were saved as plain text files (.txt) and used for subsequent spectral analysis.

Peak parameters were extracted through a spectral fitting procedure implemented in Python.
Each spectrum was modeled as the sum of multiple Lorentzian components corresponding to predefined characteristic Raman bands associated with the mineral and organic components of dentin. A non linear least squares minimization approach was used to optimize the fitting parameters. For each fitted band, peak position, peak height, full width at half maximum (FWHM), and integrated band area were obtained from the fitted profiles.

Derived compositional and structural indices were calculated from the extracted numerical parameters.
These included mineral related parameters (phosphate band intensity and area at 960 cm^{-1} , carbonate to phosphate ratio, and crystallinity expressed as 1/FWHM of the 960 cm^{-1} band [45]) , collagen related indices, and the mineral to matrix ratio.
Ratio calculations and graphical data representation were performed using spreadsheet based data analysis (Microsoft Excel).

Chapter 3

Results

3.1 Representative Raman Spectra Before and After Irrigation

This section is dedicated to representative Raman spectra acquired illustrating the main spectral features observed across the experimental groups following the various acquisitions. That leads directly to the aim of proving a qualitative overview of the dentin chemical profile by illustrating the main spectral variations between pre treatment (T0) and post treatment (T1) conditions.

For each experimental group, five different specimens (S1—S5) were analyzed by Raman spectroscopy at two standardized depths (2 mm and 4 mm), with five measurement points per cavity in order to minimize potential local variations and increase the statistical robustness, thereby improving the reliability of measurements.
It was therefore decided to select some spectra that could illustrate some characteristic behaviors observed among the various working groups, always considering a variability factor in the quantitative analysis.

Figure 3.1, for example, reports a typical Raman spectrum acquired at T0 condition, from a sample (PA) belonging to Group (G2) at a depth of 2 mm. The representation range for each spectrum was chosen within the 800–1800 cm^{-1} region in order to best appreciate the typical vibrational profile of dentin before irrigation.

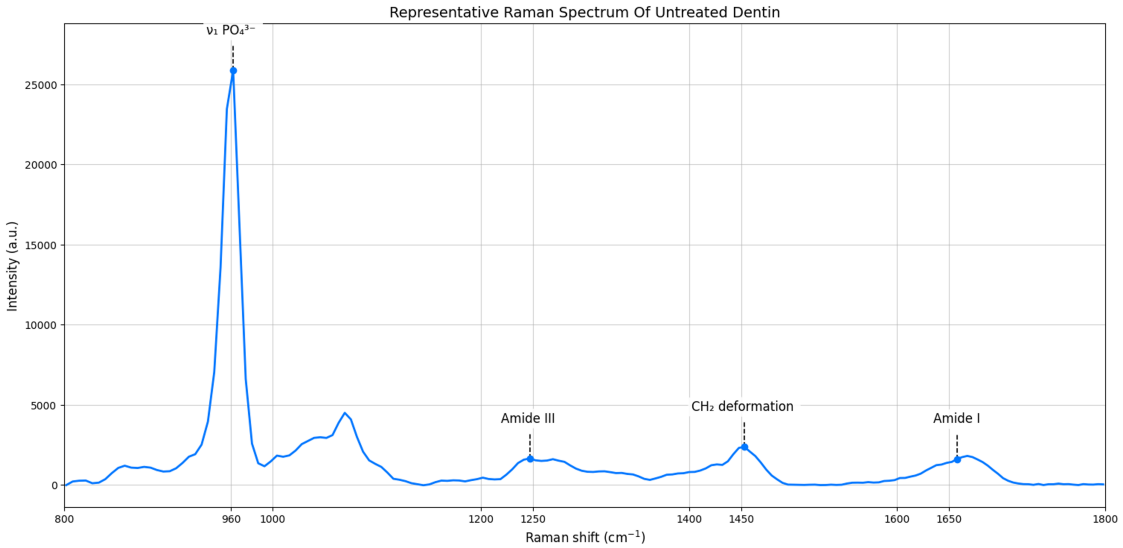

Figure 3.1: The spectrum highlights the main dentin-related bands, including the $\nu_1\,\mathrm{PO}_4^{3-}$ *symmetric stretching mode at* $\sim 960\ \mathrm{cm}^{-1}$*, the Amide III region (*$\sim$ 1240–1270 cm^{-1}*), the* CH_2 *bending mode (*$\sim 1450\ \mathrm{cm}^{-1}$*), and the Amide I band (*$\sim 1660\ \mathrm{cm}^{-1}$*).*

The characteristic peaks that concern the main dentinal components are therefore highlighted.

Having clarified this aspect, it is of interest for this study to note, instead, a typical trend after irrigation treatment as in the case in the following Figure 3.2. Indeed, it shows a reduction in overall band intensity after irrigation, particularly in the phosphate region (localized around 960 cm^{-1}) and in the collagen related bands. The spectrum, however, remains overall consistent, in terms of trend, with that of the initial dentin.

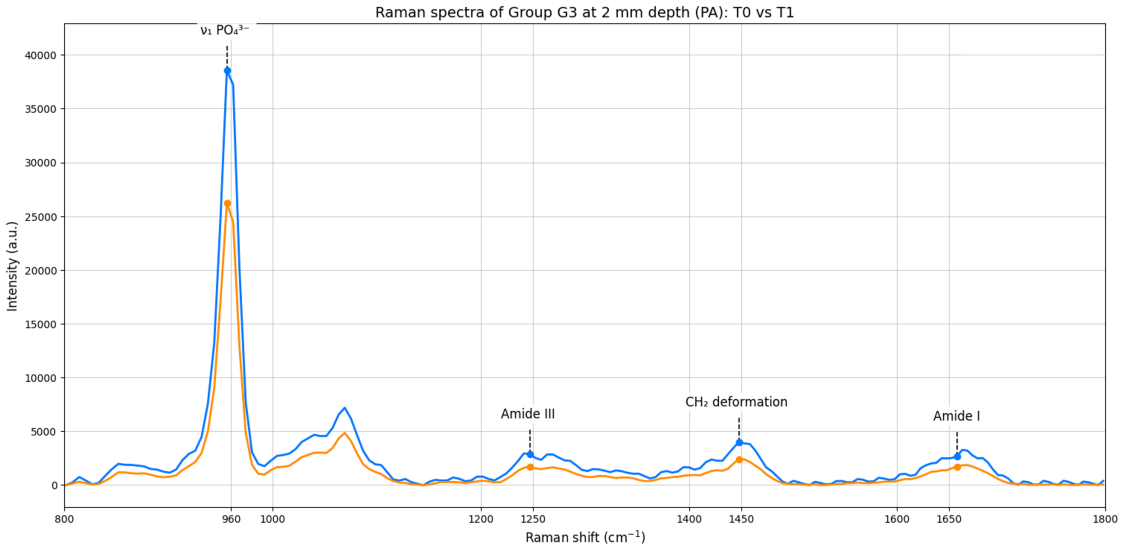

Figure 3.2: Representative Raman spectra of dentin recorded from Group G3 at 2 mm depth (PA condition) before (T0, blue line) and after (T1, orange line) irrigation with NaOCl for 60 minutes. Spectra allow direct comparison of mineral and collagen-related bands.

Finally, to complete the analysis of spectral trends, a trend at a depth of 4 mm was also reported so that the issue of treatment response dependent on scanning depth was addressed for the same protocol. The trend is overall comparable, although the differences between T0 and T1 appear less pronounced than those detected at 2 mm.

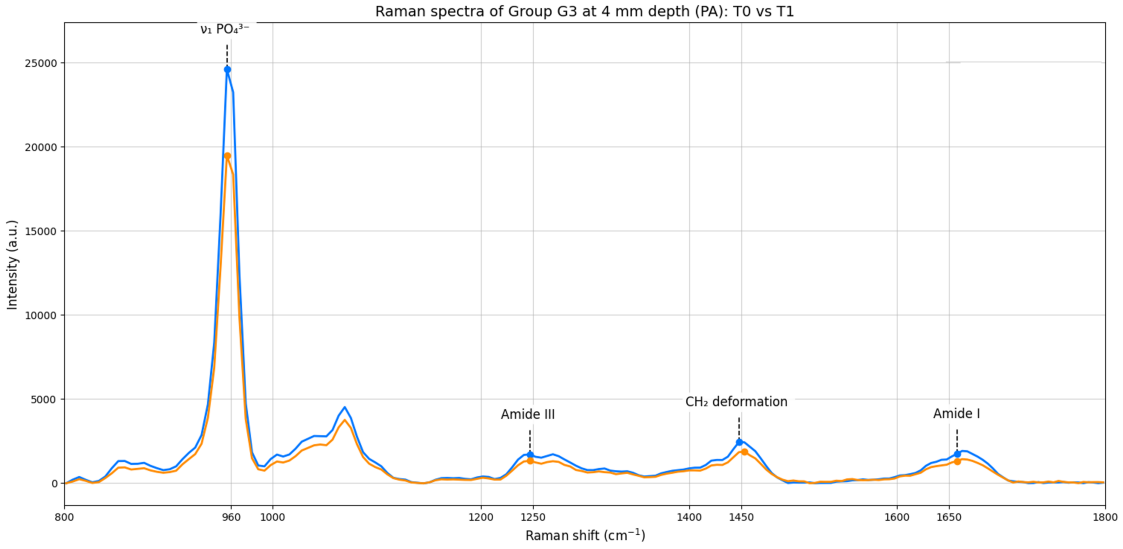

Figure 3.3: Representative Raman spectra of dentin recorded from Group G3 at 4 mm depth (PA condition) before irrigation (T0, blue line) and after irrigation (T1, orange line).

Looking at the trends, it is therefore possible to assert that the phosphate

band shows a moderate reduction after treatment, while the Amide and CH_2 regions maintain a similar spectral profile with only slight intensity variations and no evident peak shifts or new spectral features are observed.

3.2 Assessment of Chemical Modifications

For each specimen, peak intensities and selected band ratios were calculated at both investigated depths (2 mm and 4 mm) for comprehensive analysis and in-depth comparisons.

Furthermore, for each of the parameters chosen for the study, the data distribution is reported using box plots as an illustrative method, to show how the measurement distributions could vary with each experimental condition.
In order to make the following graphic representation understandable, it should be underlined the following information.
In each plot, the box represents the interquartile range encompassing the central 50% of the dataset between the 25th and 75th percentiles.

Within the box, the horizontal line indicates the median value, while the 'x' marker represents the arithmetic mean.
The whiskers extend to the minimum and maximum measured values, providing a comprehensive visualization of data dispersion and variability across the different experimental conditions. Points displayed beyond the whiskers correspond to outliers.

3.2.1 Changes in Collagen-related Raman parameters

To evaluate modifications affecting the organic component of dentin, collagen related Raman indices (reported in Tab. 3.1) were analyzed across all experimental groups and depths.

Table 3.1: Raman intensity ratios used to assess collagen related alterations and their corresponding spectral bands.

Raman ratio	**Characteristic Raman bands (cm^{-1})**	**Spectral significance**
Amide I / CH_2	(∼1650) / (∼1450)	Relative indicator of collagen integrity normalized to the organic backbone.
Amide III / CH_2	(∼1250) / (∼1450)	Sensitive to changes in collagen secondary structure and molecular organization.
Amide I / Amide III	(∼1650) / (∼1250)	Internal collagen ratio reflecting conformational and structural modifications.

Below, therefore, are synthetic and explanatory observations of the main significant parameters or ratios following the processing of the measures.

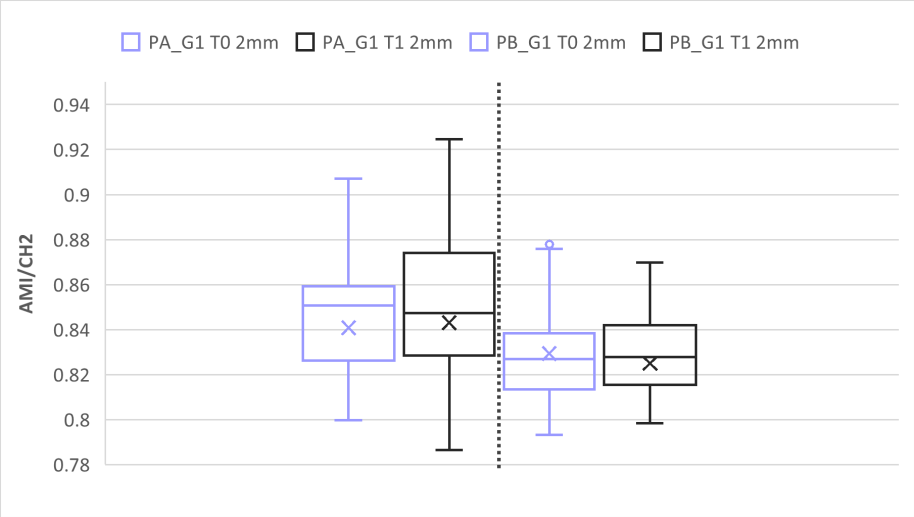

Figure 3.4: Boxplot of the Amide I/CH_2 intensity ratio for Group 1. Group A (without adhesive) on the left side of dashed line and Group B (with adhesive) on the right side. Lilac boxes represent measurements acquired before irrigation (T0), while black boxes correspond to Raman measurements performed after the irrigation protocol (T1) collected at 2 mm depth.

At 2 mm, the Amide I/CH_2 ratio showed limited differences between T0 and T1 in both PA and PB samples, and this is evident in the finding that the median values remained largely comparable over time.

In PA, the post treatment condition showed a slightly broader distribution, reflected in a slightly greater box height, more specifically, a wider interquartile

range and more extended whiskers, indicating a modest increase in dispersion. In PB, the distribution appeared stable, with no substantial change in central tendency or variability.

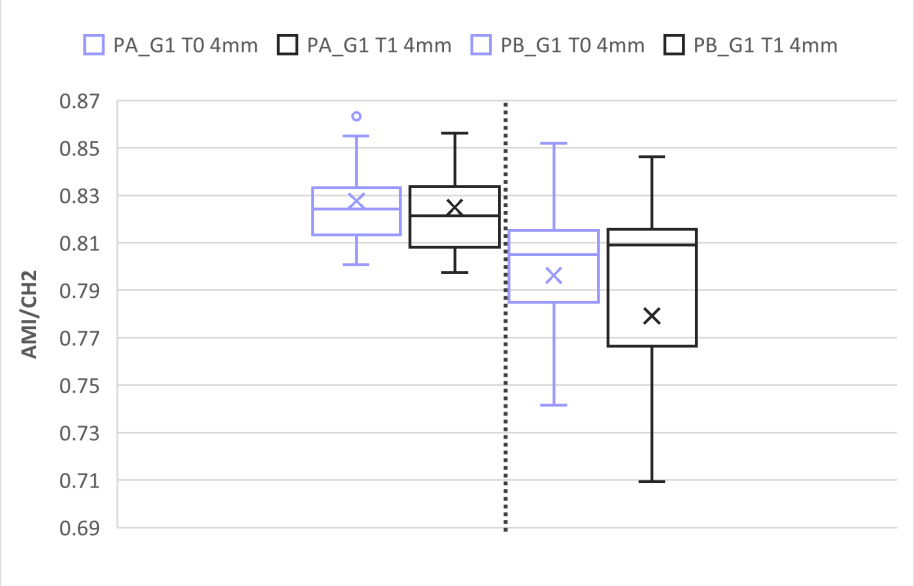

Figure 3.5: Boxplot of the Amide I/CH_2 intensity ratio for Group 1. Group A (without adhesive) on the left side of the dashed line and Group B (with adhesive) on the right side. Lilac boxes represent measurements acquired before irrigation (T0), while black boxes correspond to Raman measurements performed after the irrigation protocol (T1) collected at 4 mm depth.

At 4 mm, the first of the analyzed ratios showed no substantial differences between T0 and T1 for samples with pure dentin, and it is evident that median values remained comparable, and therefore settled around the same range of calculated values, so that the overall distribution appeared stable.

In PB, T1 condition exhibited a much broader distribution, with a wider interquartile range and higher whiskers. Median values were slightly higher compared to T0 (which is noticeable with a slight raising of the horizontal line), suggesting a modest shift accompanied by increased dispersion.

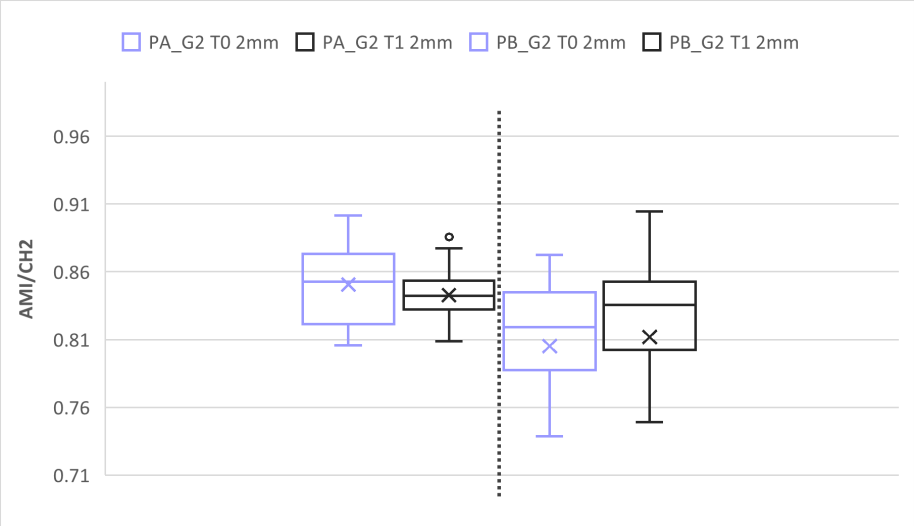

Figure 3.6: Boxplot of the Amide I/CH_2 intensity ratio for Group 2. Group A (without adhesive) on the left side of the dashed line and Group B (with adhesive) on the right side. Lilac boxes represent measurements acquired before irrigation (T0), while black boxes correspond to Raman measurements performed after the irrigation protocol (T1) collected at 2 mm depth.

Focusing now on the second working group, at 2 mm, the Amide I/CH_2 ratio, in PA showed minimal differences between T0 and T1, in terms of mean and median values, although these were more evident in the case of the pure dentin samples.

Indeed, the distribution of values, remained largely comparable, without evident shift over time.

In PB, the trend shown in T1, displayed a slightly higher median and a broader distribution compared to T0, with a modest increase in interquartile range and more extended whiskers, indicating increased dispersion.

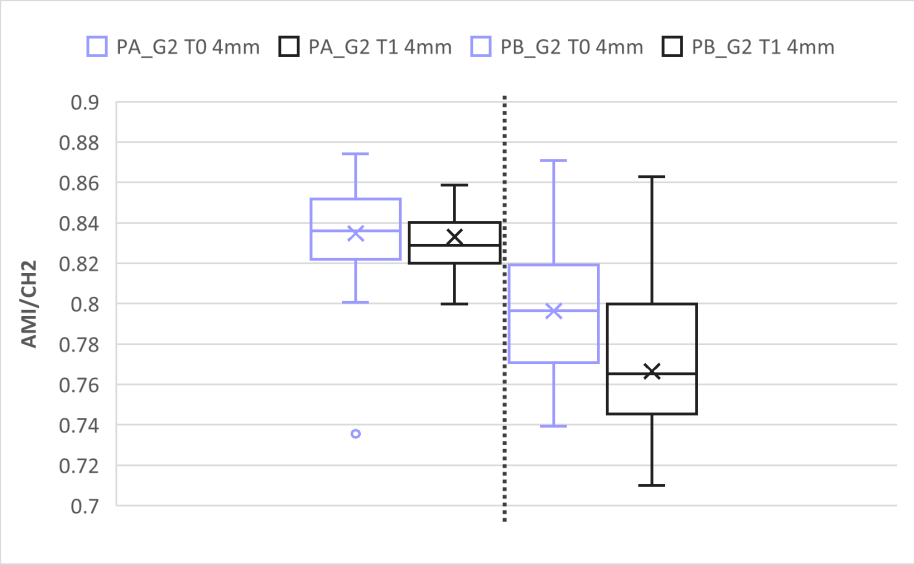

Figure 3.7: Boxplot of the Amide I/CH_2 intensity ratio for Group 2. Group A (without adhesive) on the left side of dashed line and Group B (with adhesive) on the right side. Lilac boxes represent measurements acquired before irrigation (T0), while black boxes correspond to Raman measurements performed after irrigation protocol (T1) collected at 4 mm depth.

Moving on to the analysis for the case at greater depth, the case on the left shows no substantial differences between pre e post treatment conditions, with comparable median values and a largely stable distribution.

In contrast, focusing on the right side, a significant reduction in median values can be seen at T1 compared to initial condition.

This sort of shift was accompanied by a broader interquartile range (viewable with a greater vertical width) and more extended lower whiskers, indicating increased dispersion and a tendency toward lower ratio values.

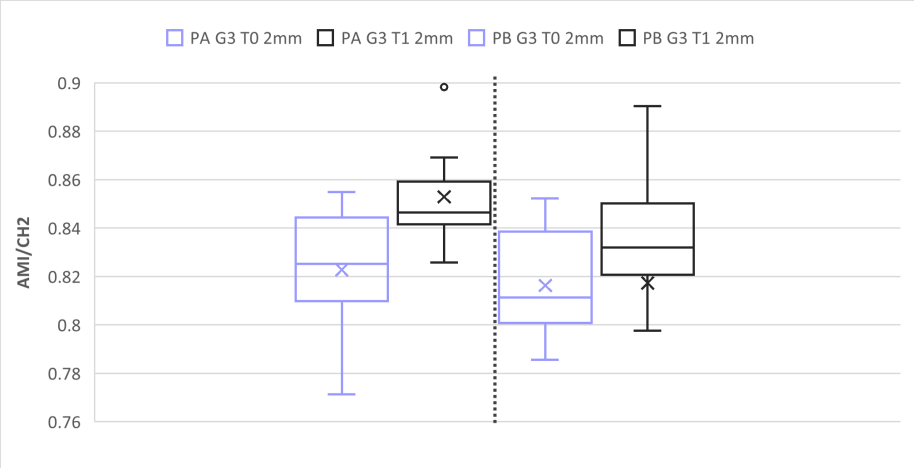

Figure 3.8: Boxplot of the Amide I/CH_2 intensity ratio for Group 3. Group A (without adhesive) on the left side of the dashed line and Group B (with adhesive) on the right side. Lilac boxes represent measurements acquired before irrigation (T0), while black boxes correspond to Raman measurements performed after irrigation protocol (T1) collected at 2 mm depth.

The penultimate working group shows how at 2 mm, in both conditions there is an increase in the Amide I/CH_2 ratio, with a significant upward shift for measurements acquired in the post treatment phases.
This is also accompanied by a trend of higher median and mean values.

The interquartile range appeared slightly more compact, indicating no increase in variability in the overall variability of the trend of measured values.

In PB, T1 exhibited a modest increase in median values compared to baseline and the overall dispersion remained comparable, although the upper whisker was slightly more extended at T1.

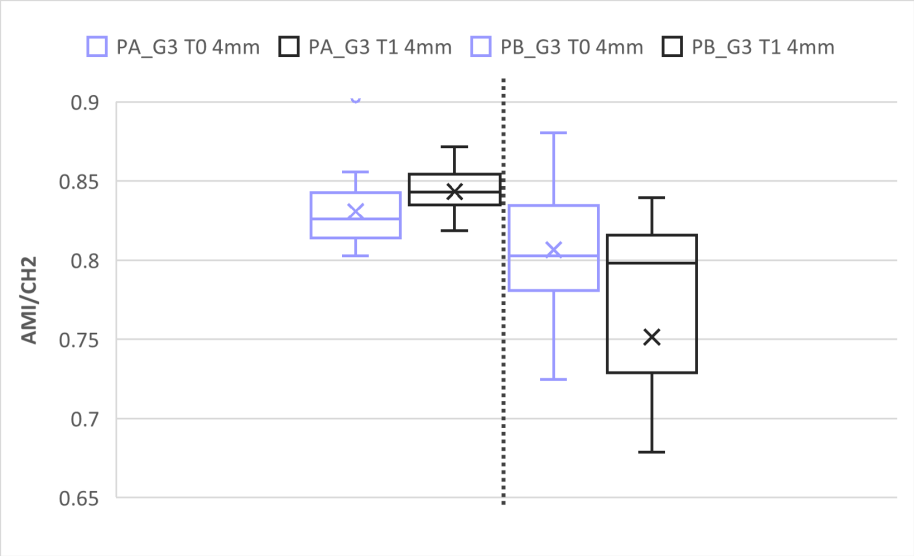

Figure 3.9: Boxplot of the Amide I/CH_2 intensity ratio for Group 3. Group A (without adhesive) on the left side of dashed line and Group B (with adhesive) on the right side. Lilac boxes represent measurements acquired before irrigation (T0), while black boxes correspond to Raman measurements performed after the irrigation protocol (T1) collected at 4 mm depth.

At 4 mm, in PA it is showed a slight increase in median and mean values at post treatment condition, compared to the values calculated in the pre-treatment phase, but overall the extent of the values obtained and the general variability remain unchanged.

In contrast, samples with dentin and adhesive exhibited a marked increase in dispersion at T1, which is characterized by a wider interquartile range and markedly extended lower whiskers.

A final observation that can be made is that although median values were broadly comparable, the distribution shifted toward lower values, so it reflects the reduced mean and greater asymmetry.

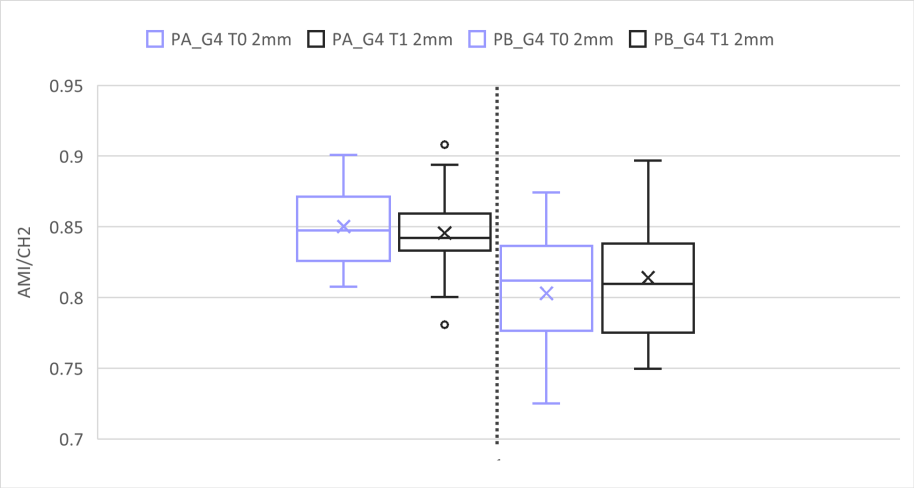

Figure 3.10: Boxplot of the Amide I/CH_2 intensity ratio for Group 4. Group A (without adhesive) on the left side of dashed line and Group B (with adhesive) on the right side. Lilac boxes represent measurements acquired before irrigation (T0), while black boxes correspond to Raman measurements performed after the irrigation protocol (T1) collected at 2 mm depth.

For the last working group it is reported that at 2 mm, the ratio showed minimal differences between T0 and T1 in both type samples and median values remained comparable over time.
In PB, T1 displayed a slightly higher median, while overall variability appeared largely unchanged.

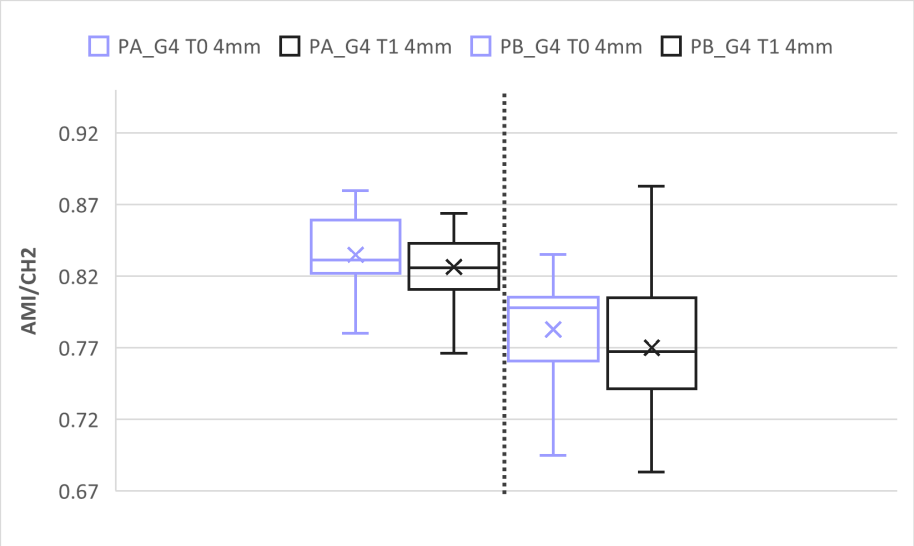

Figure 3.11: Boxplot of the Amide I/CH_2 intensity ratio for Group 4. Group A (without adhesive) on the left side of dashed line and Group B (with adhesive) on the right side. Lilac boxes represent measurements acquired before irrigation (T0), while black boxes correspond to Raman measurements performed after the irrigation protocol (T1) collected at 4 mm depth.

At 4 mm, the ratio in PA remained largely stable between T0 and T1, with comparable median values and no evident change in dispersion.

In PB, T1 state showed a slight reduction in median and mean values compared to T0, accompanied by a modest extension of the lower whisker, indicating a tendency toward lower ratio values.

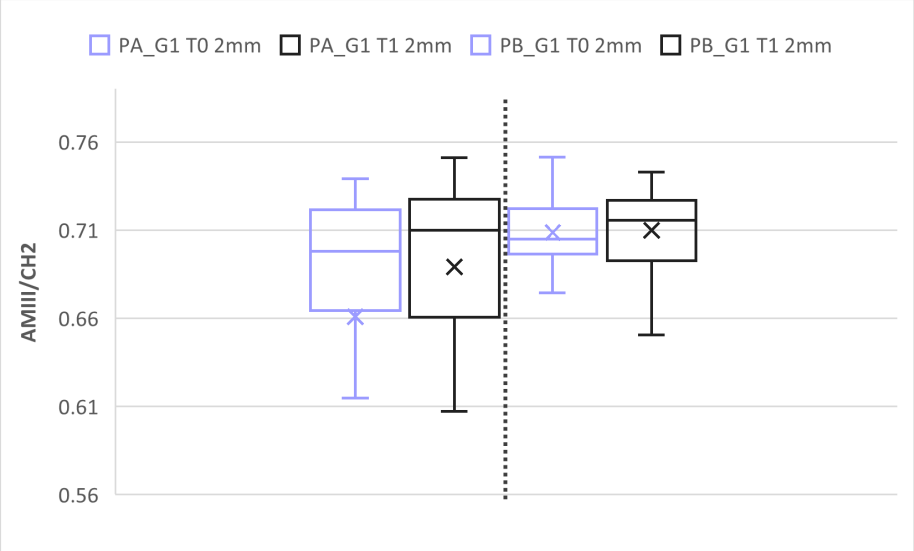

Figure 3.12: Boxplot of the Amide III/CH_2 intensity ratio for Group 1. Group A (without adhesive) on the left side of dashed line and Group B (with adhesive) on the right side. Lilac boxes represent measurements acquired before irrigation (T0), while black boxes correspond to Raman measurements performed after the irrigation protocol (T1) collected at 2 mm depth.

Continuing the analysis and considerations with a further significant ratio, namely Amide III/CH_2, which is sensitive to changes in the secondary structure and molecular organization of collagen, that allows to highlight, for the first working group, that at 2 mm and for the PA samples, a slight increase in the median and mean values was observed at T1, while the overall variability remained comparable.

In PB, median values and distribution patterns were largely unchanged between T0 and T1.

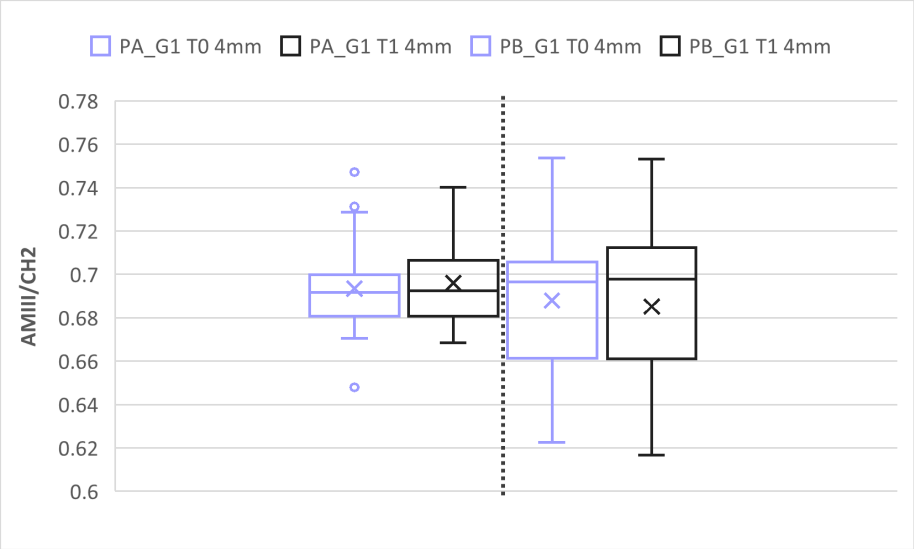

Figure 3.13: Boxplot of the Amide III/CH_2 intensity ratio for Group 1. Group A (without adhesive) on the left side of dashed line and Group B (with adhesive) on the right side. Lilac boxes represent measurements acquired before irrigation (T0), while black boxes correspond to Raman measurements performed after the irrigation protocol (T1) collected at 4 mm depth.

At 4 mm, the ratio remained stable over time for no adhesive condition, with comparable median values and no evident change in dispersion, while the adhesive and post treatment condition showed a slightly higher median along with broader distribution, more extended whiskers and increased variability.

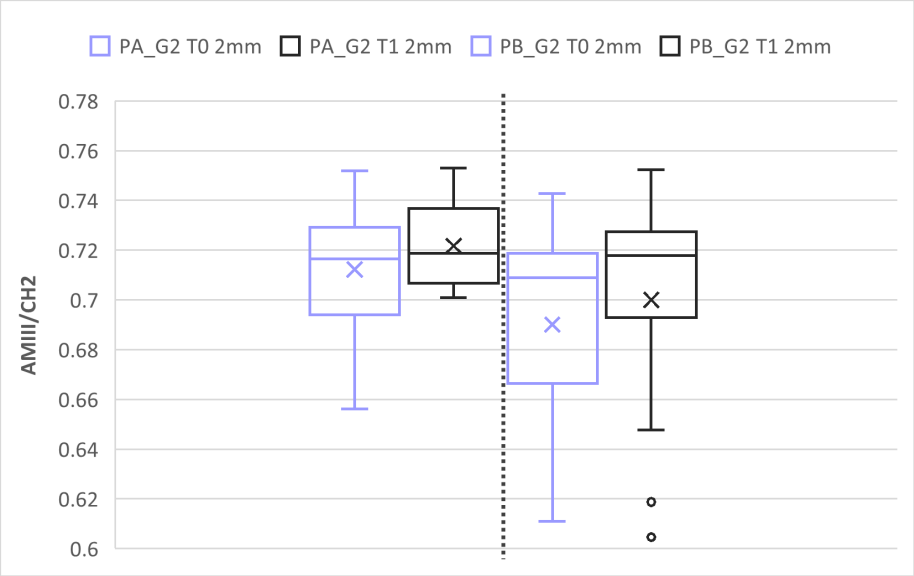

Figure 3.14: Boxplot of the Amide III/CH_2 intensity ratio for Group 2. Group A (without adhesive) on the left side of dashed line and Group B (with adhesive) on the right side. Lilac boxes represent measurements acquired before irrigation (T0), while black boxes correspond to Raman measurements performed after the irrigation protocol (T1) collected at 2 mm depth.

For the second group, at the 2 mm cavity, a trend similar to the previous one for the condition on the left is observed while in PB samples, T1 exhibited a modest rise in median values accompanied by a broader distribution, characterized by a wider interquartile range and extended lower whiskers.

Regarding the trends observed at the 4 mm depth, showed a general stability between T0 and T1 for PA, with comparable median values and no evident change in variability.

In PB, T1 showed a slight reduction in median and mean, accompanied by a modest extension of the lower whisker, indicating a tendency toward lower ratio values, as shown in the following figure.

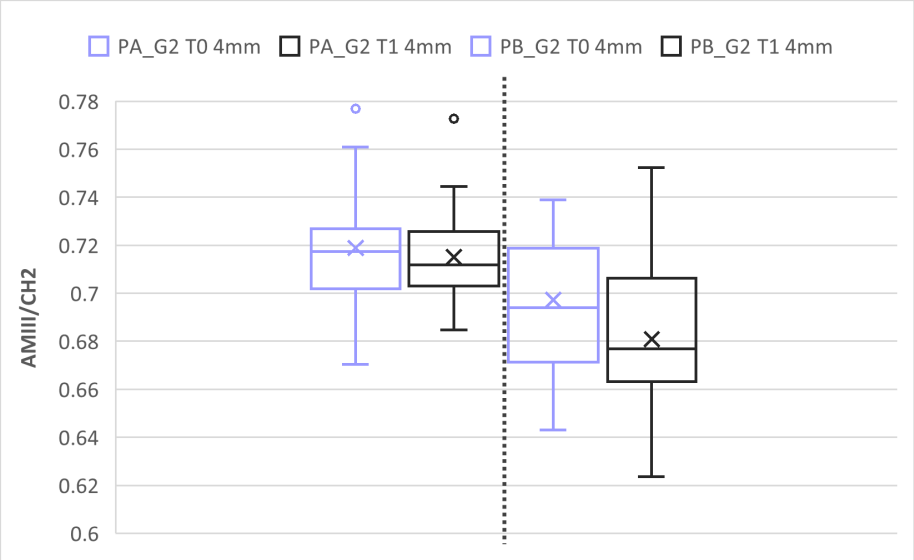

Figure 3.15: Boxplot of the Amide III/CH_2 intensity ratio for Group 2. Group A (without adhesive) on the left side of the dashed line and Group B (with adhesive) on the right side. Lilac boxes represent measurements acquired before irrigation (T0), while black boxes correspond to Raman measurements performed after the irrigation protocol (T1) collected at 4 mm depth.

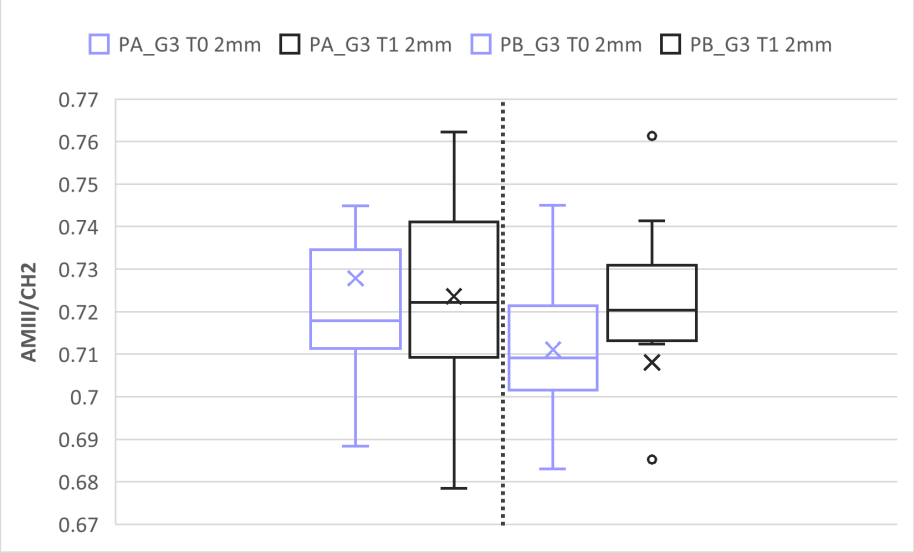

Figure 3.16: Boxplot of the Amide III/CH_2 intensity ratio for Group 3. Group A (without adhesive) on the left side of the dashed line and Group B (with adhesive) on the right side. Lilac boxes represent measurements acquired before irrigation (T0), while black boxes correspond to Raman measurements performed after the irrigation protocol (T1) collected at 2 mm depth.

Analyzing the G3, it was then noted that at 2 mm, the ratio showed a slight increase in median values at T1 for PA, accompanied by a modest widening of the interquartile range.

Focusing on the right side, the black boxes allow to observe an overall comparable variability, with a limited extension of the upper range.

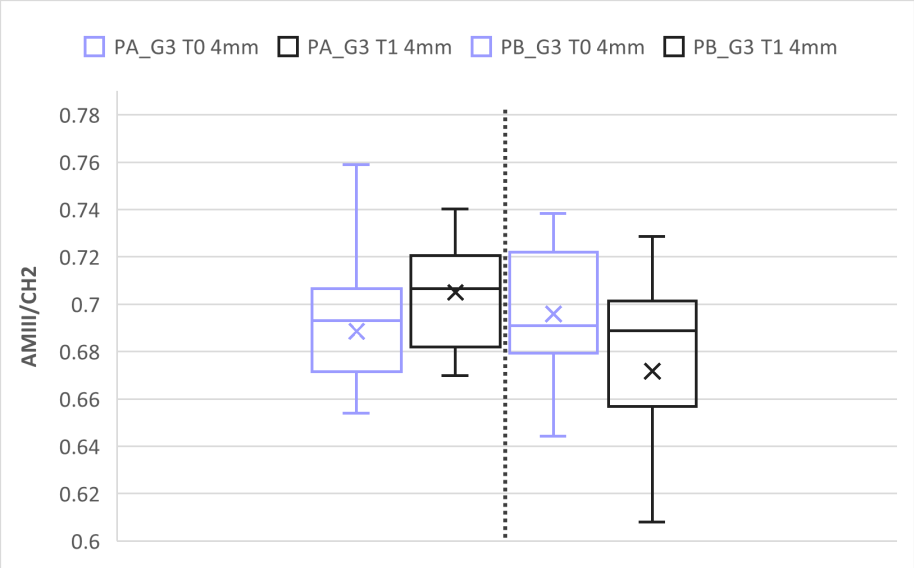

Figure 3.17: Boxplot of the Amide III/CH_2 intensity ratio for Group 3. Group A (without adhesive) on the left side of the dashed line and Group B (with adhesive) on the right side. Lilac boxes represent measurements acquired before irrigation (T0), while black boxes correspond to Raman measurements performed after the irrigation protocol (T1) collected at 4 mm depth.

Subsequently, shifting the observation of the data to the values measured at the deepest cavity allows us to highlight how the mean and median values follow opposite trends for the PA and PB cases, which in the latter case also translates into an extended lower whisker, indicating a greater dispersion toward lower ratio values.

There is therefore the focus on the last two box plots dedicated to the analysis of the second ratio reported in the 2.4, for observations regarding the changes linked to modifications of the collagen component.

For the lasting working group it can be seen that st 2 mm, PA remained largely unchanged between T0 and T1, with comparable median values and similar variability.

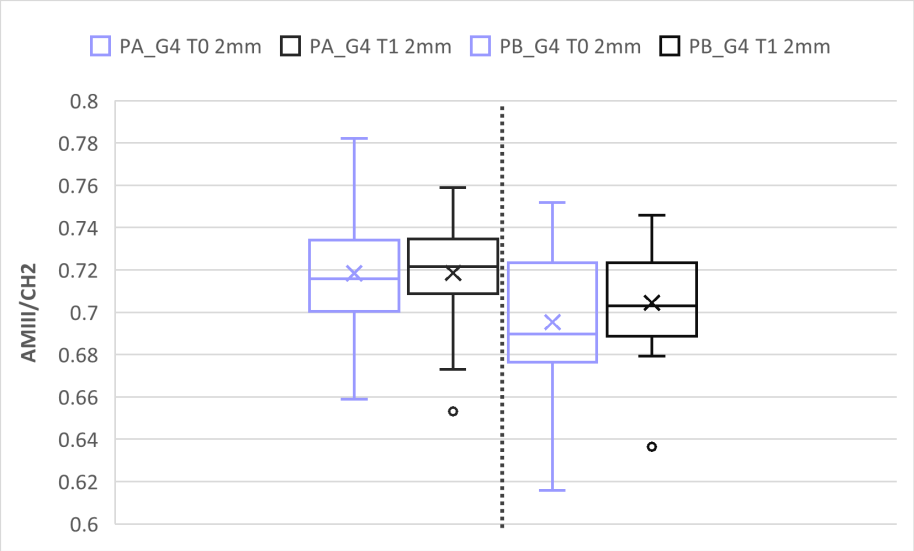

Figure 3.18: Boxplot of the Amide III/CH_2 intensity ratio for Group 4. Group A (without adhesive) on the left side of the dashed line and Group B (with adhesive) on the right side. Lilac boxes represent measurements acquired before irrigation (T0), while black boxes correspond to Raman measurements performed after the irrigation protocol (T1) collected at 2 mm depth.

Then in PB, T1 showed a slight increase in median and mean values, accompanied by a modest extension of the lower whisker, indicating mildly increased dispersion.

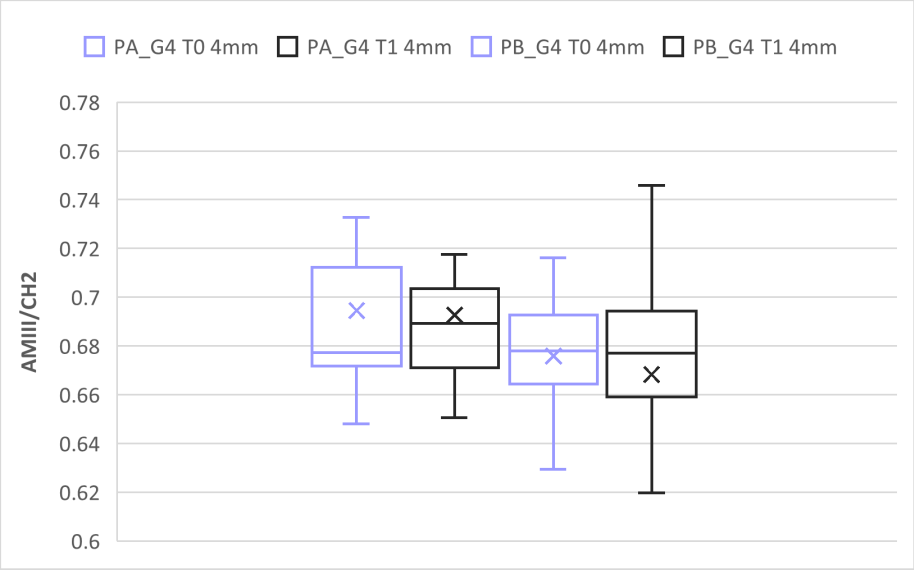

Figure 3.19: Boxplot of the Amide III/CH_2 intensity ratio for Group 1. Group A (without adhesive) on the left side of the dashed line and Group B (with adhesive) on the right side. Lilac boxes represent measurements acquired before irrigation (T0), while black boxes correspond to Raman measurements performed after the irrigation protocol (T1) collected at 4 mm depth.

At 4 mm Amide III/CH_2 ratio in PA showed comparable median values between T0 and T1, with no substantial change in variability. In PB, T1 was associated with a slight upper whisker, while overall dispersion remained broadly comparable.

The analysis then focused on the study of the parameter Amide I/Amide III ratio, to further characterize variations within the collagen related spectral components.

The rationale for this methodological choice is related to the evidence that this parameter allows a comparative assessment of the relative contribution of the two amide bands across experimental conditions, depths, and time points.

The distribution of mean values for each group is presented below.

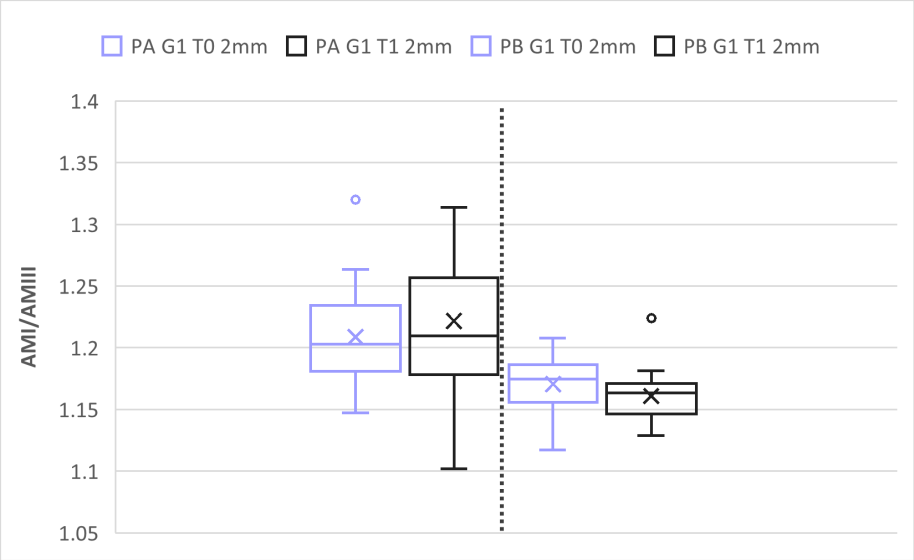

Figure 3.20: Boxplot of the Amide I/Amide III intensity ratio for Group 1. Group A (without adhesive) on the left side of the dashed line and Group B (with adhesive) on the right side. Lilac boxes represent measurements acquired before irrigation (T0), while black boxes correspond to Raman measurements performed after the irrigation protocol (T1) collected at 2 mm depth.

The first case shows that at 2 mm, there is an increase in statistical parameters, at T1, accompanied by a modest widening of the distribution. Differently, in PB, median values remained comparable over time, with no substantial change in variability.

At 4 mm, values in PA remained largely stable between the two moments of acquisition, with slight decrease in median and mean values. Furthermore, these values decrease slightly in the PB samples, accompanied by a broader distribution and more extended whiskers, indicating increased variability.

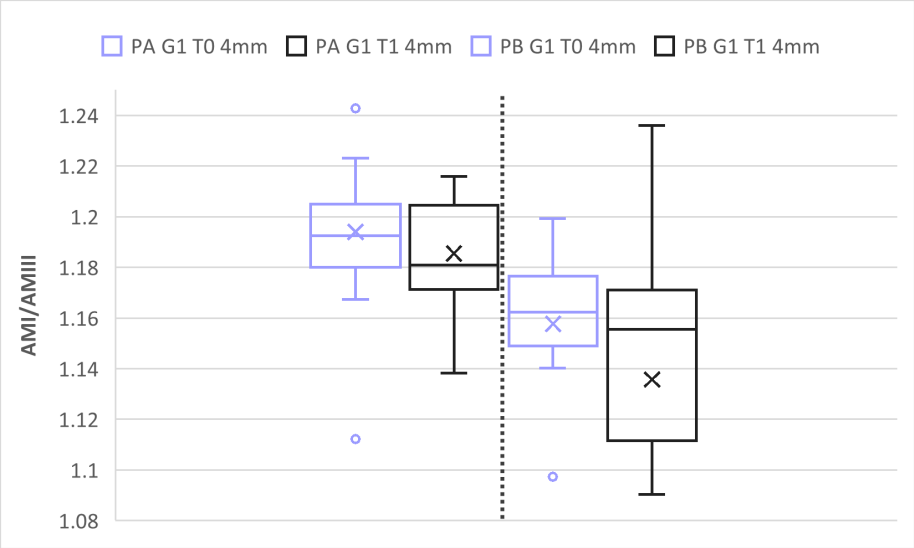

Figure 3.21: Boxplot of the Amide I/Amide III intensity ratio for Group 1. Group A (without adhesive) on the left side of the dashed line and Group B (with adhesive) on the right side. Lilac boxes represent measurements acquired before irrigation (T0), while black boxes correspond to Raman measurements performed after the irrigation protocol (T1) collected at 4 mm depth.

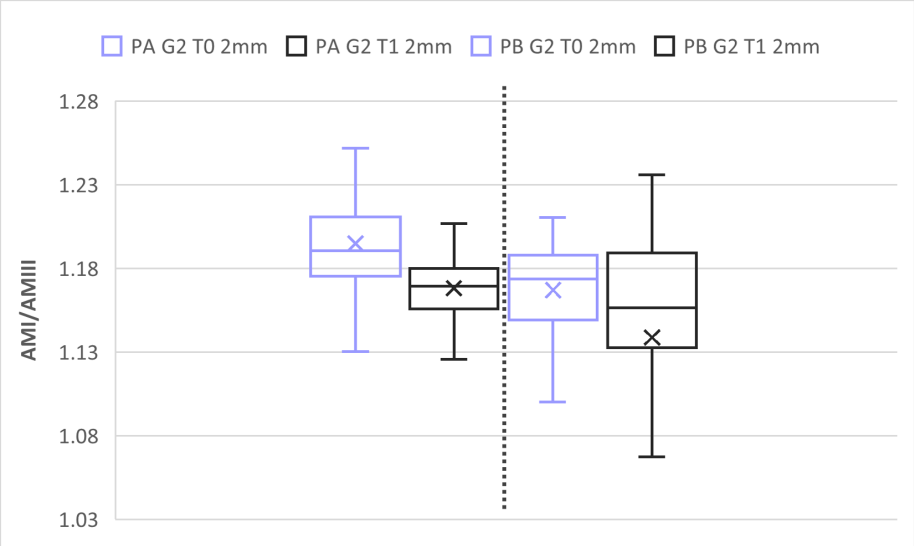

Figure 3.22: Boxplot of the Amide I/Amide III intensity ratio for Group 2. Group A (without adhesive) on the left side of the dashed line and Group B (with adhesive) on the right side. Lilac boxes represent measurements acquired before irrigation (T0), while black boxes correspond to Raman measurements performed after the irrigation protocol (T1) collected at 2 mm depth.

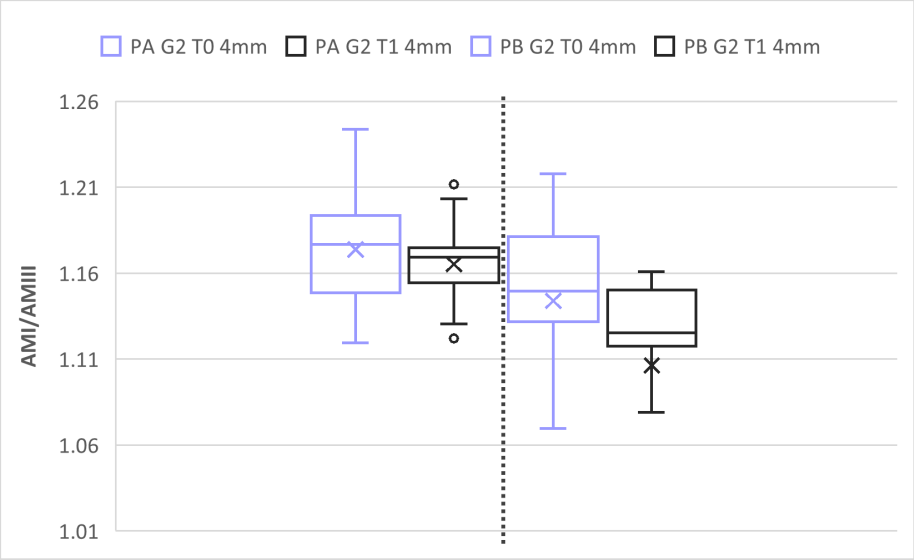

Figure 3.23: Boxplot of the Amide I/Amide III intensity ratio for Group 2. Group A (without adhesive) on the left side of the dashed line and Group B (with adhesive) on the right side. Lilac boxes represent measurements acquired before irrigation (T0), while black boxes correspond to Raman measurements performed after the irrigation protocol (T1) collected at 4 mm depth.

Analyzing the PA samples for G2, it was noted that that for both cavities there is a slight decrease in the median and mean values at T1 compared to T0, with comparable overall variability.

For the PBs, however, it was observed that at 2 mm and for post treatment condition, slightly lower central values are associated with a modest broadening of the distribution, with an extension toward lower ratio values but with a more compact distribution compared to the baseline for the 4 mm cavity.

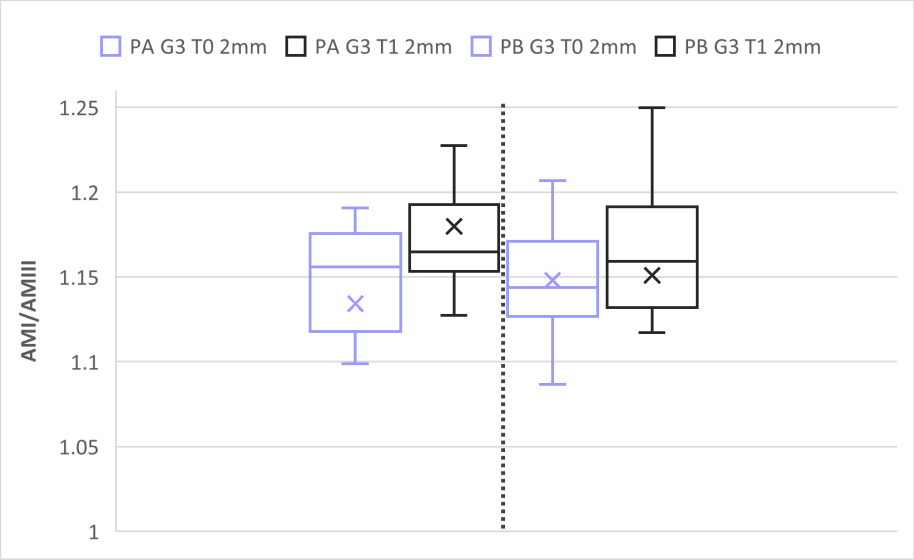

Figure 3.24: Boxplot of the Amide I/Amide III intensity ratio for Group 3. Group A (without adhesive) on the left side of the dashed line and Group B (with adhesive) on the right side. Lilac boxes represent measurements acquired before irrigation (T0), while black boxes correspond to Raman measurements performed after the irrigation protocol (T1) collected at 2 mm depth.

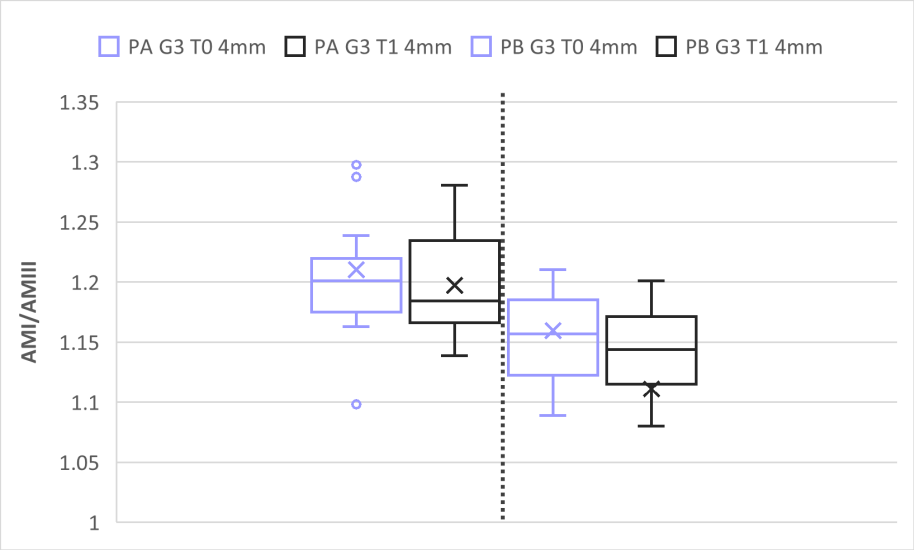

Figure 3.25: Boxplot of the Amide I/Amide III intensity ratio for Group 3. Group A (without adhesive) on the left side of the dashed line and Group B (with adhesive) on the right side. Lilac boxes represent measurements acquired before irrigation (T0), while black boxes correspond to Raman measurements performed after the irrigation protocol (T1) collected at 4 mm depth.

For Group 3 is possible to highlight that at 2 mm, the ratio in PA increased at T1, with higher median and mean values and a modest widening of the distribution. In PB, T1 was also associated with higher central values and a

slight extension of the upper range. Then, focusing on the cavity at 4 mm, ratio in PA showed a slight decrease in median and mean values at T1. In PB, T1 was associated with lower central values, while overall variability remained broadly comparable to baseline.

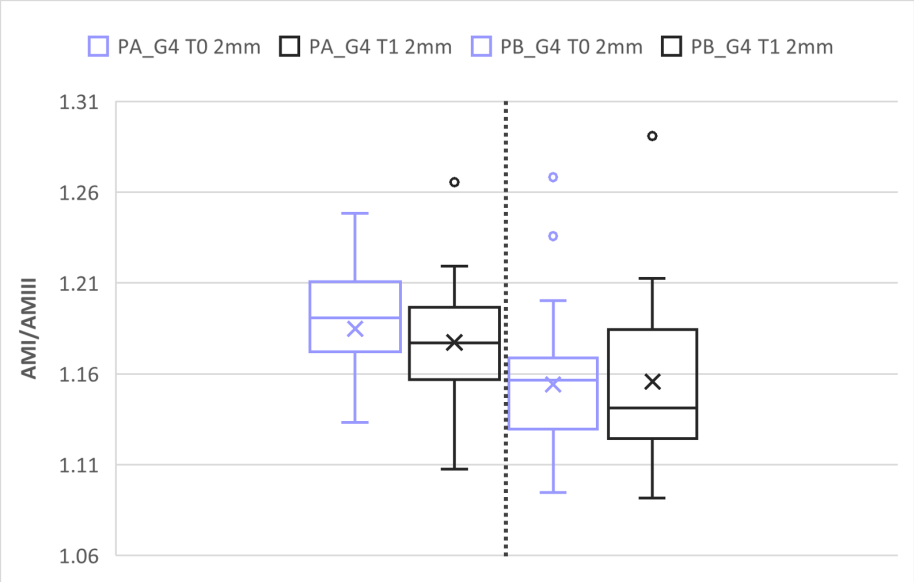

Figure 3.26: Boxplot of the Amide I/Amide III intensity ratio for Group 4. Group A (without adhesive) on the left side of the dashed line and Group B (with adhesive) on the right side. Lilac boxes represent measurements acquired before irrigation (T0), while black boxes correspond to Raman measurements performed after the irrigation protocol (T1) collected at 2 mm depth.

At 2 mm the Amide I/Amide III intensity ratio in PA showed a slight reduction in median and mean values at T1 compared to T0, while variability remained comparable. In PB, T1 was associated with lower central values and a distribution largely similar to baseline, with occasional higher outliers.

At 4 mm, the ratio in PA showed comparable median values between T0 and T1. In PB, T1 was associated with a modest reduction in median values, while overall variability remained largely unchanged.

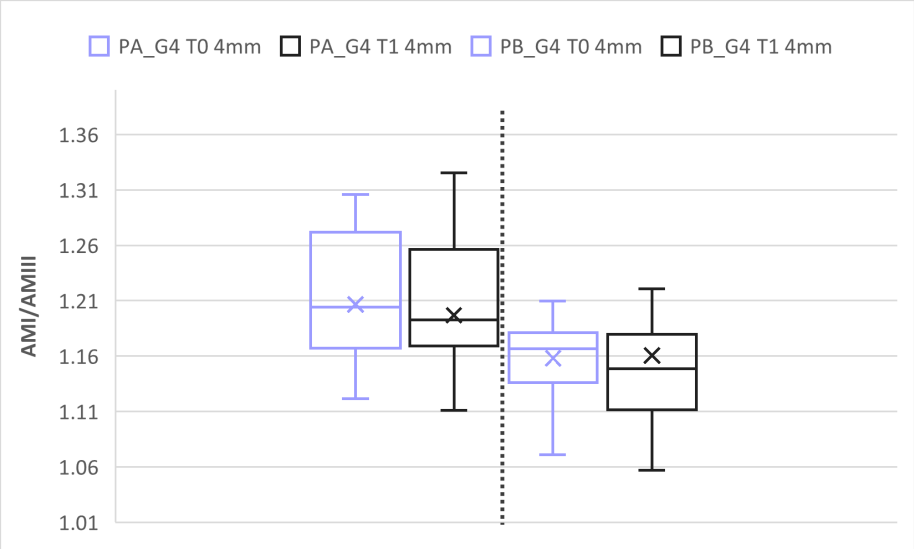

Figure 3.27: Boxplot of the Amide I/Amide III intensity ratio for Group 4. Group A (without adhesive) on the left side of dashed line and Group B (with adhesive) on the right side. Lilac boxes represent measurements acquired before irrigation (T0), while black boxes correspond to Raman measurements performed after the irrigation protocol (T1) collected at 4 mm depth.

3.2.2 Changes in Mineral-Related parameters

Mineral related modifications were assessed through analysis of the Raman peak intensity at 960 cm^{-1}, the crystallinity index, and the C/P ratio.

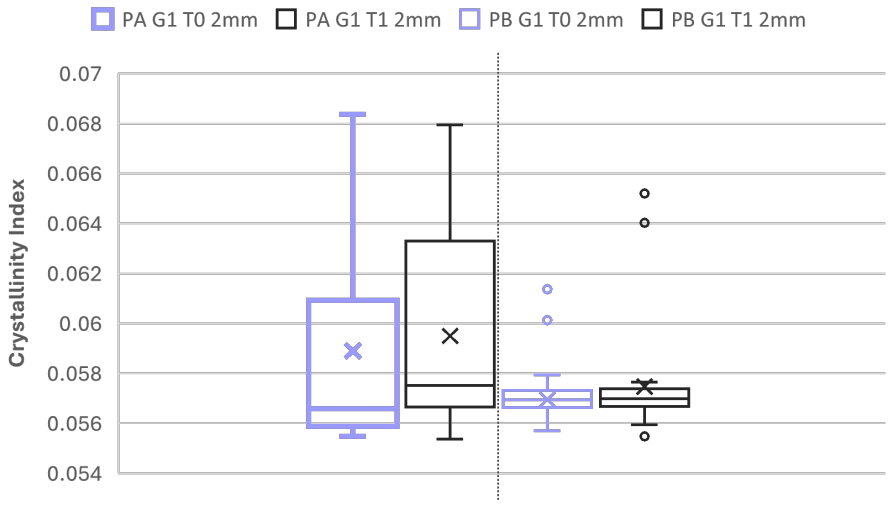

Figure 3.28: Boxplot of the Cristallinity Index for Group 1. Group A (without adhesive) on the left side of the dashed line and Group B (with adhesive) on the right side. Lilac boxes represent measurements acquired before irrigation (T0), while black boxes correspond to Raman measurements performed after the irrigation protocol (T1) collected at 2 mm depth.

For the first working group it can be observed that at 2 mm, in PA there was a slight increase in the statistical parameters for the post treatment condition. It is also accompanied by a broader interquartile range and extended whiskers. Different scenario was observed for PB samples as median values remained comparable over time, with similar central dispersion and the presence of occasional higher outliers at T1.

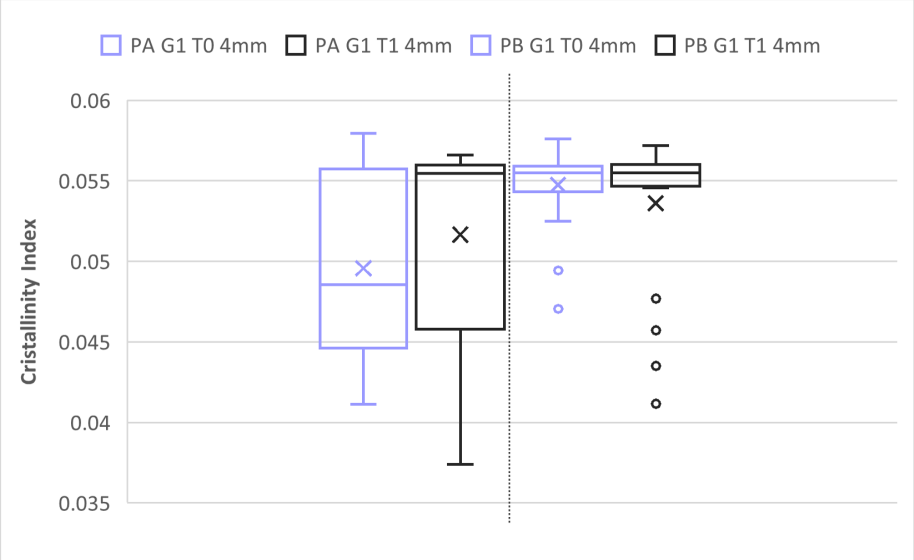

Figure 3.29: Boxplot of the Cristallinity Index for Group 1. Group A (without adhesive) on the left side of the dashed line and Group B (with adhesive) on the right side. Lilac boxes represent measurements acquired before irrigation (T0), while black boxes correspond to Raman measurements performed after the irrigation protocol (T1) collected at 4 mm depth.

At 4 mm and for PA, the Crystallinity Index showed, at T1, higher median and mean values, accompanied by a wide distribution and extended lower whiskers. Contrariwise, in PB, median values remained comparable over time, while T1 presented several lower outliers despite a similar central dispersion.

Then, follows the comparison at different depths for the G2 which highlight that at 2 mm, the Index analized showed comparable statistical values for PA and between pre e post treatment condition. Then, in PB, T1 was associated with slightly higher central values and a broader distribution, characterized by an increased interquartile range and extended whiskers.

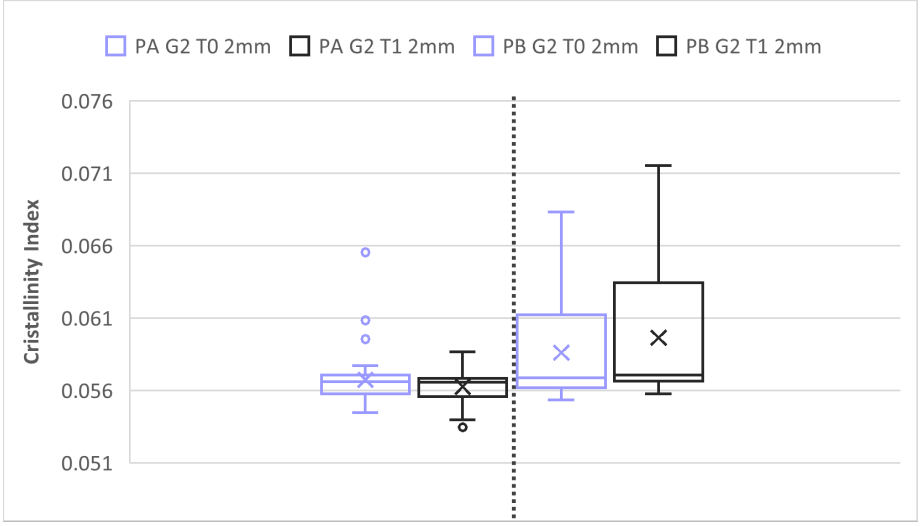

Figure 3.30: Boxplot of the Cristallinity Index for Group 2. Group A (without adhesive) on the left side of dashed line and Group B (with adhesive) on the right side.Lilac boxes represent measurements acquired before irrigation (T0), while black boxes correspond to Raman measurements performed after the irrigation protocol (T1) collected at 2 mm depth.

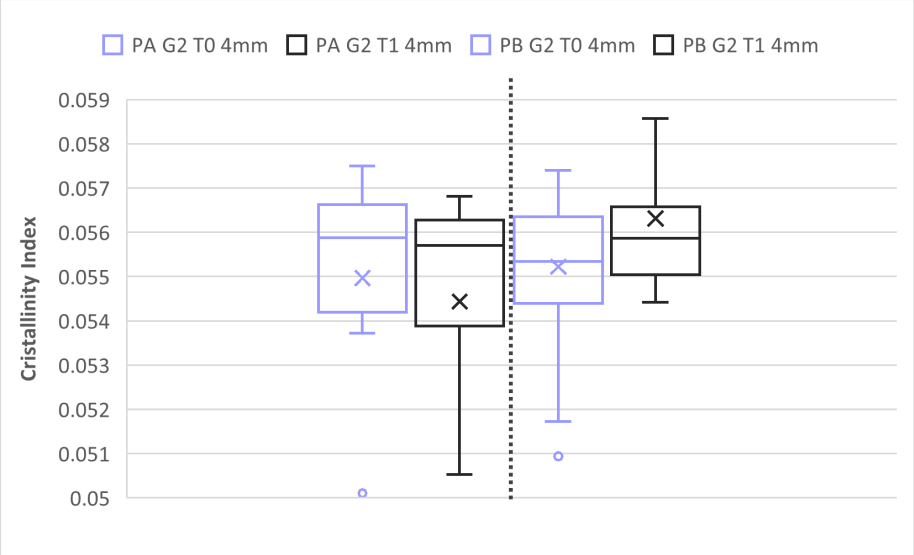

Figure 3.31: Boxplot of the Cristallinity Index for Group 2. Group A (without adhesive) on the left side of the dashed line and Group B (with adhesive) on the right side. Lilac boxes represent measurements acquired before irrigation (T0), while black boxes correspond to Raman measurements performed after the irrigation protocol (T1) collected at 4 mm depth.

At 4 mm, the Crystallinity Index in PA showed comparable median values between T0 and T1, with a slightly extended lower whisker at T1. In PB, T1 was associated with mildly higher central values and a modest widening of the distribution compared to baseline.

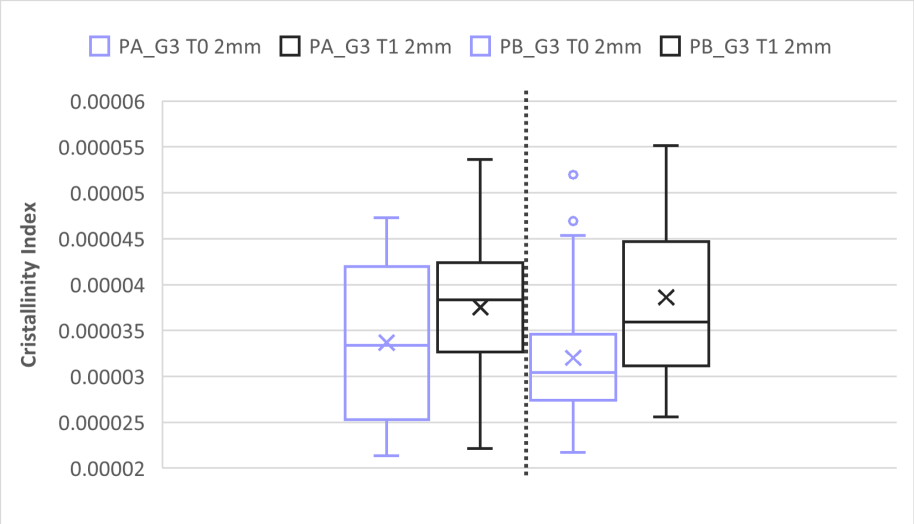

Figure 3.32: Boxplot of the Cristallinity Index for Group 3. Group A (without adhesive) on the left side of the dashed line and Group B (with adhesive) on the right side. Lilac boxes represent measurements acquired before irrigation (T0), while black boxes correspond to Raman measurements performed after the irrigation protocol (T1) collected at 2 mm depth.

At 2 mm, the Crystallinity Index increased at T1 compared to T0 in both PA and PB, with higher median and mean values. In both conditions, T1 was associated with a larger distribution, reflected by a wider interquartile range and more extended whiskers.

At 4 mm, the Index in PA showed higher median and mean values at T1, while the interquartile range appeared slightly more compact. In PB, T1 was associated with a modest increase in median values and a distribution broadly comparable to baseline, with the presence of occasional higher outliers.

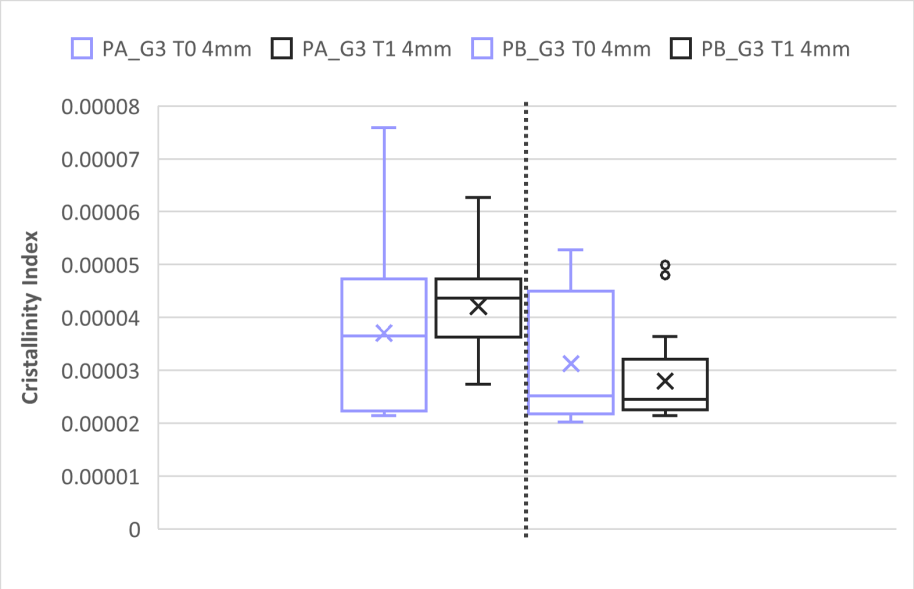

Figure 3.33: Boxplot of the Cristallinity Index for Group 3. Group A (without adhesive) on the left side of the dashed line and Group B (with adhesive) on the right side. Lilac boxes represent measurements acquired before irrigation (T0), while black boxes correspond to Raman measurements performed after the irrigation protocol (T1) collected at 4 mm depth.

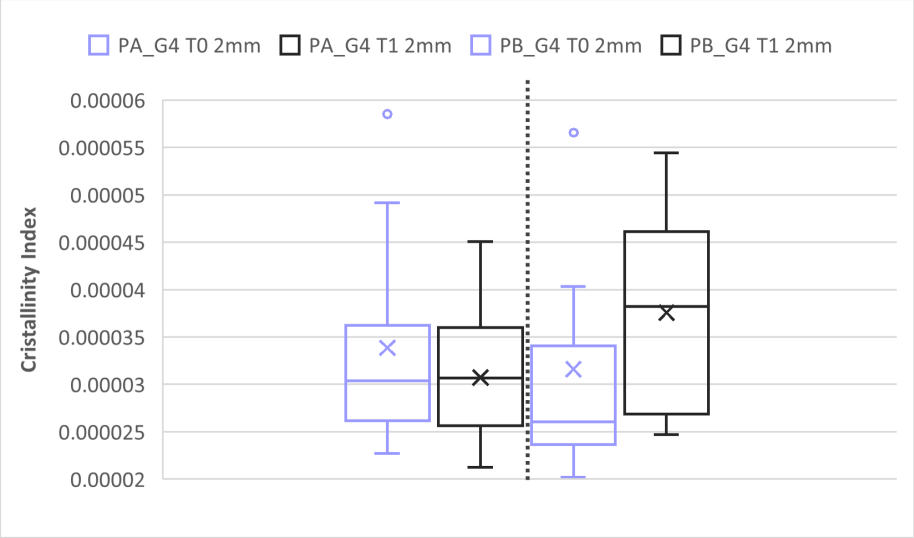

Figure 3.34: Boxplot of the Cristallinity Index for Group 4. Group A (without adhesive) on the left side of the dashed line and Group B (with adhesive) on the right side. Lilac boxes represent measurements acquired before irrigation (T0), while black boxes correspond to Raman measurements performed after the irrigation protocol (T1) collected at 2 mm depth.

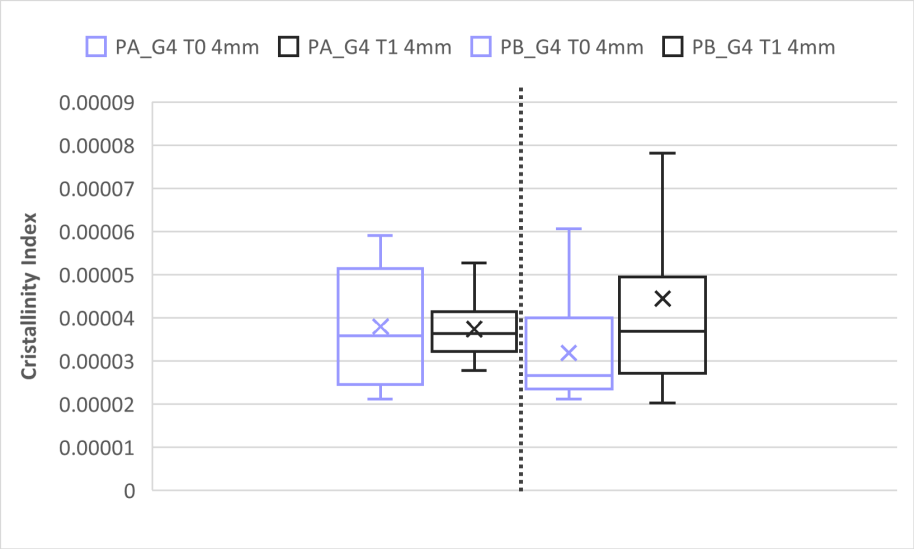

Figure 3.35: Boxplot of the Cristallinity Index for Group 4. Group A (without adhesive) on the left side of the dashed line and Group B (with adhesive) on the right side. Lilac boxes represent measurements acquired before irrigation (T0), while black boxes correspond to Raman measurements performed after the irrigation protocol (T1) collected at 4 mm depth.

For the penultimate working group, statistical evidence at the two depths showed that PAs had comparable statistical values between the two different acquisition times for the shallower depth, with no significant changes in variability, unlike the deeper depth, where a more compact interquartile range was observed.
For the samples to which adhesive had been applied, higher mean median and central values were observed, with a marked extension of the upper whisker.

Below, therefore, are reported the statistical evidences regarding one of the most significant and important parameters of the analysis and experimentation conducted.

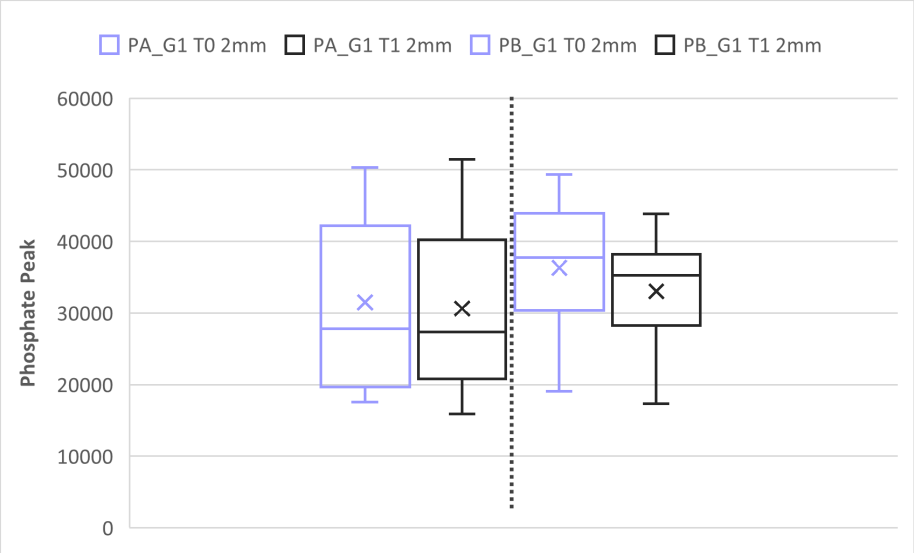

Figure 3.36: Boxplot of the Phosphate Peak for Group 1. Group A (without adhesive) on the left side of the dashed line and Group B (with adhesive) on the right side. Lilac boxes represent measurements acquired before irrigation (T0), while black boxes correspond to Raman measurements performed after the irrigation protocol (T1) collected at 2 mm depth.

At 2 mm, the Phosphate peak intensity in PA showed slightly higher median and mean values at T0, with a broad distribution in both time conditions. The post treatment condition for PB, was also associated with reduced central values, while overall variability remained comparable to baseline.

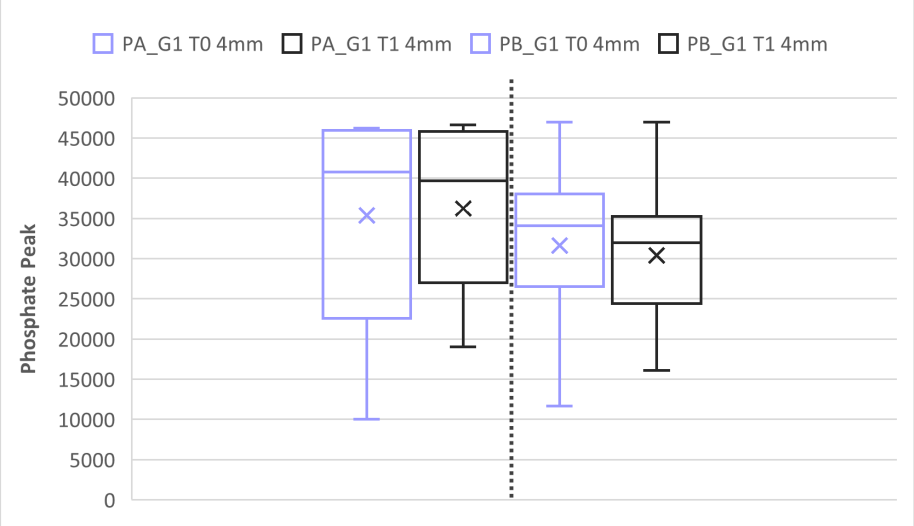

Figure 3.37: Boxplot of the Phosphate Peak for Group 1. Group A (without adhesive) on the left side of dashed line and Group B (with adhesive) on the right side. Lilac boxes represent measurements acquired before irrigation (T0), while black boxes correspond to Raman measurements performed after the irrigation protocol (T1) collected at 4 mm depth.

Analyzing the deeper depth, the intensity of the peak, in PA showed slightly lower median and mean values at T1, with a wider distribution also for the T0 condition.
In PB, T1 was associated with reduced central values and a slightly more compact distribution relative to baseline.

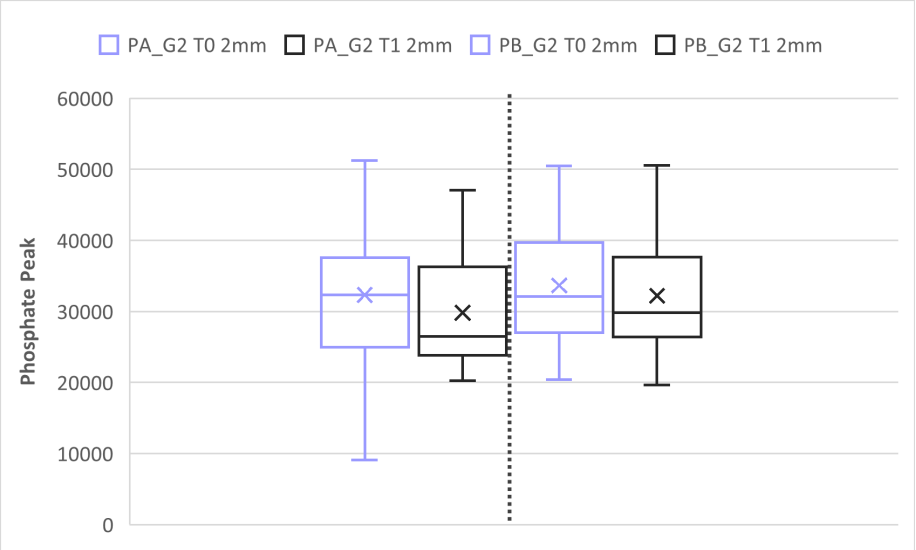

Figure 3.38: Boxplot of the Phosphate Peak for Group 2. Group A (without adhesive) on the left side of dashed line and Group B (with adhesive) on the right side. Lilac boxes represent measurements acquired before irrigation (T0), while black boxes correspond to Raman measurements performed after the irrigation protocol (T1) collected at 2 mm depth.

At 2 mm, the Phosphate peak intensity in PA showed slightly lower median and mean values at T1, while overall variability remained broad but comparable.
In PB, median values were largely unchanged, with a similar distribution pattern over time.

At 4 mm, the intensity noticed in PA increased post treatment compared to T0, with higher median and mean values and a broader distribution.
In PB, T1 was associated with lower central values and a distribution that appeared slightly more compact than baseline.

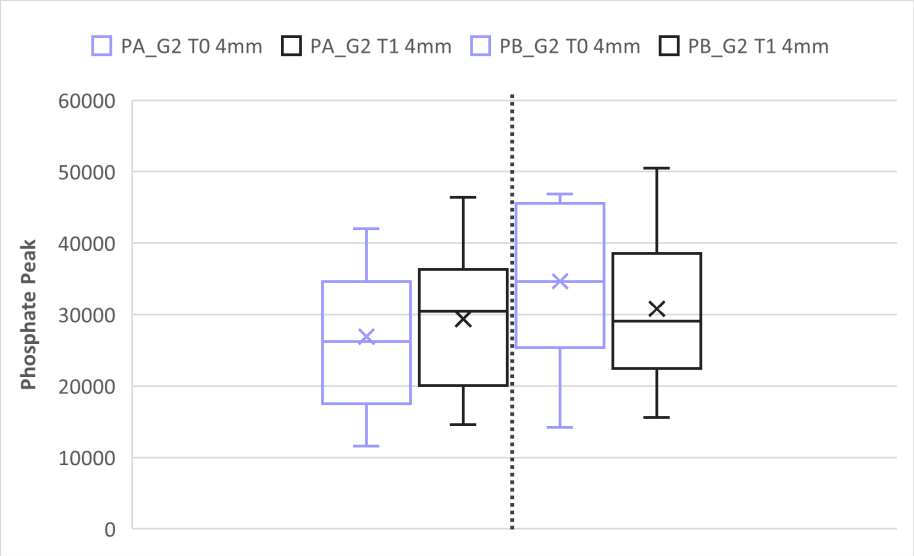

Figure 3.39: Boxplot of the Phosphate Peak for Group 2. Group A (without adhesive) on the left side of dashed line and Group B (with adhesive) on the right side. Lilac boxes represent measurements acquired before irrigation (T0), while black boxes correspond to Raman measurements performed after the irrigation protocol (T1) collected at 4 mm depth.

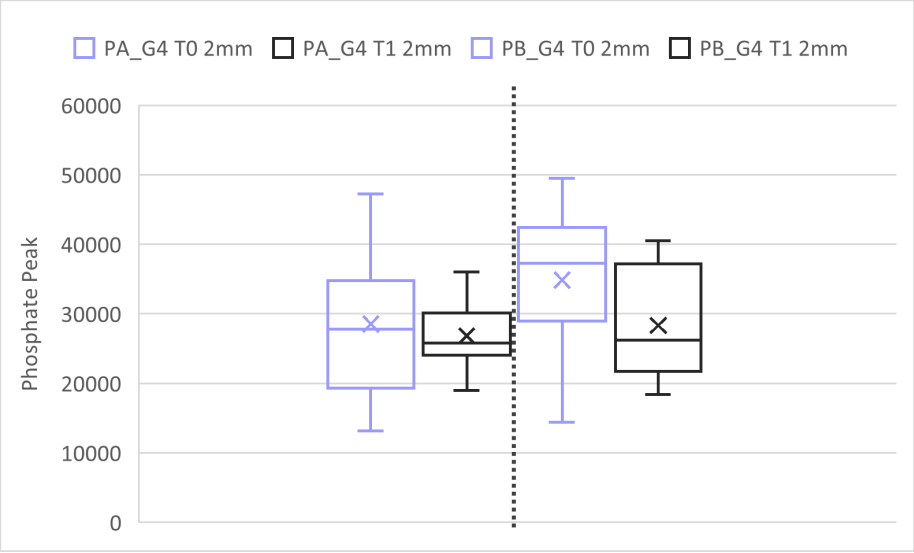

Figure 3.40: Boxplot of the Phosphate Peak for Group 4. Group A (without adhesive) on the left side of dashed line and Group B (with adhesive) on the right side. Lilac boxes represent measurements acquired before irrigation (T0), while black boxes correspond to Raman measurements performed after the irrigation protocol (T1) collected at 2 mm depth.

Continuing to look at the evidence for the G4, at 2 mm, the Phosphate peak in PA showed slightly lower median and mean values at T1 compared to T0, with comparable variability.
In PB, T1 was associated with reduced central values and a more compact distribution relative to baseline.

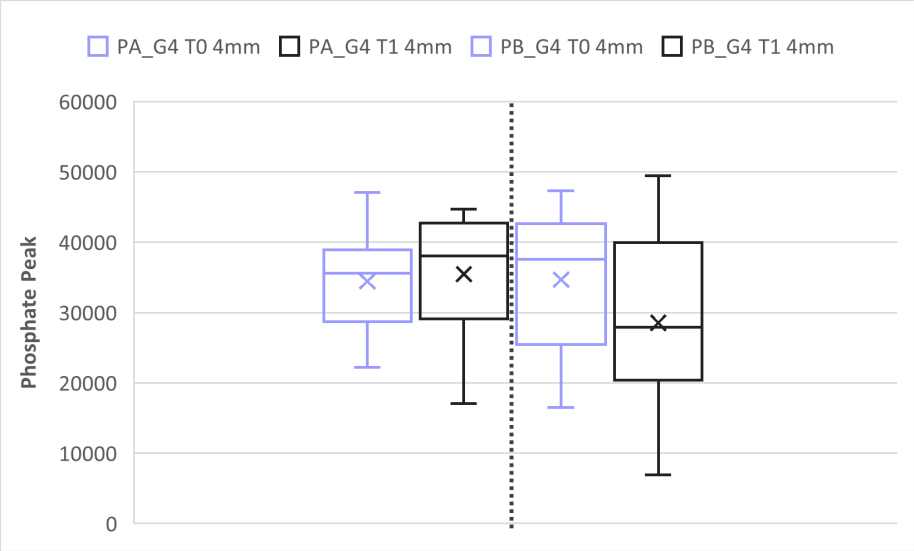

Figure 3.41: Boxplot of the Phosphate Peak for Group 4. Group A (without adhesive) on the left side of dashed line and Group B (with adhesive) on the right side. Lilac boxes represent measurements acquired before irrigation (T0), while black boxes correspond to Raman measurements performed after the irrigation protocol (T1) collected at 4 mm depth.

A different trend is observed for the statistical parameters at the 4 mm cavity, with a modest widening of the distribution.
In PB, T1 was associated with lower central values and a broader distribution, characterized by an extended lower whisker.

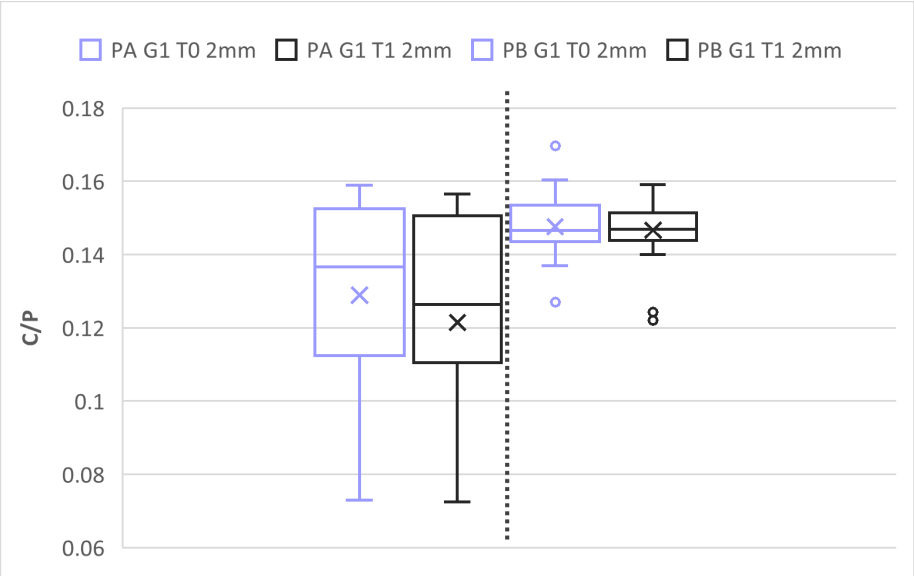

Figure 3.42: Boxplot of the C/P ratio for Group 1. Group A (without adhesive) on the left side of dashed line and Group B (with adhesive) on the right side. Lilac boxes represent measurements acquired before irrigation (T0), while black boxes correspond to Raman measurements performed after the irrigation protocol (T1) collected at 2 mm depth.

The calcium phosphate ratio allows us to highlight, for G1, that at 2 mm and for PA, there was a slight decrease in median and mean values at T1.
In PB, median values remained largely unchanged over time, while T1 presented a few lower outliers despite comparable central dispersion.

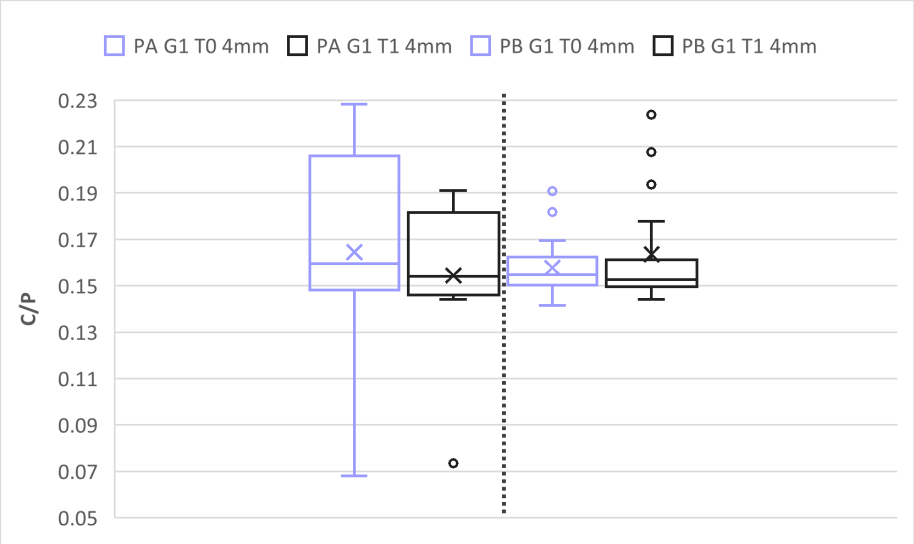

Figure 3.43: Boxplot of the C/P ratio for Group 1. Group A (without adhesive) on the left side of dashed line and Group B (with adhesive) on the right side. Lilac boxes represent measurements acquired before irrigation (T0), while black boxes correspond to Raman measurements performed after the irrigation protocol (T1) collected at 4 mm depth.

At 4 mm, variability increased overall. In PA, treatment was associated with a modest reduction compared to baseline, whereas PB maintained a largely stable profile, with only a subtle upward tendency at T1. Differences between the two conditions were more apparent at baseline; after treatment, central values became closer, although PA continued to show greater spread.

Focusing, therefore, on the second working group, it is notable that at 2 mm, C/P ratio in PA showed a slight increase in median and mean values at T1 compared to T0, with comparable variability.
In PB, T1 was associated with lower central values and a broader distribution, characterized by an extended lower whisker.

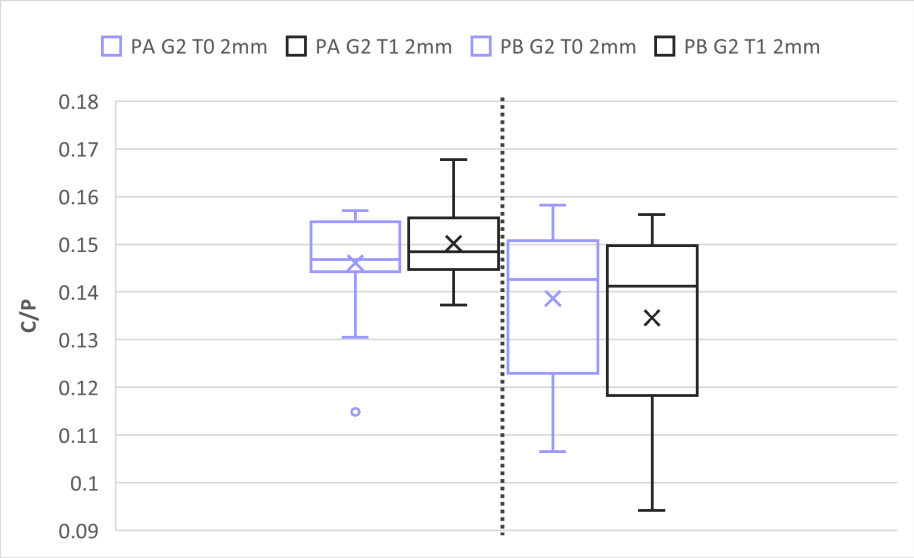

Figure 3.44: Boxplot of the C/P ratio for Group 2. Group A (without adhesive) on the left side of dashed line and Group B (with adhesive) on the right side. Lilac boxes represent measurements acquired before irrigation (T0), while black boxes correspond to Raman measurements performed after the irrigation protocol (T1) collected at 2 mm depth.

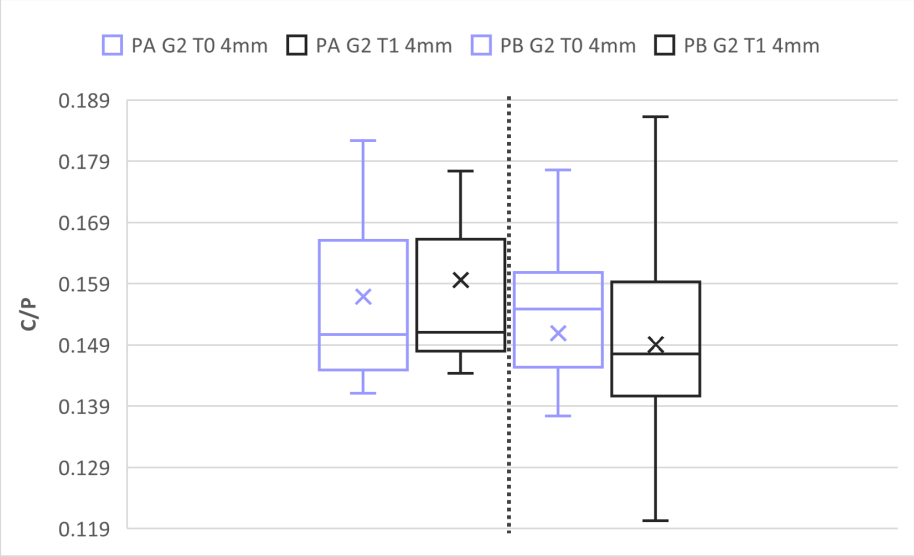

Figure 3.45: Boxplot of the C/P ratio for Group 2. Group A (without adhesive) on the left side of dashed line and Group B (with adhesive) on the right side. Lilac boxes represent measurements acquired before irrigation (T0), while black boxes correspond to Raman measurements performed after the irrigation protocol (T1) collected at 4 mm depth.

At 4 mm, the ratio in PA showed slightly higher median and mean values at T1 compared to T0, with comparable general spread.
In PB, T1 was associated with lower central values and an extended lower whisker, indicating increased dispersion toward reduced ratio values.

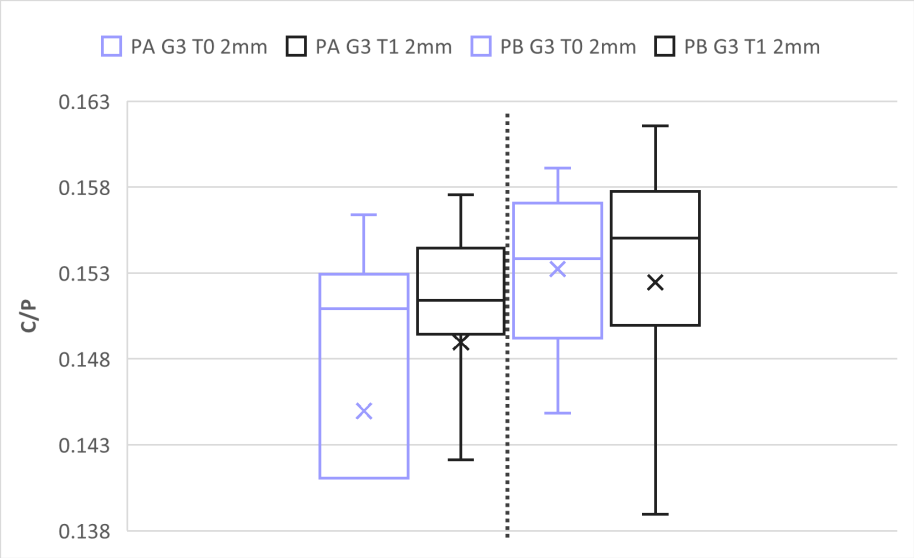

Figure 3.46: Boxplot of the C/P ratio for Group 3. Group A (without adhesive) on the left side of dashed line and Group B (with adhesive) on the right side. Lilac boxes represent measurements acquired before irrigation (T0), while black boxes correspond to Raman measurements performed after the irrigation protocol (T1) collected at 2 mm depth.

The third working group highlights that at the shallowest depth and for PA, the C/P ratio showed a slight increase in median and mean values at T1. In PB, T1 was associated with higher central values and a modest widening of the distribution, reflected by an extended lower whisker.

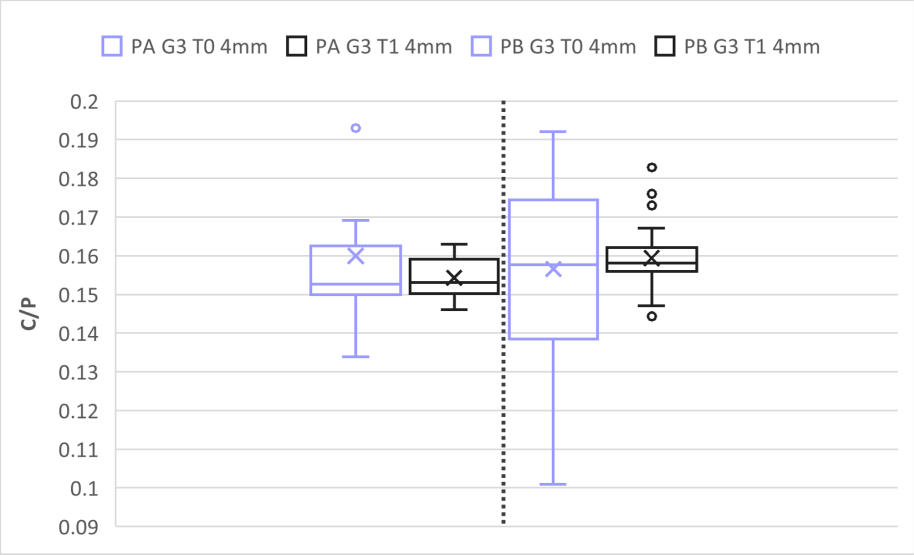

Figure 3.47: Boxplot of the C/P ratio for Group 3. Group A (without adhesive) on the left side of dashed line and Group B (with adhesive) on the right side. Lilac boxes represent measurements acquired before irrigation (T0), while black boxes correspond to Raman measurements performed after the irrigation protocol (T1) collected at 4 mm depth.

A different trend, in some respects, can be found when observing what was obtained for the 4 mm cavity. In PA it is showed slightly lower median and mean values at T1 compared to T0, with a more compact distribution.
In PB, T1 was associated with a modest increase in central values and a similar interquartile range, although several higher outliers were observed.

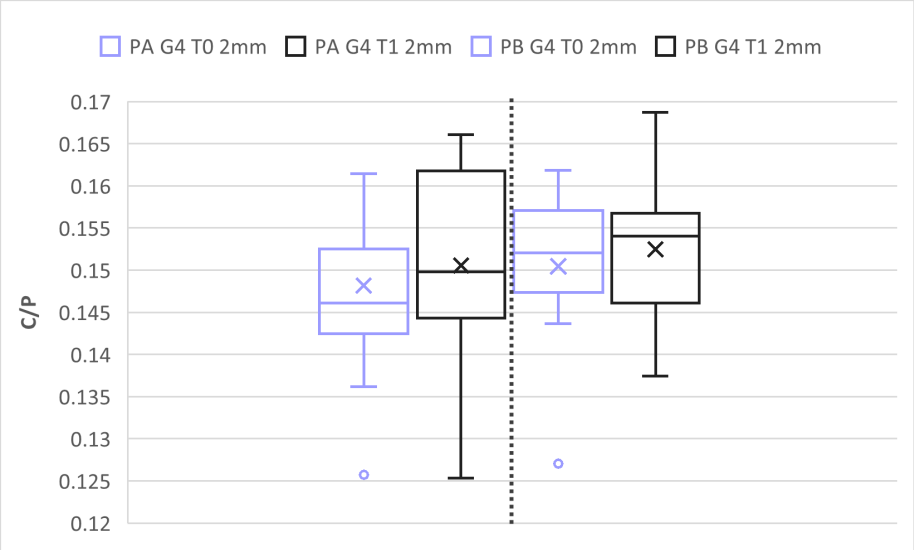

Figure 3.48: Boxplot of the C/P ratio for Group 4. Group A (without adhesive) on the left side of dashed line and Group B (with adhesive) on the right side. Lilac boxes represent measurements acquired before irrigation (T0), while black boxes correspond to Raman measurements performed after the irrigation protocol (T1) collected at 2 mm depth.

At 2 mm, the Carbonate to Phosphate ratio in PA increased at T1 compared to T0, with higher median and mean values and a broader interquartile range.
In PB, T1 was also associated with slightly higher central values, while overall variability remained largely comparable to baseline.

At 4 mm, the ratio calculated in PA showed higher median and mean values at T1, accompanied by a marked widening of the interquartile range and extended whiskers.
In PB, median values remained largely comparable over time, with a slightly more compact distribution at T1.

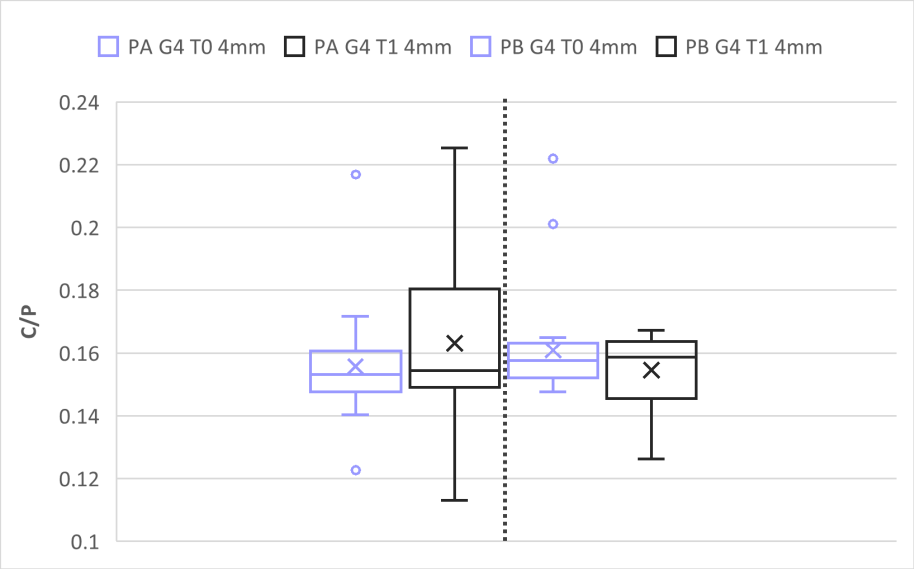

Figure 3.49: Boxplot of the C/P ratio for Group 4. Group A (without adhesive) on the left side of dashed line and Group B (with adhesive) on the right side. Lilac boxes represent measurements acquired before irrigation (T0), while black boxes correspond to Raman measurements performed after the irrigation protocol (T1) collected at 4 mm depth.

The M/M ratio was subsequently evaluated to further characterize variations within the mineral component across experimental groups, depths, and time points. The results for each protocol are presented below.

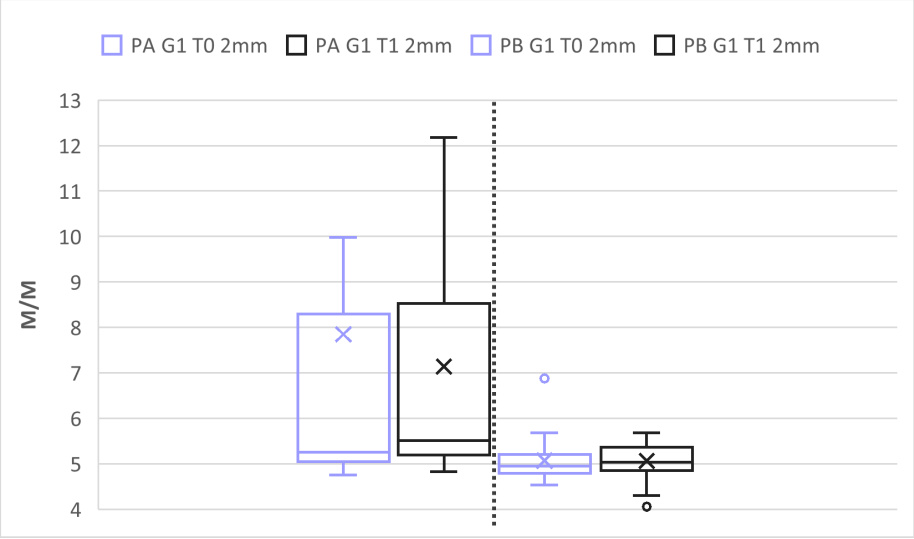

Figure 3.50: Boxplot of the M/M ratio for Group 1. Group A (without adhesive) on the left side of dashed line and Group B (with adhesive) on the right side. Lilac boxes represent measurements acquired before irrigation (T0), while black boxes correspond to Raman measurements performed after the irrigation protocol (T1) collected at 2 mm depth.

At 2 mm, the M/M ratio in PA showed slightly lower median and mean

values at post treatment condition, with a wide distribution in both conditions. In PB, median values remained comparable over time, with a more compact distribution and limited variability.

At 4 mm, the Mineral to Matrix has allowed us to highlight that in PA higher median and mean values can be found at T1 compared to T0, accompanied by a broader interquartile range.
In PB, T1 was also associated with increased central values and a slightly wider distribution, with occasional higher outliers.

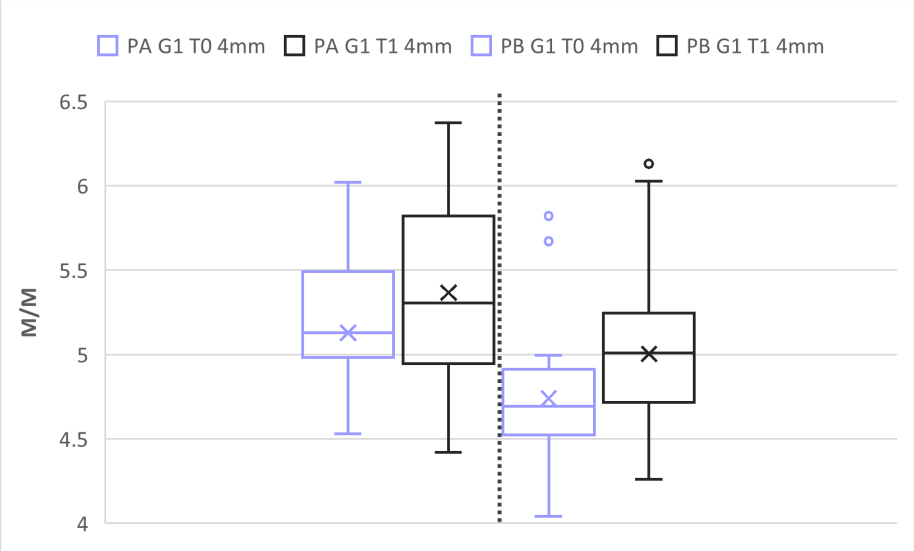

Figure 3.51: Boxplot of the M/M ratio for Group 1. Group A (without adhesive) on the left side of dashed line and Group B (with adhesive) on the right side. Lilac boxes represent measurements acquired before irrigation (T0), while black boxes correspond to Raman measurements performed after the irrigation protocol (T1) collected at 4 mm depth.

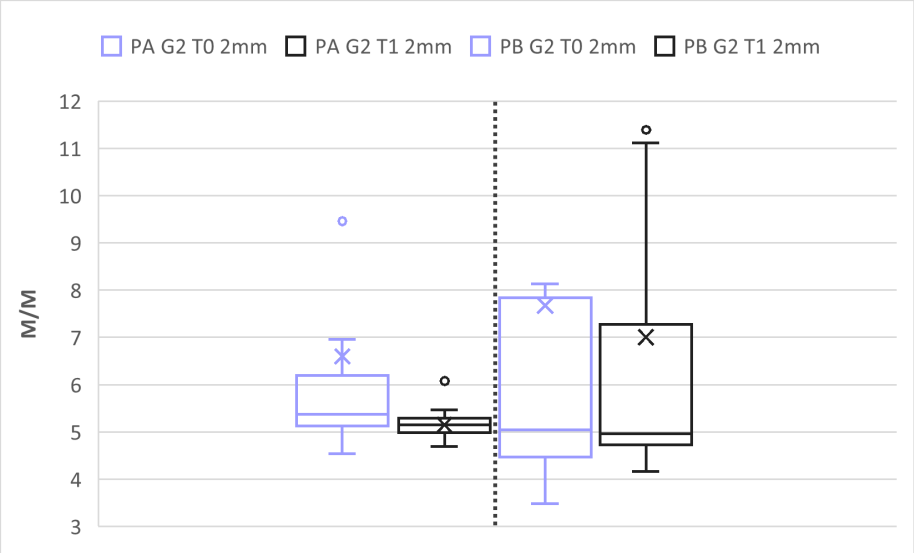

Figure 3.52: Boxplot of the M/M ratio for Group 2. Group A (without adhesive) on the left side of dashed line and Group B (with adhesive) on the right side. Lilac boxes represent measurements acquired before irrigation (T0), while black boxes correspond to Raman measurements performed after the irrigation protocol (T1) collected at 2 mm depth.

At 2 mm, the M/M ratio in PA showed slightly lower median and mean values at T1 compared to T0, with a more compact distribution. In PB, T1 was associated with reduced central values and a wide dispersion, characterized by an extended upper whisker and the presence of high outliers.

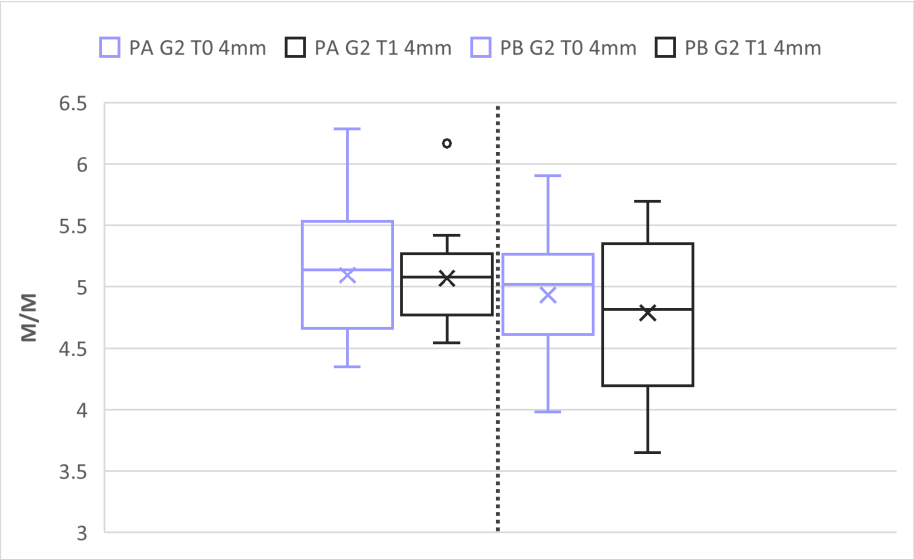

Figure 3.53: Boxplot of the M/M ratio for Group 2. Group A (without adhesive) on the left side of dashed line and Group B (with adhesive) on the right side. Lilac boxes represent measurements acquired before irrigation (T0), while black boxes correspond to Raman measurements performed after the irrigation protocol (T1) collected at 4 mm depth.

At 4 mm, the M/M ratio in PA showed comparable median and mean values between T0 and T1, with a largely stable distribution. In PB, T1 was associated with slightly lower central values and a broader distribution, characterized by an extended lower whisker.

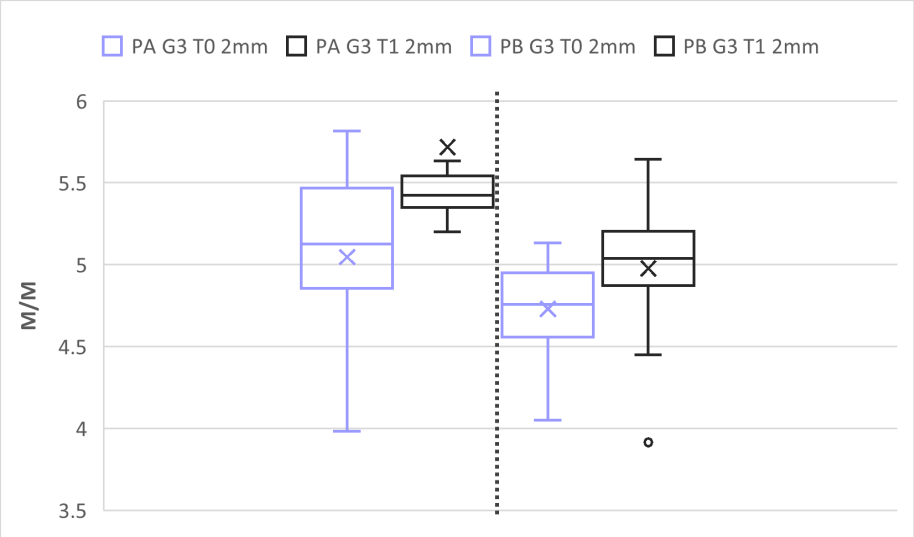

Figure 3.54: Boxplot of the M/M ratio for Group 3. Group A (without adhesive) on the left side of dashed line and Group B (with adhesive) on the right side. Lilac boxes represent measurements acquired before irrigation (T0), while black boxes correspond to Raman measurements performed after the irrigation protocol (T1) collected at 2 mm depth.

The observations regarding the penultimate working group allow us to highlight that the 2 mm depth is associated to higher median and mean values along with slightly more compact distribution between T0 and T1.
For samples covered with adhesive, and T1 state, it was associated with a modest increase in central values, while overall variability remained comparable, despite the presence of a lower outlier.

At 4 mm, the M/M ratio in PA showed a clear increase in median and mean values at T1 compared to T0, accompanied by a wider interquartile range. In PB, T1 was associated with slightly higher central values and a somewhat more compact distribution.

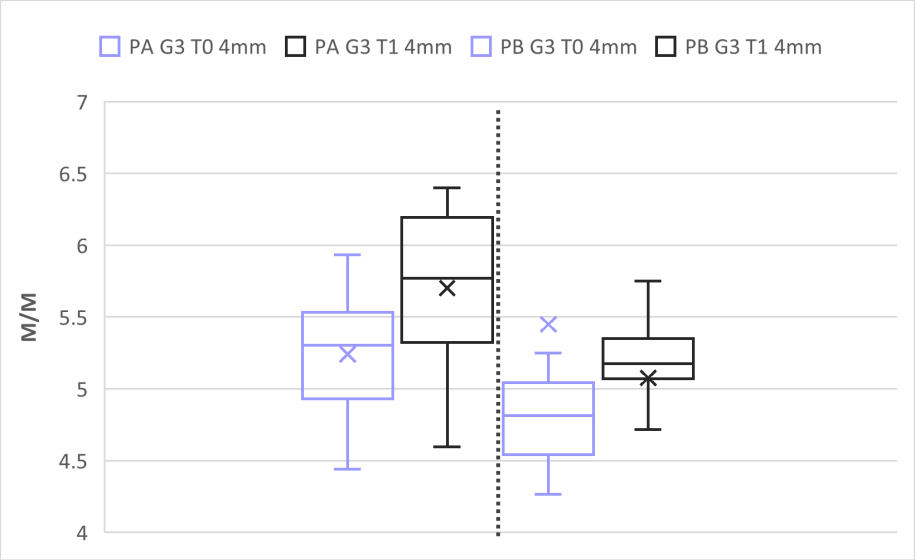

Figure 3.55: Boxplot of the M/M ratio for Group 3. Group A (without adhesive) on the left side of dashed line and Group B (with adhesive) on the right side. Lilac boxes represent measurements acquired before irrigation (T0), while black boxes correspond to Raman measurements performed after the irrigation protocol (T1) collected at 4 mm depth.

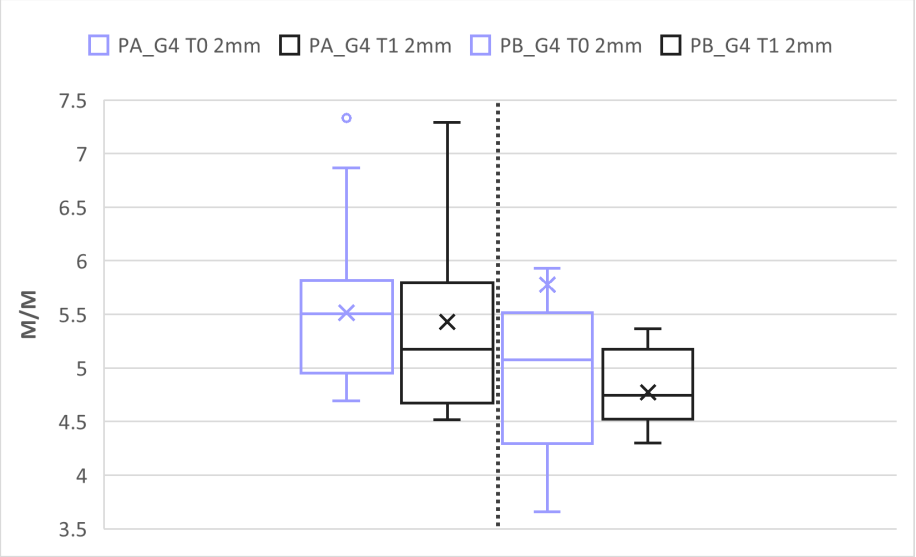

Figure 3.56: Boxplot of the M/M ratio for Group 4. Group A (without adhesive) on the left side of the dashed line and Group B (with adhesive) on the right side. Lilac boxes represent measurements acquired before irrigation (T0), while black boxes correspond to Raman measurements performed after the irrigation protocol (T1) collected at 2 mm depth.

Finally, analyzing the trends of the last working group, G4, at 2 mm, the trend of M/M ratio dysplayed comparable median and mean values between T0 and T1, for PA. Although that, T1 exhibited a broader interquartile range and more extended whiskers.

In PB, T1 was associated with lower central values and a more compact distribution compared to baseline.

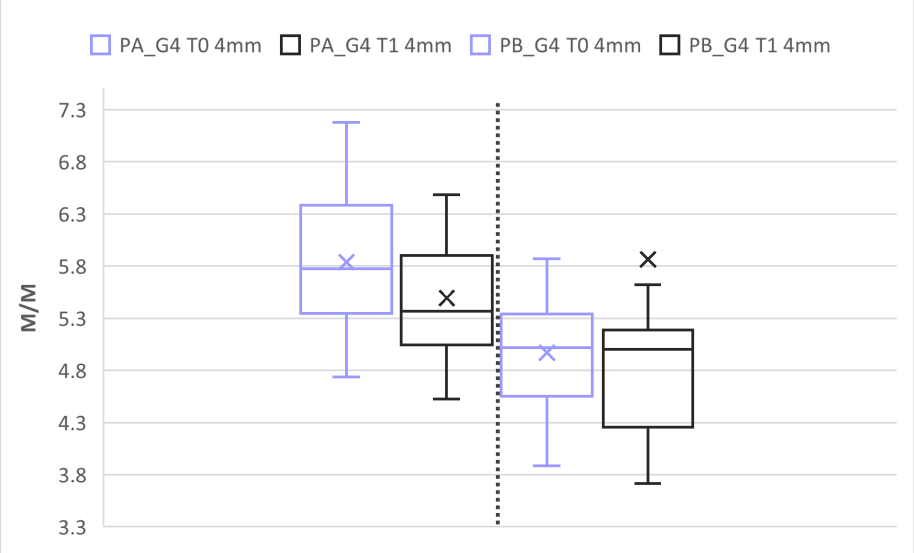

Figure 3.57: Boxplot of the M/M ratio for Group 1. Group A (without adhesive) on the left side of dashed line and Group B (with adhesive) on the right side. Lilac boxes represent measurements acquired before irrigation (T0), while black boxes correspond to Raman measurements performed after the irrigation protocol (T1) collected at 4 mm depth.

This concludes with what concerns the 4mm cavity: lower median and mean values at T1 for PA, with a slightly more compact distribution. This is accompanied by a modest increase in central values, stable overall variability for PB in T1 state.

3.3 Depth-Dependent Chemical Analysis: Comparison Between 2 mm and 4 mm

The comparison between superficial (2 mm) and deeper (4 mm) dentin revealed a depth dependent behavior that was not uniform across all Raman derived parameters, but strongly influenced by the specific type of irrigation protocol.

In more detail when examining what was measured and analyzed for collagen related indices, the parameter of depth mainly affected data dispersion.
In protocols based on the usage of NaOCl alone (Groups G1 and G3), measurements acquired at 2 mm generally exhibited wider distributions, indicating

greater heterogeneity of the component of organic matrix mainly regarding the superficial dentin.

Focusing instead on what was possible to notice at the greatest depth of analysis, the same parameters mentioned, tended to show overall more compact profiles.
This type of consideration can suggest a more homogeneous collagen response.

In contrast, in Groups G2 and G4, which were characterized by the combined usage of NaOCl and EDTA, collagen related ratios showed overlapping distributions between depths, without consistent or systematic depth related trend.

In addition to that, mineral associated parameters displayed a comparable behavior. For example, phosphate peak intensity and crystallinity index varied between 2 mm and 4 mm depending on the protocol, rather than following a monotonic superficial to deep gradient. In Groups G1 and G3, depth related differences were mainly reflected in terms of variability, with superficial dentin often showing wider spreads.

Conversely, in combined G2 and G4 protocols, mineral parameters at the two depths were largely comparable, indicating that the chemical treatment dominated over depth related effects.

In light of this, the results obtained during the various comparative analyses indicate that dentin depth modulates the heterogeneity of the Raman response rather than imposing a consistent directional change.

The recurring relationship between depth and type of chemical treatment, which often occurs throughout this study, is undoubtedly complex.
Indeed, it suggests that depth-related effects cannot be interpreted independently of the specific type of irrigation regime applied.

3.4 Comparative Evaluation of the Shielding Ff-fect: Group A vs Group B (30 min)

At 30 minutes, the comparison between PA and adhesive protected dentin, does not indicate a uniform shielding effect, but rather differences that vary according to the irrigation protocol and dentin depth.

For collagen related parameters, in several collagen related parameters, differences between PA and PB were more evident in data dispersion than in median values. In NaOCl only treatments (G1), measurements collected at 2 mm showed a wider dispersion in PA, while PB values remained more compact both before and after irrigation. This difference became less evident at 4 mm, where collagen related ratios were comparable in the two conditions.

In combined protocols (like G2), differences between PA and PB were more evident at 2 mm, with PB often showing a more compact distribution after treatment.

At greater depth, however, this distinction largely disappeared. Furthermore, a similar, but for some aspects not identical, behavior was observed for the mineral related parameters considered. In some cases, phosphate intensity and crystallinity values in PB were characterized by narrower distributions compared to PA, particularly in superficial dentin.
This effect was not systematically observed across all groups and was negligible in NaOCl only treatments.

Putting together the considerations made for this section, for protocols that have a shorter duration, it can be seen that a possible adhesive application does not prevent the chemical interaction with the dentin, but can have an influence in terms of response variability in the superficial regions, which results in a greater dispersion in the median values.

3.5 Impact of Prolonged Exposure: Long - Term Chemical Stability (60 min)

Considering the experimental condition characterized by a prolonged exposure time, it was possible to assess that the evolution of Raman derived parameters did not correspond direclty to a uniform increase in the magnitude of the changes observed at shorter exposure.
Instead, the response varied according to the irrigation protocol and the depth of the cavity.

In the case of G3, collagen related indices at 2 mm showed modest additional changes in that case, compared to the shorter exposure, while at 4 mm their distributions remained largely overlapping with baseline values.
For parameters related to collagen component, the values collected for 60 minutes exposure, largely overlapped those observed at shorter exposure, without evidence of a consistent additional shift.

A different behavior was observed in G4. The combined usage of irrigants detected that at 2 mm, prolonged exposure was associated with increased dispersion of collagen related ratios, reflecting increased variability among samples rather than a uniform shift in median values.
Then, focusing on the 4 mm depth, by contrast, collagen parameters remained comparatively stable in both PA and PB conditions.

A similar pattern was also reflected in mineral related parameters. Phosphate intensity and crystallinity did not increase progressively with time. In NaOCl based protocols, values at prolongued exposure largely overlapped those measured at shorter exposure, whereas in combined treatments extended exposure mainly resulted in greater variability at superficial depth, with limited effects in deeper dentin.

These observations indicate that prolonged irrigation was not associated with a consistent increase in the magnitude of the measured Raman parameters.

Instead, the impact of exposure time varied according to irrigant combination and dentin depth, with superficial regions showing a more heterogeneous response under extended chemical challenge.

Chapter 4

Discussion

4.1 Interpretation of Raman-Derived Chemical Changes

The Raman analysis performed across the four experimental protocols revealed that chemical modifications induced by NaOCl, with or without EDTA, were neither homogeneous nor depth independent. However, specific trends emerged when individual parameters were examined in relation to protocol intensity and substrate condition.

Indeed, it is possible to ntoice that NaOCl acts as a strong oxidant that degrades the organic matrix, leading to a relative increase in the 960 cm^{-1} (ν_1 PO_4^{3-}) peak intensity. In dentinal substrates, NaOCl induced degradation of the organic matrix may result in a relative increase of the mineral signal intensity. This phenomenon can be seen as an artifact of surface deproteinization rather than a true recrystallization; indeed, the increased FWHM indicates the presence of smaller or more defective crystals following the oxidative attack.

Conversely, EDTA promotes selective demineralization through Ca^{2+} chelation, resulting in a measurable decrease in I_{960}. The simultaneous increase in FWHM further confirms the dissolution of the crystalline structure and the resulting increase in lattice disorder.
It can also be attentioned that, thanks to depth dependent analysis, chemical

alterations at 2 mm depth, NaOCl generates maximum HA exposure, whereas at 4 mm the magnitude of the changes was generally reduced.

The increase in the Carbonate to Phosphate ratio (I_{1072}/I_{960}) reflects selective demineralization, as EDTA preferentially dissolves phosphate rich hydroxyapatite while B type carbonates (CO_3^{2-}) exhibit higher resistance to chelation. For that reason, depth dependent results reveal a distinct penetration gradient, at 2 mm the synergistic action of NaOCl and EDTA is most effective, resulting in carbonate enrichment.
On the other hand, it has to be taken in consideration that, at 4 mm, the limited diffusion of irrigants through the tubules preserves the more stable mineral phase, minimizing the risk of structural collapse in deeper dentinal regions.

The observed increase in this contribution following NaOCl exposure indicates the preferential removal of non collagenous proteins and hydrophobic moieties. This has the result to lead to a relative surface enrichment of structured collagen fibrils as the more labile organic components are dissolved by the oxidative action of the irrigant.
Protected dentin, conversely, the reduction in the I_{1650}/I_{1450} ratio for samples treated with a protective adhesive indicates that the adhesive layer successfully acted as a chemical barrier.
By limiting the diffusion and oxidative potential of NaOCl, the adhesive preserves the original organic framework while modifying the spectral signature.

Finally, AMI/AMIII decrease confirms collagen structural damage post treatment, directly correlating with compromised hybrid layer durability. More pronounced dentin at 2 mm depth, where treatment penetration is maximal.

Taken together, the Raman-derived parameters indicate that NaOCl induced modifications affect both mineral and organic components, but the direction and magnitude of these changes depend on protocol composition, exposure time, depth, and the presence of adhesive sealing as demonstrated in studies [8] [23] .

Superficial dentin consistently showed greater variability and reactivity, whereas deeper dentin exhibited more protocol-specific and condition-dependent behavior.

4.2 Influence Of Exposure Time On Dentin Integrity

The comparison between 30 minute protocols (G1 and G2) and 60 minute protocols (G3 and G4) allows a direct evaluation of the role of exposure time on dentin chemical stability.

In NaOCl-only protocols, extending exposure from 30 minutes (G1) to 60 minutes (G3) resulted in more consistent alterations of both mineral and organic parameters. In G3, crystallinity increased at both 2 mm and 4 mm in PA, whereas in G1 changes were limited and less systematic. Similarly, the M/M ratio showed a clear upward shift in G3 at both depths, while in G1 variations were mild and mainly restricted to superficial dentin. These findings suggest that prolonged NaOCl exposure may promote structural reorganization of the mineral phase.

The effect on collagen related parameters also differed with time. In G3, the AMI/CH_2 and AMI/AMIII ratios showed significant changes at 2 mm, with increases indicating superficial conformational modifications of the collagen matrix. In G1, variations were present but overall they could be described as less pronounced. This indicates that extended exposure amplifies detectable changes in the organic matrix, particularly in the most superficial.

When EDTA was included, time-dependent effects became more complex. Comparing G2 (30 min) and G4 (60 min), the longer exposure did not simply intensify the response. At 2 mm, G4 showed reductions in the M/M ratio in both PA and PB, whereas G2 displayed opposite tendencies between conditions. At 4 mm, G4 was associated with a clearer decrease in mineral-related ratios in PA, while G2 remained relatively stable. This suggests that when chelation is combined with prolonged exposure, the balance between organic

degradation and mineral modification is altered rather than uniformly intensified.

Across all parameters, superficial dentin consistently exhibited greater sensitivity to prolonged exposure, particularly in G3, where both mineral organization and collagen-related ratios were affected. At 4 mm, time-dependent differences were present but less uniform, indicating that depth modulates the impact of extended chemical action.

Increasing exposure time from 30 to 60 minutes does not merely amplify the effects observed at shorter durations. Instead, it modifies the pattern of chemical response, especially in protocols without EDTA (G3), where prolonged NaOCl exposure produces more coherent alterations in both mineral and organic components. This supports the view that exposure time is a critical determinant of dentin chemical integrity, with superficial layers being the most responsive to extended treatment.

4.3 Protective Effect of Adhesive Sealing On Dentin Chemistry

The comparison between specimens without adhesive (PA) and with adhesive (PB) shows that the adhesive layer does not simply attenuate the chemical effect of the irrigating solutions.
Instead, it modifies the pattern of response of both mineral and organic components, particularly in deeper dentin and under prolonged exposure.

In NaOCl 60 min treatment, the more evident reduction of the phosphate band in PB may partly reflect the presence of the adhesive layer, which can attenuate the mineral signal from the underlying dentin. Consistently, PB and PA showed different trends in mineral-related Raman parameters at both depths. A similar pattern was observed for crystallinity in G4 at 2 mm, where PB exhibited a clearer post-treatment increase compared with PA, suggesting that these parameters may be influenced by the presence of the adhesive layer.

The influence of the adhesive becomes more evident in deeper layers when collagen-related parameters are considered. In G2 and G4 at 4 mm, the AMI/CH_2 ratio decreased after treatment in PB, whereas PA remained comparatively stable.
Likewise, in G2 and G3 at 4 mm, the AMI/AMIII ratio showed a more pronounced reduction in PB samples. These types of findings indicate that collagen-related ratios at deeper cavity, differ more clearly between PA and PB, particularly when EDTA or prolonged exposure is involved.

The C/P ratio confirms that the organic mineral balance is also differentially affected. In G2 at 2 mm, PA exhibited a post-treatment increase while PB decreased; in G4 at 4 mm, PA slightly increased, whereas PB decreased. These opposite trends confirm that the adhesive does not produce a uniform effect across conditions.

The M/M ratio further supports this interpretation. Baseline values were generally higher in PA, especially at 2 mm. After treatment, differences between PA and PB either persisted (G4) or narrowed (G1 and G3), suggesting that the adhesive influences both initial chemical characteristics and the magnitude of subsequent changes.

Overall, adhesive application was associated with protocol and depth-dependent differences in both mineral and collagen-related parameters. The effect was more evident at 4 mm and under prolonged or combined chemical exposure.

4.4 Study Limitations

Some limitations of the present study should be acknowledged when interpreting the findings.

The Raman measurements performed on adhesive-coated specimens reflect a composite surface consisting of polymerized adhesive, interface region, and underlying dentin. Although this approach was chosen to simulate a clinically relevant condition, the spectral contribution of the bonding material

may have influenced specific parameters, particularly those involving CH_2 and phosphate-related bands. Consequently, changes observed in adhesive coated samples cannot be attributed exclusively to dentin modifications.

A fundamental aspect to consider is the biological variability closely related to the type of samples used. Extracted teeth may vary considerably in terms of the donor's age, health status, hygiene and dietary habits, and the presence of any pathological conditions. All of this can directly impact the composition of the dentin used for analysis.

Furthermore, the analysis was based solely on Raman spectroscopy. While this technique provides detailed chemical information regarding mineral and organic components, it does not directly assess mechanical properties or ultrastructural morphology. Complementary methods such as microhardness testing, bond strength evaluation, or high-resolution imaging could provide additional insight into the functional implications of the chemical changes detected.

It should also be noted that the study was conducted under in vitro conditions. The absence of pulpal pressure, saliva, and biological variability may limit direct extrapolation to the clinical setting. Chemical interactions observed in a controlled laboratory environment may differ from those occurring in vivo.

A significant limitation can also be found in the fact that this study employed static and controlled application, which does not fully reflect the behavior of irrigants in a real clinical setting. In this specific case, the dentin is isolated, and the irrigant remains in direct and continuous contact with the surface. Furthermore, the exposure time is precisely controlled, meaning there is no flow of liquid, no moving endodontic instruments, or dilution of other fluids. This undoubtedly allows for control of the variables of interest, but it represents a simplified situation. This differs from actual root canal therapy, as non continuous contact with the dentin and variable diffusion may occur. This leads us to conclude that the conditions chosen for this study accurately describe the chemical behavior of the system under controlled conditions, but

do not perfectly represent what happens during a real treatment.

Moreover, although multiple parameters were analyzed, the sample size per group was limited. While the consistency of trends across different indices strengthens the internal validity of the findings, larger sample sizes would improve statistical robustness and external generalizability.

Despite these limitations, the standardized experimental design, the inclusion of multiple protocols and exposure times, and the integrated evaluation of mineral and organic Raman indices provide a structured framework for understanding the chemical response of dentin to irrigation procedures.

Chapter 5

Conclusion

This study, thanks to Raman spectroscopy analisys, has highlighted that the chemical response of dentin to NaOCl based protocols can be strongly influenced by parameters like: exposure time, depth of the analyzed area, and the presence of an adhesive layer previously applied.

Prolonged NaOCl exposure (60 minutes, G3) induced more consistent modifications of both mineral organization and collagen component compared to 30 minute protocols (G1), particularly at 2 mm. These observed changes were reflected by alterationsin crystallinity and shifts in collagen-sensitive ratios, indicating structural reorganization rather than simple degradation.

When EDTA was combined with NaOCl (G2 and G4), the response became less linear so that at 4 mm, some mineral and collagen related parameters showed divergent trends between PA and PB, suggesting that chelation and extended exposure modify the organic mineral balance in a depth-dependent manner.

Furthermore, it can be noted that the application of an adhesive layer should not be interpreted exclusively as a uniform and protective barrier. Instead, PB specimens exhibited, in the majority of cases, distinct patterns of mineral signal intensity and collagen ratio variation, especially at 4 mm and in prolonged or combined protocols. This indicates that the adhesive interface modulates the chemical behavior of dentin rather than shielding it from chemical action.

Superficial dentin consistently demonstrated greater reactivity across parameters, while deeper dentin exhibited protocol-specific and condition-dependent responses.

The combined evaluation of crystallinity, phosphate peak, carbonate to phosphate, collagen-related ratios, and mineral to matrix revealed that the way of reaction of mineral and organic components highlights the complexity of dentin chemical modification under irrigating protocols.

The findings demonstrate that NaOCl-based treatments induce measurable alterations in dentin chemistry, but the magnitude and direction of these changes depend on exposure time, chelating association, depth, and adhesive condition. The study provides a Raman-based framework for understanding how different clinical protocols may differentially affect dentin at both superficial and deeper levels. Therefore, the information obtained can be useful for customizing the various dental protocols in clinical practice and can contribute to the optimization of clinical protocols aimed at improving the long-term stability of post-endodontic restorations.

Acknowledgements

First, I would like to express my sincere thanks to Professor Sabrina Grassini and the Istitute of Dental School for her availability, guidance, and support throughout the development of this thesis; a proper supervision were essential to the completion of this project.

To Ali, because even though time and distance kept us apart for a while, we always found our way back to each other with laughter, hugs, and sometimes tears. We are day and night, sea and mountains, blue and pink, and yet our connection is something rare. We almost never say "I love you" out loud; instead it's in the small things: "You look good with your hair tied back," "Hold my hand while the teacher decides who to call on," or laughing uncontrollably on a warm summer evening in Sardinia. We know how much we love each other, even if we rarely say it, and we have always wanted the best for one another.

To Davide, who welcomed every version of me with open arms. You never judged me, only met me with the kind of quiet, genuine affection that comes from someone who truly understands how much you might need it. I will never stop being grateful to you and to life, for bringing someone like you into my world. Your words somehow always arrive exactly when I need them. You seem to know what I'm thinking, what I'm hiding, and how I'm feeling without me having to say a thing. And that kind of presence has been a light in some of my darkest tunnels.

To Franci, one of the purest and kindest souls life could have placed on my path. We are different in so many ways, and yet deeply alike where it matters most. The love we share is genuine, simple, and sincere. Talking to you is

one of the most freeing things I know: you listen, and somehow the chaos in my head begins to make sense again. You have always reminded me of my worth, especially in the moments when I needed that reminder the most. To Matthew, who always seems to have a kind word ready for me, and who never fails to see the beauty and the good in things. Souls like yours are rare, and I feel lucky to have someone so thoughtful and genuine in my life.

To Luca, because I will probably never be able to thank you enough for the kindness you have always shown me. Only a friend like you could listen to me talk about the same topic for hours and still never seem tired of it. You made me laugh, sing, smile, and lifted me up more times than you know. You truly are one of the good ones — determined, brilliant, and kind. You deserve the very best life has to offer, and I already know that one day I will be there, listening to the stories of everything you have achieved.

To my dearest friends (There, Matthew, Fla, Franci, Laura, Tere, Giuli, Iri, Manu, Dani, Clas, Gianmaria, Gianmarco, Lori, Gios, Kev, Ali, Cami), because with you it has always felt natural to be completely myself. You are all so different from one another, and yet each of you adds something unique to my life. I probably don't say it often enough, but every single one of you is powerful and special in your own way. Little by little you have become pieces of a chaotic puzzle that somehow fits perfectly together. And never more than in these past few months have you shown me how real that is. Some of you have been there since school, others arrived later, but all of you have given me so much kindness and support, more than I ever thought I deserved. You are the grit when I am full of energy, but also the calm when I find myself looking at you with tears in my eyes, trying to understand what just happened. These are not words written out of formality. This just feels like the right moment to tell you how much people like you truly mean to me.

To my coaches (Andre, Matte, Gio, Doc, Gabri), who pushed my nervous system to the limit, but with patience taught it to function correctly again, without fear but with grit, helping me to bring it out again when, for a moment, I had put it aside.

To my friend Auro, whom I unfortunately shared too little time with, but who I know to be one of the best people I met at this university. A simple, sharp, and wonderfully ironic person who managed to lighten the weight that a course of study can sometimes place on your shoulders and did so with the most effortless naturalness. I don't know which directions our lives will take, but I am certain that you will go far. And I hope I can carry your spontaneous and contagious laughter with me for a little while longer.

To my parents, who have learned to welcome the roller coaster that often lives inside my head. You have always tried to understand the chaos and confusion that so often filled my thoughts, and little by little you helped me see where I was going wrong and how to find my way out again, with the determination and strength you always reminded me I had. This is certainly the end of an important journey, one that has taken a lot from me, but that I hope will slowly give back everything I have tried to sow along the way. Thank you for always believing in me. You have always seen my achievements long before I even knew I was capable of entering the race. You have always chosen to see the good and the beauty in me, in my actions and in my words, celebrating with me in the joyful moments and wiping away my tears in the difficult ones. Having parents like you is not something to take for granted. You have your imperfections and have made mistakes, like anyone else, but you are also learning to live this life for the first time, just like I am. I hope the full sunlight returns within me, so that we can continue to celebrate our milestones together.

To my grandparents and my uncles, for always having kind and comforting words for me, and for constantly encouraging me to do better and aim higher. You have always reminded me not to stop, to stay curious, to keep learning, and never to settle, no matter what. With this achievement, I hope I can make you proud to have a granddaughter and niece who might be a little unconventional, just like me.

To **Turin**, because with this we place a full stop. Dear Turin, you welcomed me just two and a half years ago when I arrived fragile, insecure, and confused,

yet full of hopes and dreams, and with a quiet determination to prove, to myself and only to myself, that perhaps I could face the challenges of the feared Politecnico. I would be lying if I said I fully realized how many days and months I spent walking your streets, riding your trams, and living under your grey skies; skies that, strangely enough, almost always seemed to offer a brilliant sun on Sundays. I would be lying because it all feels like it passed so quickly that sometimes I can still picture the first boxes I had to unpack, slowly filling shelves and wardrobes. And yet time did pass, and somewhere along the way I changed, perhaps for the better. Because, despite everything, I came to understand that you were exactly what I needed: a kind of shock therapy. Not gentle comfort or soft reassurance, but an unexpected, almost refreshing cold shower. Little by little, you made me understand far more than I ever imagined I would need to learn. That exam days will probably always mean a white T-shirt and rusks with blueberry jam for breakfast (I don't really believe they bring me luck... but maybe a little). That the hug of a brother can quietly lift you back up. That maybe electronics and electrical engineering aren't so terrible after all; and that, somehow, I can manage them too. You watched me pack and unpack suitcases, return home and then come back to you again, happy, sad, angry, disappointed, with swollen eyes from crying, but always ready to begin again, one step at a time, quietly. Perhaps because, in the end, you became a kind of home too. Sometimes small, very small, sometimes enormous and dispersive, almost without walls, as if you wanted me to learn how to find my own direction. Even if only towards the end, you taught me something important: that studying alone is something I can do well, and even enjoy. But doing it with friends is far better. Because in the end, they believed in me more than I remembered to believe in myself. They probably don't even know it, but they made things lighter for me. They made me smile, laugh, reflect. They cooked me dinner, helped me blow out candles, and listened when I needed it most. You gave me new friends, so different from me, so different from each other in passions, ideas, rhythms, and ambitions, and yet all so equally ready to care for me in the most sincere and spontaneous way. You made me understand that waking up at five in the morning to watch the sunrise, revise for an exam, go to the gym, or run is somehow written in my DNA, but that going to bed at ten probably is too. That sometimes turning up

the volume of my favourite Marshall speakers doesn't silence the noise inside my own thoughts. Because not everything depends on me, or on what I can prove or give. But there is one thing you did not manage to teach me: how to shake off the terrible feeling that everything can slip through my hands, that just when it feels like you finally hold what you have always imagined for yourself, it suddenly seems to be over. No, in that you were not a very good teacher. Perhaps because what you are really teaching me is patience. That sometimes things simply take time. That sometimes the path needs to be longer before reaching the destination. That rushing can burn a garden that might have had the chance to bloom. That haste may have defeated me before, but it never has the final word. That truly anything can happen, and very often when you least plan for it. And in the end, I do not know what will become of me, or of you and me. But for now, dear Turin, let's place a full stop.

Bibliography

[1] Ahmed IM Al-Rubaie and Abdulla MW Al-Shamma. Effect of immediate pre-endodontic dentin sealing on the cuspal deflection and fracture strength of endodontically treated teeth. *Clinical Oral Investigations*, 29(6):297, 2025.

[2] Ana Flávia Sanches Borges, Renata Andrade Bittar, Fernanda Miori Pascon, Lourenço Correr Sobrinho, Airton Abrahão Martin, and Regina Maria Puppin-Rontani. Naocl effects on primary and permanent pulp chamber dentin. *Journal of Dentistry*, 36(9):745–753, 2008.

[3] Hayaki Nakatani, Atsushi Mine, Mariko Matsumoto, Yuko Tajiri, Ryosuke Hagino, Masahiro Yumitate, Shintaro Ban, Jiro Miura, Takuya Minamino, and Hirofumi Yatani. Effectiveness of pretreatment with phosphoric acid, sodium hypochlorite and sulfinic acid sodium salt on root canal dentin resin bonding. *Journal of Prosthodontic Research*, 64(3):272–280, 2020.

[4] Ana Flávia Sanches Borges, Renata Andrade Bittar, Fernanda Miori Pascon, Lourenço Correr Sobrinho, Airton Abrahao Martin, and Regina Maria Puppin Rontani. Naocl effects on primary and permanent pulp chamber dentin. *journal of dentistry*, 36(9):745–753, 2008.

[5] Ayfer Atav, Alessio Zanza, Aysenaz Gunes, Luca Testarelli, Massimo Galli, Qorri Erda, Michela Relucenti, Orlando Donfrancesco, and Gianluca Gambarini. Recent innovations in endodontic irrigation and effects on smear layer removal: an ex-vivo study. *Clinical Oral Investigations*, 29(6):309, 2025.

[6] Andrea Frassetto, Lorenzo Breschi, Gianluca Turco, Giulio Marchesi, Roberto Di Lenarda, Franklin R. Tay, David H. Pashley, and Milena Cadenaro. Mechanisms of degradation of the hybrid layer in adhesive

dentistry and therapeutic agents to improve bond durability: A literature review. *Dental Materials*, 32(2):e41–e53, 2016.

[7] Lorenzo Breschi, Tatjana Maravic, Claudia Mazzitelli, Uros Josic, Edoardo Mancuso, Milena Cadenaro, Carmem S Pfeifer, and Annalisa Mazzoni. The evolution of adhesive dentistry: From etch-and-rinse to universal bonding systems. *Dental Materials*, 41(2):141–158, 2025.

[8] Luca De Rose, I Krejci, and Tissiana Bortolotto. Immediate endodontic access cavity sealing: fundamentals of a new restorative technique. *Odontology*, 103(3):280–285, 2015.

[9] Andrea Martín-Vacas, Vicente Vera-González, Julio Ramírez-Castellanos, Diego González-Gil, and Manuel Joaquín de Nova García. Sem/eds analysis of tubules and mineral deposition in the dentin of children with osteogenesis imperfecta. *Applied Sciences*, 13(22), 2023.

[10] Marco A Carvalho, Priscilla C Lazari-Carvalho, Paulo ET Maffra, Thábata F Izelli, Marco Gresnigt, Carlos Estrela, and Pascal Magne. Immediate pre-endodontic dentin sealing (ipds) improves resin-dentin bond strength. *Journal of Esthetic and Restorative Dentistry*, 37(1):39–47, 2025.

[11] Giulia Orilisi, Riccardo Monterubbianesi, Valentina Notarstefano, Vincenzo Tosco, Flavia Vitiello, Giampaolo Giuliani, Angelo Putignano, and Giovanna Orsini. New insights from raman microspectroscopy and scanning electron microscopy on the microstructure and chemical composition of vestibular and lingual surfaces in permanent and deciduous human teeth. *Spectrochimica Acta Part A: Molecular and Biomolecular Spectroscopy*, 260:119966, 2021.

[12] Lamia Sami Mokeem, Isadora Martini Garcia, and Mary Anne Melo. Degradation and failure phenomena at the dentin bonding interface. *Biomedicines*, 11(5), 2023.

[13] Steve Armstrong, Lorenzo Breschi, Mutlu Özcan, Frank Pfefferkorn, Marco Ferrari, and Bart Van Meerbeek. Academy of dental materials guidance on in vitro testing of dental composite bonding effectiveness to dentin/enamel using micro-tensile bond strength (μtbs) approach. *Dental Materials*, 33(2):133–143, 2017.

[14] Manon Fraulob, Siyuan Pang, Sophie Le Cann, Romain Vayron, Mathilde

Laurent-Brocq, Soorya Todatry, Julio A. N. T. Soares, Iwona Jasiuk, and Guillaume Haïat. Multimodal characterization of the bone-implant interface using raman spectroscopy and nanoindentation. *Medical Engineering & Physics*, 84:60–67, 2020.

[15] Adrianna Gliszczyńska, Magdalena Gibas-Dorna, Barbara Wróbel, and Bartłomiej Czyżniewski. Application of raman spectroscopy in dentistry: current state of knowledge, future developments and clinical potential. *Biuletyn Głównej Biblioteki Lekarskiej*, 58(385):33–56, 2025.

[16] Yong Wang, Xinglin Guo, Xiaomei Yao, and Viviane Hass. Mapping water and monomer gradients in the adhesive/dentin interface with confocal micro-raman imaging. *Dental Materials*, 41(4):473–481, 2025.

[17] Yuan Zou, Steven R Armstrong, and JL Jessop. Using raman spectroscopy to determine adhesive distribution in hybrid layer of dental bonding. *Journal of Biomedical Optics*, 11(4):044011, 2006.

[18] Fernanda Miori Pascon, Kamila Rosamilia Kantovitz, Luís Eduardo Silva Soares, Ana Maria do Espírito Santo, Airton Abrahão Martin, and Regina Maria Puppin-Rontani. Morphological and chemical changes in dentin after using endodontic agents: Fourier transform raman spectroscopy, energy-dispersive x-ray fluorescence spectrometry, and scanning electron microscopy study. *Journal of Biomedical Optics*, 17(7):075008, 2012.

[19] Julia Menezes Savaris, Maria Eduarda Paz Dotto, Lucas da Fonseca Roberti Garcia, Emmanuel João Nogueira Leal da Silva, Bruno Alexandre Pacheco de Castro Henriques, Cleonice da Silveira Teixeira, and Eduardo Antunes Bortoluzzi. Effect of final irrigation protocols on the structural integrity and mechanical properties of the root dentine. *Brazilian Oral Research*, 38:e072, 2024.

[20] Yuanyuan Liu, Leo Tjäderhane, Lorenzo Breschi, Anna Mazzoni, Nan Li, Jian Mao, David H. Pashley, and Franklin R. Tay. Limitations in bonding to dentin and experimental strategies to prevent bond degradation. *Journal of Dental Research*, 90(8):953–968, 2011.

[21] Yong Wang, Paulette Spencer, and Mary P Walker. Chemical profile of adhesive/caries-affected dentin interfaces using raman microspectroscopy. *Journal of Biomedical Materials Research Part A: An Official Journal*

of The Society for Biomaterials, The Japanese Society for Biomaterials, and The Australian Society for Biomaterials and the Korean Society for Biomaterials, 81(2):279–286, 2007.

[22] Lorenzo Breschi. Buonocore memorial lecture 2023: changing operative mindsets with universal adhesives and cements. *Operative Dentistry*, 50(1):12–32, 2025.

[23] Cristian Fernando Sanchez Puetate, Aline Carvalho Girotto, Joissi Ferrari Zaniboni, Mariana Bena Gelio, João Felipe Besegato, and Milton Carlos Kuga. Sealing of pulp chamber dentin in endodontics: Influence of bond strategy and time-point application. *Journal of Conservative Dentistry and Endodontics*, 27(5):514–519, 2024.

[24] Rong Wang, Donggao Zhao, and Yong Wang. Characterization of elemental distribution across human dentin–enamel junction by scanning electron microscopy with energy-dispersive x-ray spectroscopy. *Microscopy Research and Technique*, 84(5):881–890, 2021.

[25] Kai Zhang, Franklin R Tay, Young Kyung Kim, Jan K Mitchell, Jong Ryul Kim, Marcela Carrilho, David H Pashley, and Jun-qi Ling. The effect of initial irrigation with two different sodium hypochlorite concentrations on the erosion of instrumented radicular dentin. *Dental Materials*, 26(6):514–523, 2010.

[26] Hamza Elfarraj, Franco Lizzi, Kerstin Bitter, and Paul Zaslansky. Effects of endodontic root canal irrigants on tooth dentin revealed by infrared spectroscopy: a systematic literature review. *Dental Materials*, 40(8):1138–1163, 2024.

[27] Joana A. Marques, Rui I. Falacho, Sara Fateixa, Francisco Caramelo, João Miguel Santos, João Rocha, Markus B. Blatz, João Carlos Ramos, and Paulo J. Palma. Advancing adhesive strategies for endodontically treated teeth—part i: Impact of endodontic irrigation protocols on the chemical composition and structural integrity of coronal dentin. *Journal of Esthetic and Restorative Dentistry*, 37(7):1848–1864, 2025.

[28] Mohammed E. Grawish, Lamyaa M. Grawish, Hala M. Grawish, Mahmoud M. Grawish, Ahmed A. Holiel, Nessma Sultan, and Salwa A. El-Negoly. Demineralized dentin matrix for dental and alveolar bone tissues

regeneration: An innovative scope review. *Tissue Engineering and Regenerative Medicine*, 19(4):687–701, 2022.

[29] Fereshteh Shafiei and Maryam S Tavangar. Pre-sealing of endodontic access cavities for the preservation of anterior teeth fracture resistance. *Clinical and Experimental Dental Research*, 10(4):e936, 2024.

[30] Mohammad Anwar Alebrahim. *ATR-FTIR and raman imaging to study permanent and primary teeth from different places and ages*. PhD thesis, Jena, Friedrich-Schiller-Universität Jena, Diss., 2013, 2013.

[31] Indu Padmakumar, Dharam Hinduja, Abdul Mujeeb, Raghu Kachenahalli Narasimhaiah, Ashwini Kumar Saraswathi, Mubashir Baig Mirza, Ali Robaian, Syed Nahid Basheer, Mohmed Isaqali Karobari, and Giuseppe Alessandro Scardina. Evaluation of effects of various irrigating solutions on chemical structure of root canal dentin using ftir, sem, and eds: an in vitro study. *Journal of Functional Biomaterials*, 13(4):197, 2022.

[32] Arefin Alam, Monica Yamauti, Abu Faem Mohammad Almas Chowdhury, Xiaohong Wang, Pedro Álvarez-Lloret, Enrique-Ezra Zuniga-Heredia, Carolina Cifuentes-Jiménez, Rupak Dua, Masahiro Iijima, and Hidehiko Sano. Evaluating the advancements in a recently introduced universal adhesive compared to its predecessor. *Journal of Dental Sciences*, 19(3):1609–1619, 2024.

[33] Ario Santini and Vesna Miletic. Quantitative micro-raman assessment of dentine demineralization, adhesive penetration, and degree of conversion of three dentine bonding systems. *European journal of oral sciences*, 116(2):177–183, 2008.

[34] Malik H Mahmood, László Himics, Tamás Váczi, István Rigó, Roman Holomb, Barbara Beiler, and Miklós Veres. Raman spectroscopic study of gamma radiation-initiated polymerization of diethylene glycol dimethacrylate in different solvents. *Journal of Raman Spectroscopy*, 52(10):1735–1743, 2021.

[35] Nellie Elizabeth Pretorius, A. Power, M. Tennant, A. Forrest, and Daniel Cozzolino. The use of vibrational spectroscopy in the geographic characterization of human teeth: a systematic review. *Applied Spectroscopy Reviews*, 55(2):105–127, 2020.

[36] Ying-Sing Li, Yu Wang, Tuan Tran, and Anshion Perkins. Vibrational spectroscopic studies of (3-mercaptopropyl) trimethoxylsilane sol–gel and its coating. *Spectrochimica Acta Part A: Molecular and Biomolecular Spectroscopy*, 61(13-14):3032–3037, 2005.

[37] Agnieszka Nawrocka, Ireneusz Piwonski, Salvatore Sauro, Annalisa Porcelli, Louis Hardan, and Monika Lukomska-Szymanska. Traditional microscopic techniques employed in dental adhesion research—applications and protocols of specimen preparation. *Biosensors*, 11(11), 2021.

[38] O Belaidi, M Adjim, T Bouchaour, and U Maschke. Ft-ir and ft-raman spectra of 2-hydroxyethyl methacrylate–a conformational and vibrational analysis. *Spectrochimica Acta Part A: Molecular and Biomolecular Spectroscopy*, 148:396–404, 2015.

[39] Thibaud Coradin, André Luís Porporatti, and Julia Bosco. Assessing in vitro remineralization of primary artificial caries: A systematic review of multi-techniques characterization approaches. *Dentistry Review*, 3(4):100073, 2023.

[40] José Reyes-Gasga, Esmeralda L Martínez-Piñeiro, Galois Rodríguez-Álvarez, Gaby E Tiznado-Orozco, Ramiro García-García, and Etienne F Brès. Xrd and ftir crystallinity indices in sound human tooth enamel and synthetic hydroxyapatite. *Materials science amp; engineering. C, Materials for biological applications*, 33(8):4568—4574, December 2013.

[41] Katarzyna Kaczmarek, Andrzej Leniart, Barbara Lapinska, Slawomira Skrzypek, and Monika Lukomska-Szymanska. Selected spectroscopic techniques for surface analysis of dental materials: A narrative review. *Materials*, 14(10):2624, 2021.

[42] Chiara Navarra. *Raman spectroscopy analysis of dentin-adhesive interface*. PhD thesis, Università degli studi di Trieste, 2009.

[43] Iulian Otel. Overall review on recent applications of raman spectroscopy technique in dentistry. *Quantum Beam Science*, 7(1), 2023.

[44] Diego Martins De-Paula, Alessandro D Loguercio, Alessandra Reis, Natasha Marques Frota, Radamés Melo, Kumiko Yoshihara, and Victor Pinheiro Feitosa. Micro-raman vibrational identification of 10-mdp bond to zirconia and shear bond strength analysis. *BioMed research international*, 2017(1):8756396, 2017.

[45] M Oliveira, F Chasqueira, S Arantes-Oliveira, and S Pessanha. The use of micro-raman spectroscopy for the analysis of caries-affected dentin adhesive interfaces. *International Journal of Adhesion and Adhesives*, 87:216–222, 2018.